SANDIA REPORT SAND82—0445 • Unlimited Release • UC—80
Printed May 1982

Description and Analysis of the Sandia Pulse Reactor-IV (SPR-IV)

J. S. Philbin, J. L. Tills, T. F. Luera, T. R. Schmidt

Prepared by
Sandia National Laboratories
Albuquerque, New Mexico 87185 and Livermore, California 94550
for the United States Department of Energy
under Contract DE-AC04-76DP00789

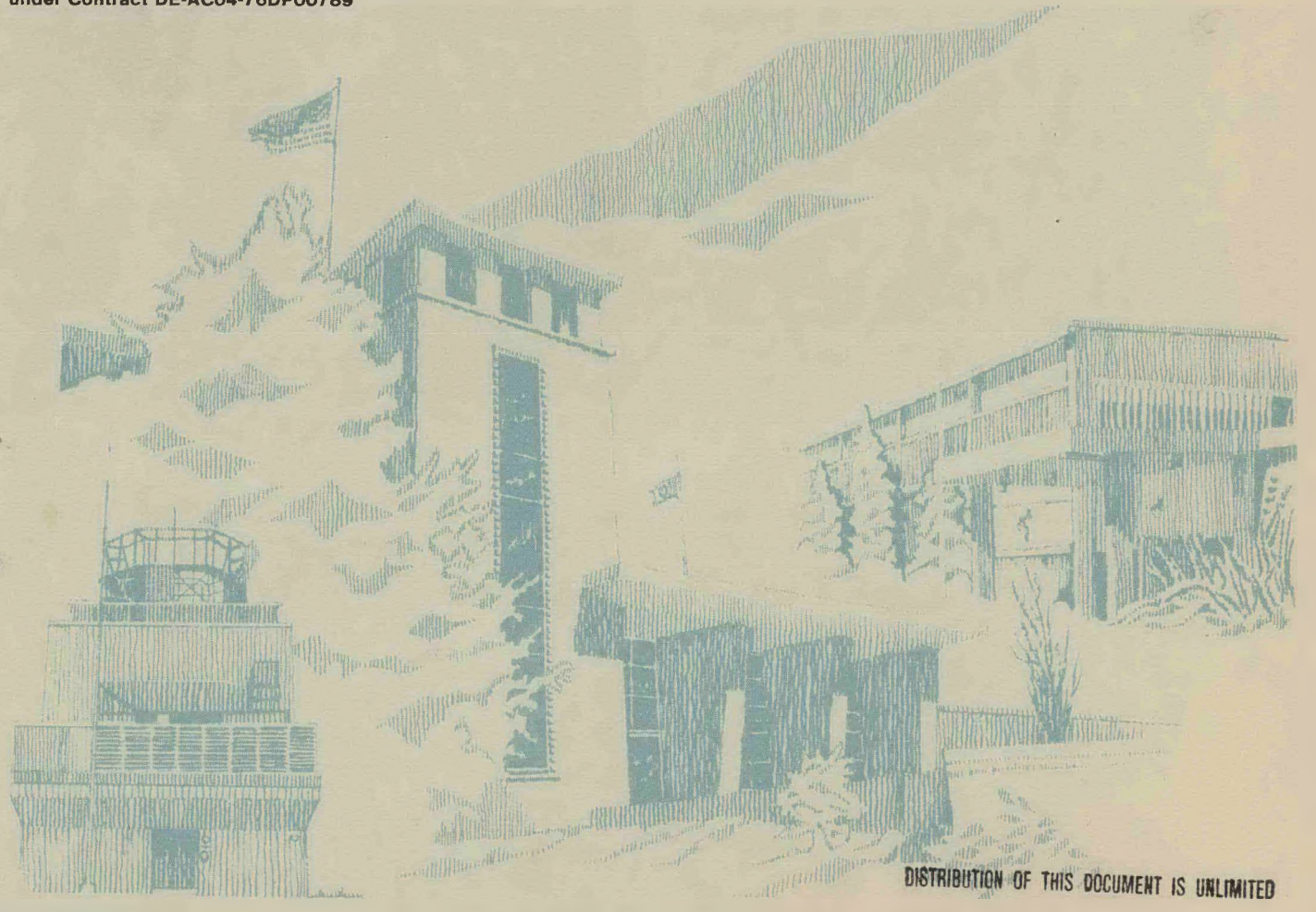

SF 2900-Q(6-82)

Issued by Sandia National Laboratories, operated for the United States Department of Energy by Sandia Corporation.

Printed in the United States of America
Available from
National Technical Information Service
U.S. Department of Commerce
5285 Port Royal Road
Springfield, VA 22161

NTIS price codes
Printed copy: A07
Microfiche copy: A01

SAND--82-0445

SAND82-0445
Unlimited Distribution
UC-80

DE82 018330

DESCRIPTION AND ANALYSIS OF THE SANDIA PULSE REACTOR-IV (SPR-IV)

J. S. Philbin
Experimental Systems Design Division, 4452

J. L. Tills
Science And Engineering Associates, Inc.

T. F. Luera
Neutron Effects Simulation Staff, 4450A

T. R. Schmidt
Reactor Applications Division, 4451

Sandia National Laboratories
Albuquerque, New Mexico 87185

Printed May 1982

Abstract

This report presents a description and analysis of the Sandia Pulse Reactor-IV (SPR-IV), an all metal, fast burst reactor, designed by Sandia National Laboratories in Albuquerque, NM. The reactor will have a large central irradition cavity, 34 cm diameter by 51 cm high, for the exposure of electronic and nuclear components to hard-spectrum pulsed neutron fluences as high as 5.6E+14 nvt. The methods, models, and results of the nuclear, thermomechanical and heat transfer design are given. Operating characteristics of the reactor as well as the reactivity worth of the control elements and some typical experiment materials are also included.

ACKNOWLEDGEMENT

The authors wish to thank D. N. Cox, 4421, and R. E. Stinebaugh, 4452, for their contributions to the mechanical design of the reactor and for drawings of the reactor that appear in this report. We also wish to acknowledge the BDM Corp. of Albuquerque, NM, for their contributions to the external nitrogen cooling system design and description.

Contents

Illustrations

Illustrations (cont.)

Tables

1.0 Introduction

Sandia National Laboratories has designed the Sandia Pulse Reactor-IV for the irradiation of large electronic and nuclear components which require high-level, hard-spectrum, neutron pulses of short duration. The SPR-IV cavity will have a usable inside diameter of 34.3 cm (13.5 inches) and a fuel height of 50.8 cm (20.0 inches) giving a cavity volume five times greater than that of SPR-III. The important feature is the increased diameter which will permit irradiation of components too large for irradiation in SPR-III. The fuel alloy will be gamma-phase-stabilized fully enriched uranium alloyed with 10 weight-percent molybdenum.

The reactor is designed for neutron vulnerability and hardening tests of Sandia-designed electronic components of advanced tactical and strategic nuclear weapon systems. Current proposed designs for these advanced electronic systems packages will not fit in SPR-III; hence, SPR-IV is designed to accommodate the development, proof testing and hardness assurance required for the new systems. Also, the SPR-IV facility will permit exposure of nuclear weapon fissile components to fast-burst neutron fluences for basic materials studies and neutron hardness testing. These components also will not fit in the SPR-III cavity.

This report describes the calculations that were performed for the reactor core of SPR-IV. Included are results from the nuclear, thermomechanical, and thermal analyses. The nuclear analysis was performed using both discrete ordinates and Monte Carlo multi-energy-group calculations. These calculations provide information on criticality, fission density distributions, flux distributions, neutron spectra, reactivity worths, neutron lifetime (hence kinetic behavior), and experiment effects. The thermomechanical analysis addressed the dynamic stresses generated in the fuel plates and the supporting structure. This analysis includes the effects of pulse width and temperature. The thermal analysis examined the reactor cooling system and heat transfer from the fuel plates and included experiments with SPR-III to determine effective heat transfer coefficients for nitrogen gas cooling on the exterior of the fuel.

The design philosophy for SPR-IV is based on SPR- III which has been proven with seven years of successful operation. SPR-III has produced approximately 900 pulses in a total of 1900 operations. However, several aspects of the SPR-III design have been identified for possible improvement. These include the cooling system, the safety block drive mechanism, the burst element drive system, axial and auxiliary radial reflectors, the shroud, the thermocouple installations, the reactor storage pit, and the reactor handling equipment. Items that do not relate directly to the nuclear, thermomechanical or

heat transfer aspects of the core itself are outside the scope of this report and are only briefly discussed here.

The increased core dimensions, the flow-thru cooling system, and the shielded shroud are perhaps the most obvious and important changes that a person familiar with SPR-III will notice.

The cooling system for SPR-IV has been designed to efficiently cool the reactor either after a pulse when the safety block is in the down position or during a steady state operation when the safety block is in the up position. Two separate gas plena circulate gas between the fuel plates of the individual core blocks. This design provides an efficient cooling geometry regardless of safety block position. The lower plenum moves with the safety block as a unit. This coupling does not alter or interfer with the safety block's function of providing a large negative reactivity to terminate an operation. Cooling between the plates provides rapid cooldown following pulse operations as well as efficient steady state cooling during power run operations.

The shroud for the reactor has been designed to include a layer of lead. The lead will attenuate gamma rays from the core more so than the neutrons thereby increasing the neutron-to-gamma ratio for experiments exposed around the periphery of the reactor. It will also serve as personnel shielding during experiment set up and reactor check out and maintenance.

Description and evaluation of the core-related design features are given in subsequent chapters of this report. Chapter 2 gives a description of the reactor, Chapter 3 presents a nuclear analysis, Chapter 4 contains the thermomechanical analysis, and Chapter 5 gives a description and analysis of the cooling system.

2.0 The Reactor

2.1 Description of the Reactor

The SPR-IV reactor core is an unmoderated cylindrical assembly of uranium metal fuel plates enriched to 93 percent ^{235}U and alloyed with 10 wt.% molybdenum. Eighteen annular fuel rings (35.4 cm ID x 45.7 cm OD x 2.75 cm high--nominal dimensions) plus steel support rings comprise the assembly which is divided at the horizontal midplane. The height of each core half including the central support ring but not the outer support ring 1.9 cm thick) is 25.96 cm (10.22 in). Refer to Figure 2.1-1 for a sketch of the reactor. Drawings of the individual fuel rings are given in Figures 2.1-2, 2.1-3, and 2.1-4. The B rings are similar to the B1 rings except for the absence of the thermocouple holes. An assembly drawing of a core block is shown in Figure 2.1-5. The critical fuel mass is approximately 550 kg.

The reactor is brought close to critical (sub-delayed critical) by raising the movable lower half of the core into contact with the upper half. Criticality is achieved through the adjustment of three nickel-plated copper control elements which move axially near the outer surface of the core. The reflector control elements are curved solid pieces, 3.2 cm (1.25 in) thick, that conform to the outside curvature of the fuel. These pieces are 43.2 cm (17 in) high and subtend an arc of 60°. (One of the elements, No. 2, subtends only 30°, however.) Each of four reflectors (three control elements plus one burst element) is centered in a 90° quadrant around the lateral surface of the core.

Experiments are placed within the 34.3 cm (13.5 in) diameter by 50.8 cm (20 in) high central cavity or positioned around the outside of the core. The control element critical positions and the adjustment required to produce the desired pulse yield are influenced by the effects of experiments on core reactivity and neutron lifetime. A fourth external control element, called the pulse (or burst) element, is moved upward rapidly by electromechanical means, thus adding sufficient reactivity to drive the reactor above prompt critical. The pulse element is made of graphite and is enclosed in an aluminum sheath.

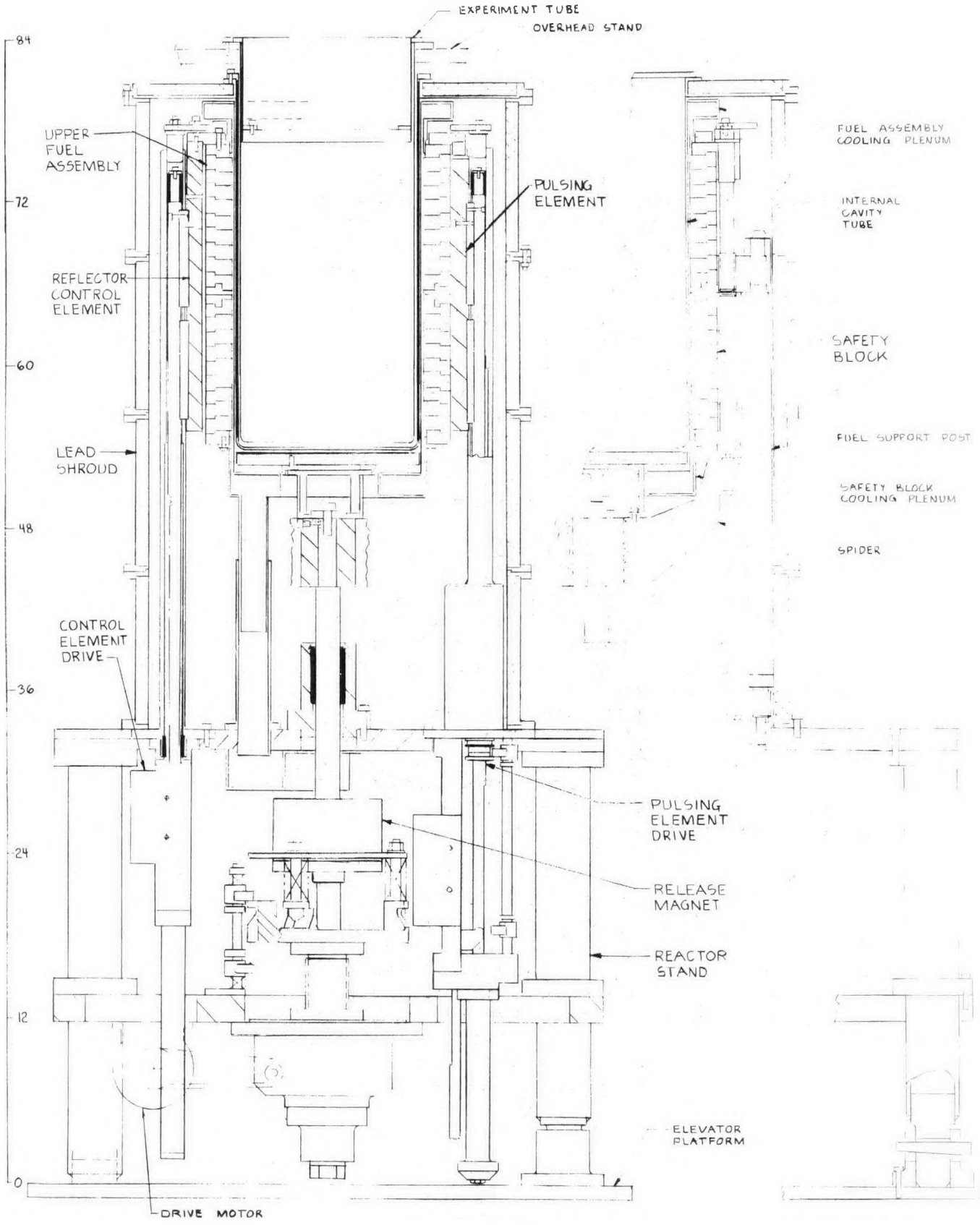

SPR IV REACTOR

Figure 2.1-1

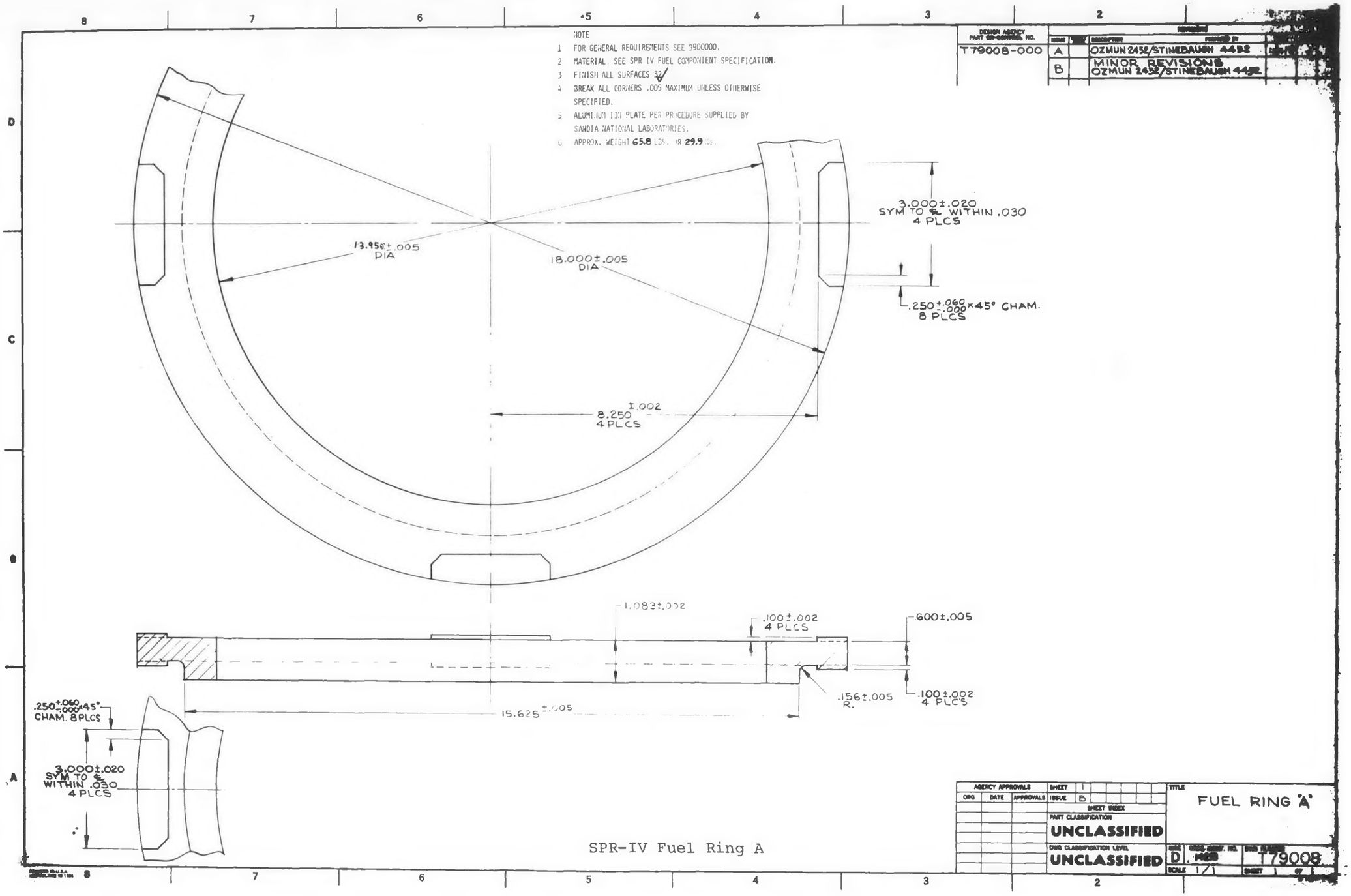

SPR-IV Fuel Ring A

Figure 2.1-2

NOTES

1. FOR GENERAL REQUIREMENTS SEE 9900000.
2. MATERIAL: SEE SPR IV FUEL COMPONENT SPECIFICATION.
3. FINISH ALL SURFACES 32
4. BREAK ALL CORNERS .005 MAXIMUM UNLESS OTHERWISE SPECIFIED.
5. ALUMINUM ION PLATE PER PROCEDURE SUPPLIED BY SANDIA NATIONAL LABORATORIES.
6. APPROX. WEIGHT 65.8 Lbs. OR 29.9 Kg.

DESIGN AGENCY PART OR IDENTIFYING NO.	ZONE	LTR	DESCRIPTION
T79007-000		A	OZMUN 2452/STINE
		B	MINOR REVISION OZMUN 2452/STINE

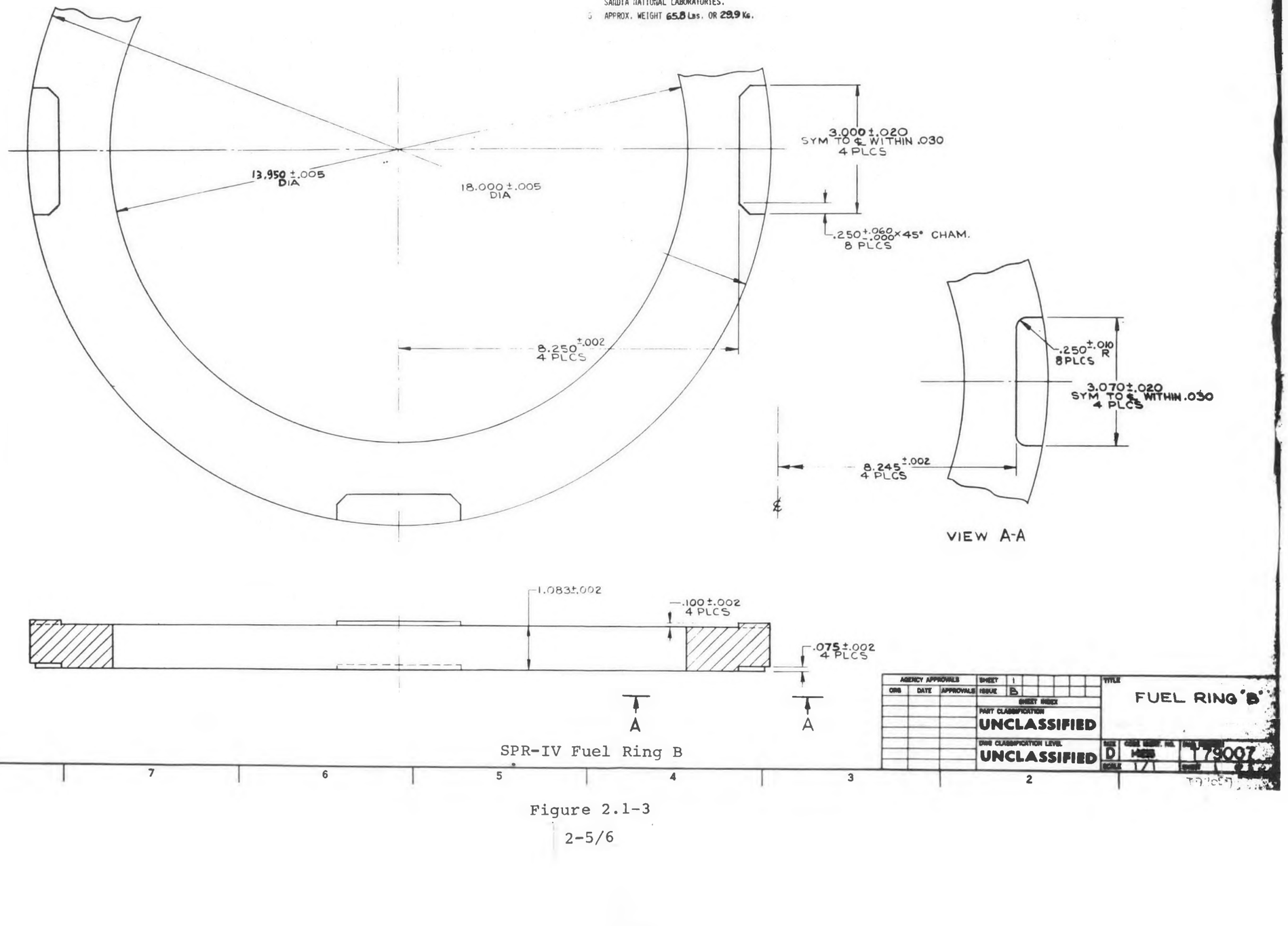

SPR-IV Fuel Ring B

AGENCY APPROVALS			SHEET 1
ORG	DATE	APPROVALS	ISSUE B

SHEET INDEX

PART CLASSIFICATION: UNCLASSIFIED

DWG CLASSIFICATION LEVEL: UNCLASSIFIED

TITLE: FUEL RING "B"

SIZE D | CAGE IDENT. NO. M88 | DWG. NO. T79007 | REV. B

SCALE 1/1 | SHEET 1 OF 1

Figure 2.1-3

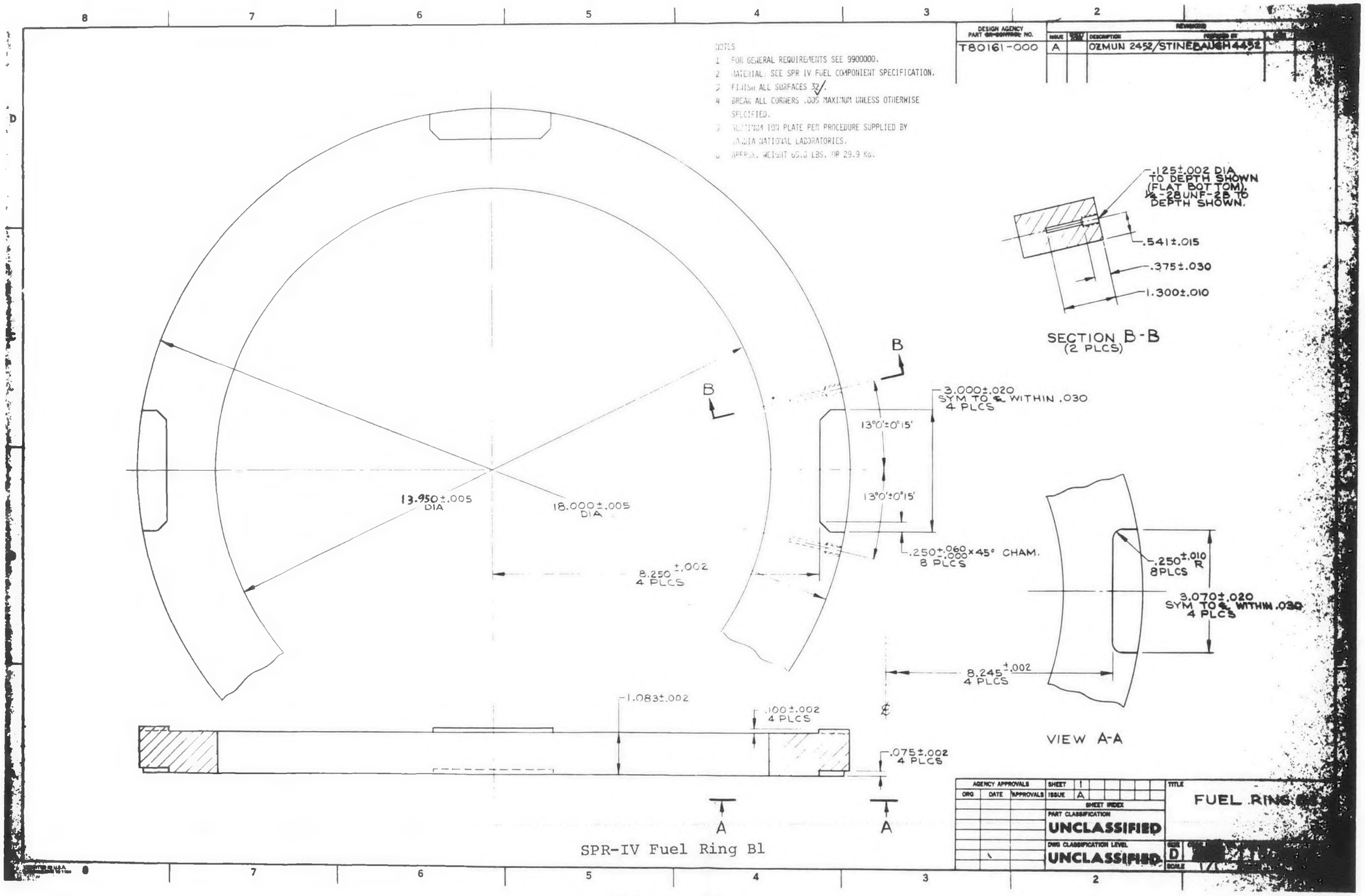

SPR-IV Fuel Ring B1

Figure 2.1-4

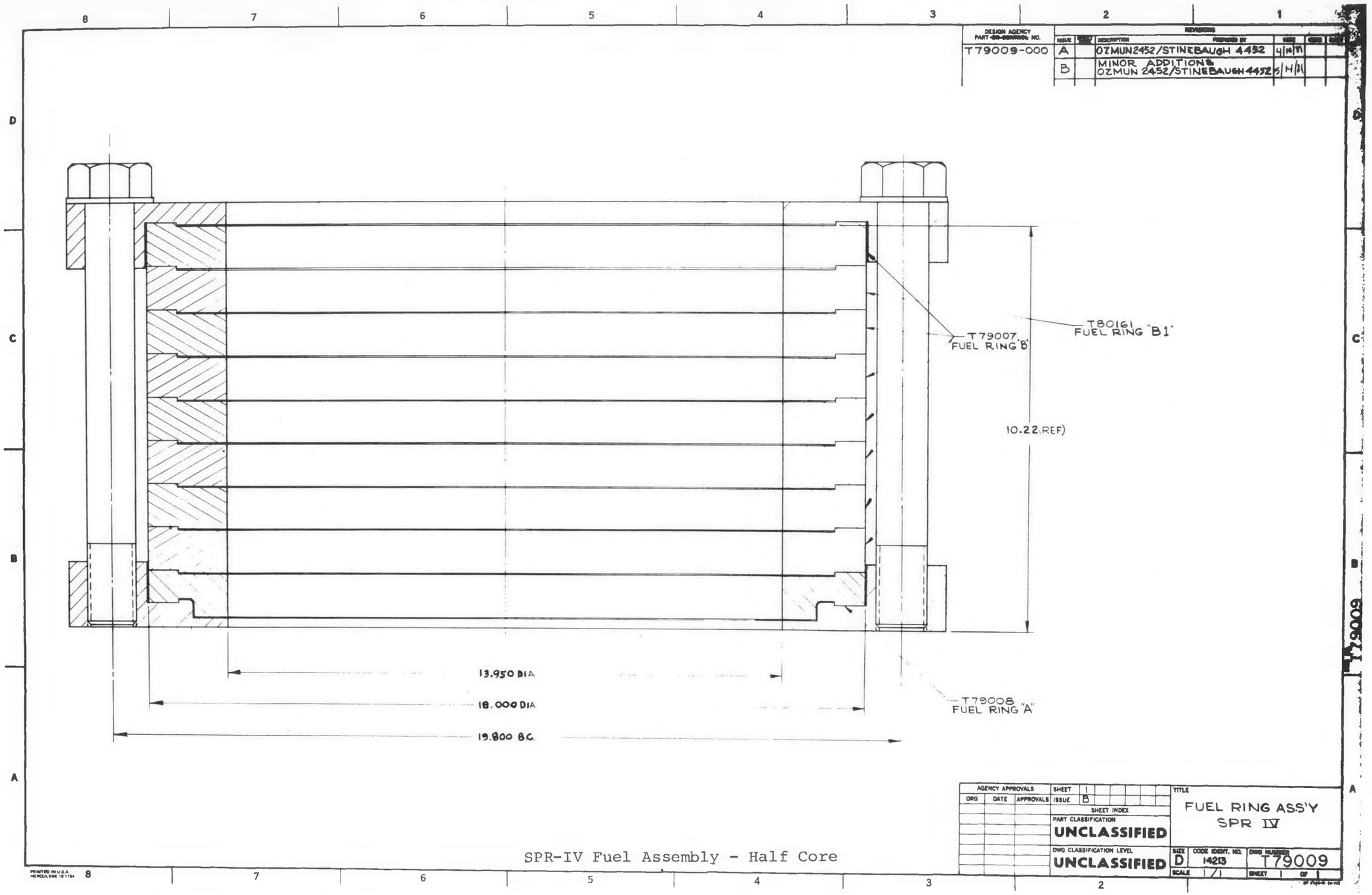
T79009-000
A
OZMUN2452/STINEBAUGH 4452
4/11/11
B
MINOR ADDITIONS
OZMUN 2452/STINEBAUGH 4452
5/11/11
T80161
FUEL RING "B1"
T79007
FUEL RING "B"
10.22 (REF)
13.950 DIA
18.000 DIA
19.800 B.C.
T79008
FUEL RING "A"
FUEL RING ASS'Y
SPR IV
UNCLASSIFIED
UNCLASSIFIED
14213
T79009
SPR-IV Fuel Assembly - Half Core

Figure 2.1-5

The super prompt critical excursion is terminated by the thermodynamic expansion of the fuel driven by the large and rapid energy deposition from fission. Thermo-mechanical shock breaks a magnetic coupling holding the lower core half in place. The core is thus driven subcritical.

The axial and auxiliary radial reflectors as well as certain features of the SPR-IV burst element and safety block (lower core half) drive systems and cooling system represent noteworthy modifications or additions to earlier fast burst reactor designs.

The burst element drive system is shown in Figure 2.1-6. A linear induction motor provides the force to drive the pulse element upward. Graphite was selected as the material for the pulse element to reduce its mass relative to the aluminum element used in SPR-III. Pulse element position readout is obtained through a circular potentiometer driven by a rack-and-pinion gear system. An air-filled dashpot controls velocity and bouncing.

The SPR-IV safety block drive system is shown in Figure 2.1-7. A reduced overall height for the SPR-IV safety block drive system was made possible by combining the dashpot and drive-motor lubrication oil in a single reservoir. The magnetic coupling feature remains unchanged from previous designs, however.

The cooling system has been designed to provide efficient cooling of the core. The design will provide cooling times comparable to those for the much smaller SPR-III core. The elements of the design which represent an improvement over past designs are (i) a cooling plenum which permits the flow of nitrogen between the fuel plates, (ii) separate plena for upper and lower core halves, and (iii) provisions for large volume coolant flow and prechilling of cooling lines. By forcing nitrogen to flow between the fuel plates, the surface area through which heat can be taken from the core is greatly enhanced compared to previous designs. Separate plena for upper and lower core halves provide for efficient cooling during power runs or with the safety block down after a burst. The coolant flow rate is 50 to 90 grams per second, and a valve near the core eliminates time lost in chilling long coolant lines.

Axial reflectors--4.4 cm (1.75 in) at the top of the cavity and 2.5 cm (1 in) beneath the cavity liner--

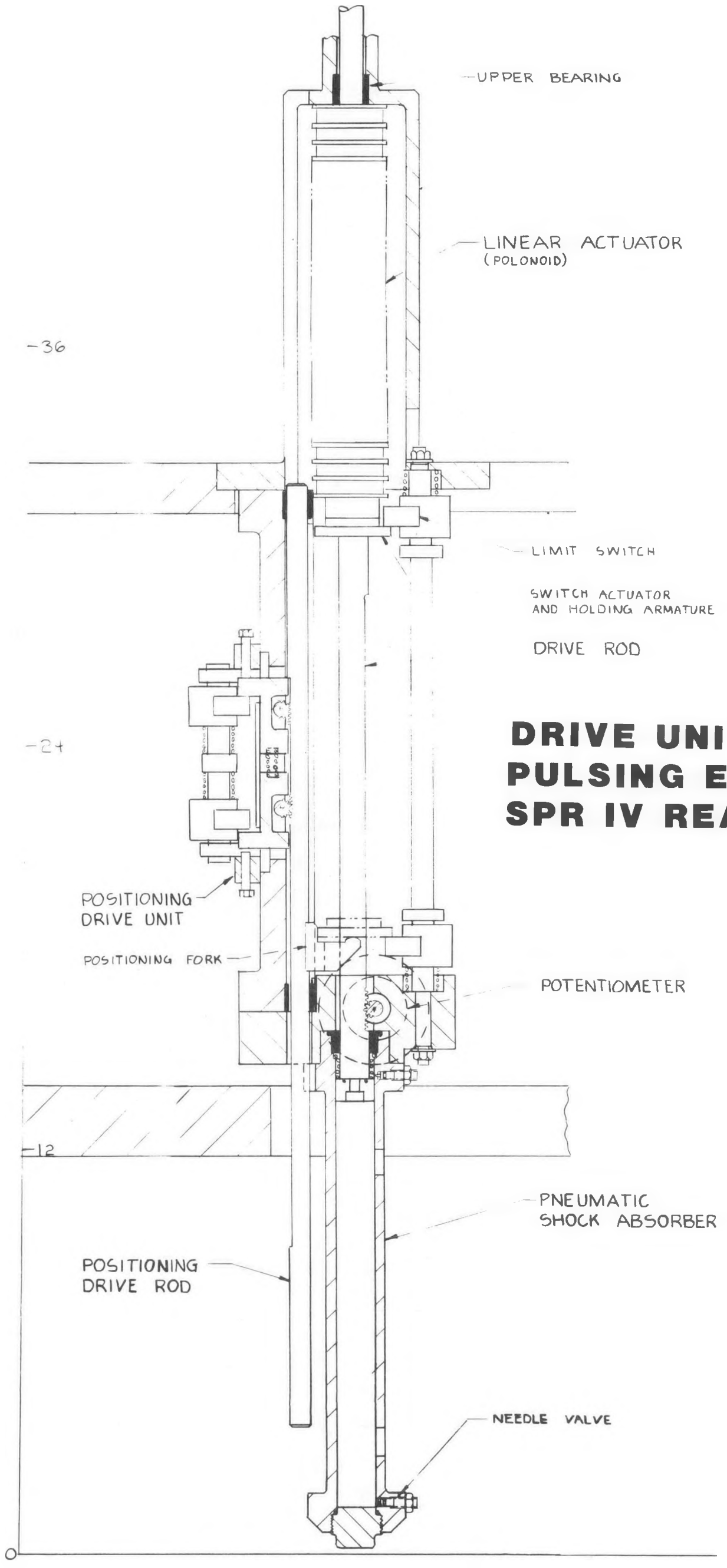

DRIVE UNIT, PULSING ELEMENT SPR IV REACTOR

Figure 2.1-6

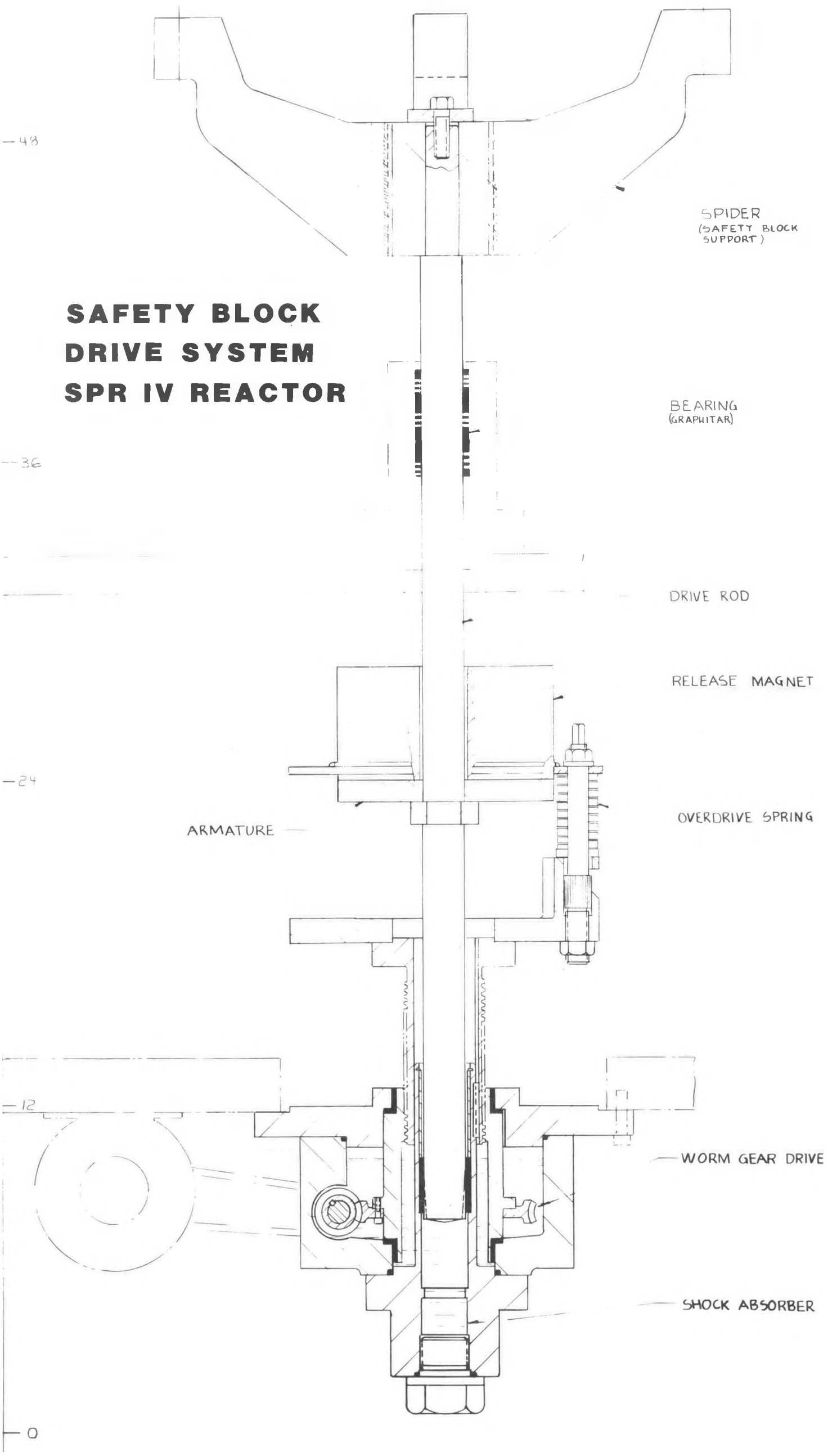
SAFETY BLOCK
DRIVE SYSTEM
SPR IV REACTOR
SPIDER
(SAFETY BLOCK
SUPPORT)
BEARING
(GRAPHITAR)
DRIVE ROD
RELEASE MAGNET
OVERDRIVE SPRING
ARMATURE
WORM GEAR DRIVE
SHOCK ABSORBER
-48
-36
-24
-12
0
2-15/16

Figure 2.1-7

are used in SPR-IV to reduce reactivity swings caused by experiments placed in the central cavity and to provide a more uniform axial distribution of neutron flux. External reflector skirts around the top three fuel rings reduce axial fission density peaking in the lower core half (caused by the control elements), increase the centerline fluence for a given hot spot temperature rise, and improve axial neutron flux uniformity in the central cavity.

Enriched boron powder (90 percent B-10) is packed (1.3 g/cm^3) into a narrow annulus, 0.15 cm (60 mils), between two steel liners to form a thimble-shaped decoupler. The decoupler reduces the influence of moderating materials in the cavity on the kinetics of the reactor. A boron-loaded (0.0240×10^{24} atoms of B-10/cm^3) silastic liner covering the cooling shroud serves a similar function by capturing slow neutrons reflected back to the reactor from the walls or from experiments located external to the reactor.

2.2 Operation of the Reactor

The reactor is controlled from the operations center. Television cameras within the Reactor Building allow visual observation of the reactor during all operations. The control console consists of a control system, a plant protection system, and environmental monitoring readouts. These systems contain instrumentation readout devices, actuators for drive motors, interlock relays that ensure safe sequencing of various operations, data recording devices, and protective circuitry. This is a one-of-a-kind, custom-designed console which complies, where applicable, to the IEEE requirements for power plant consoles.

The reactor control system permits the remote operation of the groups of devices necessary for normal reactor routines. Control cables connect the reactor room with the control room where, from the console, operators can accurately position any of the elements required to control reactivity. The safety block (lower core half) can be driven to mate with the upper core half in one of two speeds through the use of a direct current motor. To assure accurate safety block position information which is vital to the repeatability of pulse yield, precision position indication is made available at the console. The three copper control

element reflectors are driven by three independent high torque direct current motors capable of precise reflector positioning. Interlocks prevent any attempt to insert more than one reflector at a time yet allow multiple withdrawals. The graphite burst element is remotely inserted by actuating a linear induction motor on the reactor stand. Once again, duplicate position indication is made available at the console, and interlocks permit burst element insertion only after the proper reactivity assembly sequence has been completed. Furthermore, the operator is required to depress a key-locked switch as part of the assembly sequence.

Rapid shutdown--scram--is accomplished by dropping all of these reactivity control devices simultaneously. In the case of the safety block, two magnet coils which are part of the reactor protect circuitry must be energized before safety block movement can take place. Losing power to either of the two magnets drops the safety block, putting the reactor in a safe shutdown condition. Additionally, the three control element reflectors are linked to their respective drive motors with magnetic clutches which are also part of the protect circuitry. The clutches must be energized before the motors can move them, and loss of clutch power drops the reflectors. Finally, a scram signal reverses the direction of motion impressed upon the burst element by the linear induction motor so that "scram" is synonymous with having all reactivity control devices in the full down position.

For the most part, the scram signals themselves are generated by sensors in the reactor room. Thermocouples embedded in the metal fuel plates provide two independent channels of high temperature scram action. "Fast scram" detectors--photodiodes--off to the side of the reactor respond to high reactor power levels. Scram can be manually initiated either locally in the reactor room or remotely at the control console. Should a fault occur in the console itself such that reset console power is lost, a scram will also ensue. Indication of which signal initiated the scram is provided at the console as well as the status of shield and ground fault detectors which continuously monitor the protect system signal paths.

The control and protect systems are complemented by auxiliary instrumentation which is necessary for reactor operation. This includes:

- fission chamber output of reactor power for start up (two channels)
- compensated ion chamber output of reactor power for intermediate and power range operation (two channels)
- uncompensated ion chamber output of reactor power as back-up (two channels)
- reactor fuel temperature indication (four channels)
- initial reactor period measurement timers (two channels)
- nitrogen cooling system panel
- reactor room exhaust ventilation system panel
- reactor shield door and elevator control panel
- reactor control interlock panel
- program, master countdown, and sequence timers.

3.0 Nuclear Analysis of SPR-IV

3.1 Introduction to the Analysis

TWOTRAN-II and KENO-IV, two widely used, multigroup-neutron-transport codes, were used to calculate neutron flux profiles, critical mass, reflector dimensions and spacing, and the prompt neutron generation time of SPR-IV. TWOTRAN-II is a general purpose, two-dimensional, multi-energy-group code used for solving the neutron transport equation according to the discrete ordinates approximation [3-1]. KENO-IV is a general geometry, three-dimensional, Monte Carlo neutron transport code specifically designed for criticality calculations [3-2].

Flux and fission density profiles and spectral information were obtained from TWOTRAN-II while prompt neutron generation times were obtained from KENO-IV. The self-multiplication factor, k_{eff}, was obtained from both codes.

The Hansen Roach 16 group cross-sections [3-3] were used with both codes for the majority of the calculations. However, a 12-group set derived from the VITAMIN C library [3-4] was used with KENO-IV to provide independent checkpoint calculations on some normal configurations and some configurations where the reactor was modeled inside a storage pit. The Hansen Roach set contains mostly P_o cross-section data with transport corrected scattering cross-sections. Some isotopes (hydrogen and lead, for example) have specific P_1 components that were utilized, however. The 12-group set was a consistent P_3 set but only the P_o and P_1 components were used.

TWOTRAN-II and KENO-IV R-Z models of the reactor were used to derive the critical dimensions of the core and the reactivity worths of the major components (fuel and non-fuel) of the reactor. Two R-Z models were developed for each core. One was a "fine structure" model of the bare core and the other was a coarse structure model of the core and its pertinent components (including storage pit walls which were modeled in some of the KENO-IV runs). The TWOTRAN-II R-θ model, with a buckling term to simulate leakage in the Z direction, was used for reactivity worth determinations of core support posts and bolts, and the burst element.

In TWOTRAN-II the user must specify the angular quadrature. S-4 quadrature was used for all scoping calculations, S-8 quadrature was used for reactivity worth determinations ($\Delta\rho$) and S-16 and Monte Carlo results were used for the reactivity value of the bare core. S-16 runs were also used for the axial flux profiles. Changes in the self-multiplication factor, k_{eff}, compared favorably for S-8 and S-16. In the cavity region, however, the S-8 flux profiles showed evidence of ray effects. These effects were considerably reduced by using the S-16 quadrature although they were not entirely eliminated. There was roughly a factor of 3 increase in run time going from S-4 to S-8 and S-8 to S-16 (nominally 320 sec, 800 sec, and 2700 sec, respectively, on the CDC-7600).

The criticality search option in TWOTRAN-II was used for determination of important system dimensions. Reactivity worths were determined by noting the changes in the self-multiplication value (eigenvalue) resulting from deliberate changes in the system configuration. Converged fluxes from previously-run, related problems were used as input flux guesses whenever possible to reduce computer run time with TWOTRAN-II. Frequently the run time could be reduced by a factor of 4 or better by using a good flux guess.

3.2 Core Models

Information for the nuclear design was derived from three basic calculational models. A "fine structure" model describing the fuel assembly in detail was used to calculate the self-multiplication factor of the bare core and, hence, the critical dimensions and critical mass. A coarse model including a simplified fuel assembly with the shroud, lead shield, axial and radial reflectors, base plate and safety block support shaft was developed to calculate the reactivity worths of the various reactor components. This model was also used to calculate the differential reactivity worth resulting from changes (perturbations) in component dimensions. Reactivity worths of experiments were also calculated with this model. The same basic models were used for both TWOTRAN-II and KENO-IV.

The third model was in R-θ geometry. No three-dimensional KENO-IV input was developed from the R-θ model. The TWOTRAN-II calculations with this model

gave the relative reactivity worths for configurations of the radial reflectors, the reflector guide posts, clamping bolts, and core support bolts.

Figure 3.2-1 gives the dimensions and configuration of the more detailed bare fuel assembly model. Shown is the upper right quarter of an axial section of the assembly. In the calculation, a reflecting boundary condition was used at the core horizontal midplane, since both halves of the fuel assembly are identical. The experiment tube and cavity decoupler are included. The decoupler consists of 1.53 mm (60 mils) of enriched boron powder contained with stainless steel walls 0.79 mm (30 mils) thick. The 4340 steel support annuli are also shown at the outside corners. Each individual fuel plate is fully described, including the 0.635 mm (25 mil) gaps between the plates. The contact rim near the outer radius is also illustrated in the model. This configuration (without the experiment tube and decoupler) was used in determining the bare critical dimensions.

Figure 3.2-2 gives the dimensions and configuration of the coarse-detail reactor model which describes the reactor assembly down to the aluminum base plate at the top of the reactor stand. This description includes a simplified fuel assembly with 4340 steel support annuli. The cavity liner and decoupler, the shroud (also a decoupler), the lead shield, the base plate, the safety-block drive shaft, the axial reflectors, and a reflector in the delayed critical position are shown. This gives half of an axially sectioned view of the cylindrical reactor system. Reactivity worths of the various parts of the system as well as integral reactivity worths of the control and burst elements were determined with this model. The effects of core separation (safety block lowered) were also examined. Important dimensions to notice in this model are the reflector thickness--3.175 cm (1.25 in)--and the gap between the core and the reflector surfaces--0.48 cm (3/16 in).

The third configuration, shown in Figures 3.2-3A and 3.2-3B, is 1/8 of a horizontal section of the core and was used in R-θ calculations to examine reactivity worths of core bolts, support posts, and reflector perturbations. Reflecting boundary conditions were used on both radial surfaces. Figure 3.2-3A shows the simple R-θ configuration with a uniform reflector similar to an R-Z calculation with a cylindrical reflector. The radial reflector region is treated as a volume-averaged

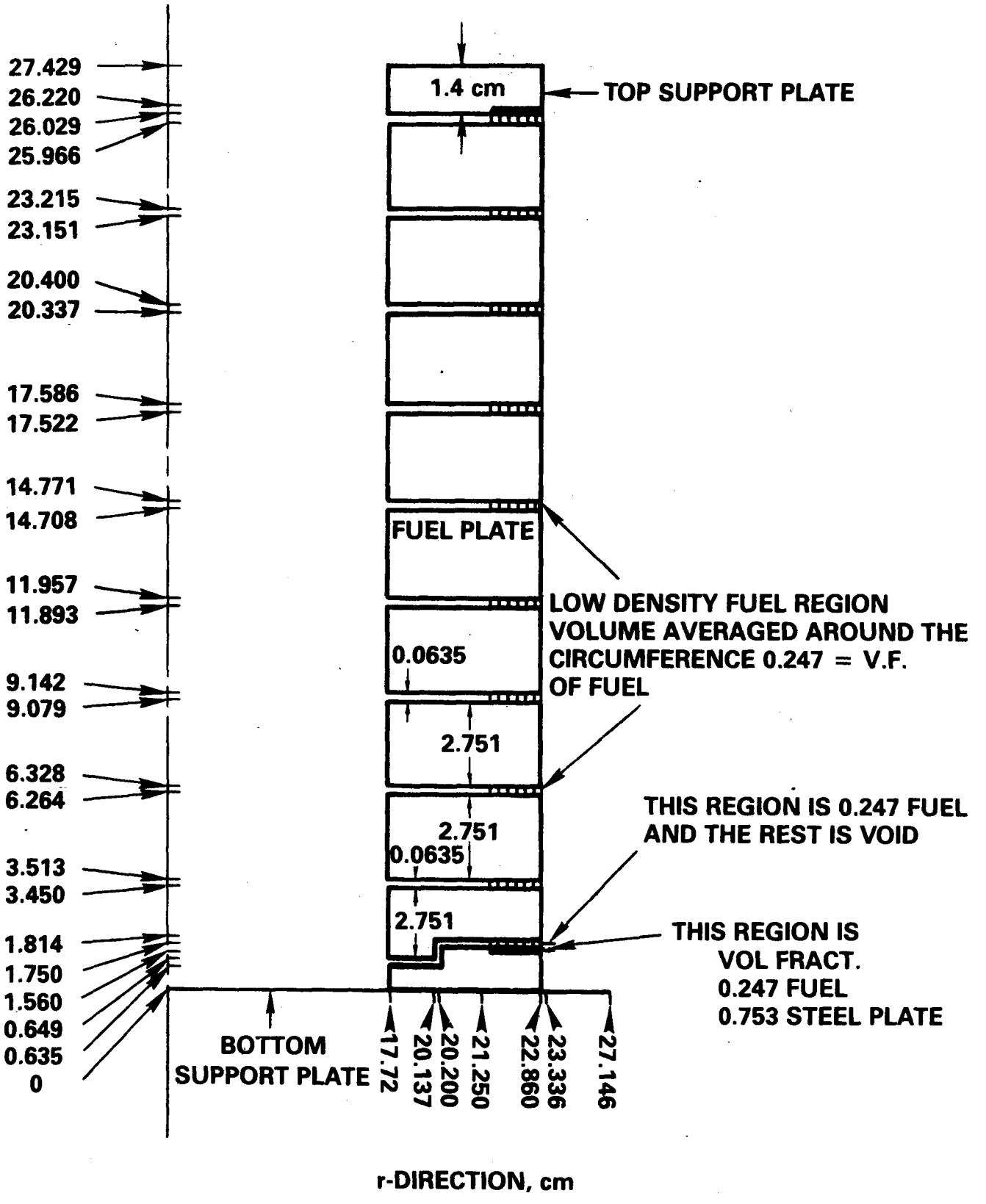

Figure 3.2-1
Fine Detail Model Of The SPR-IV Core

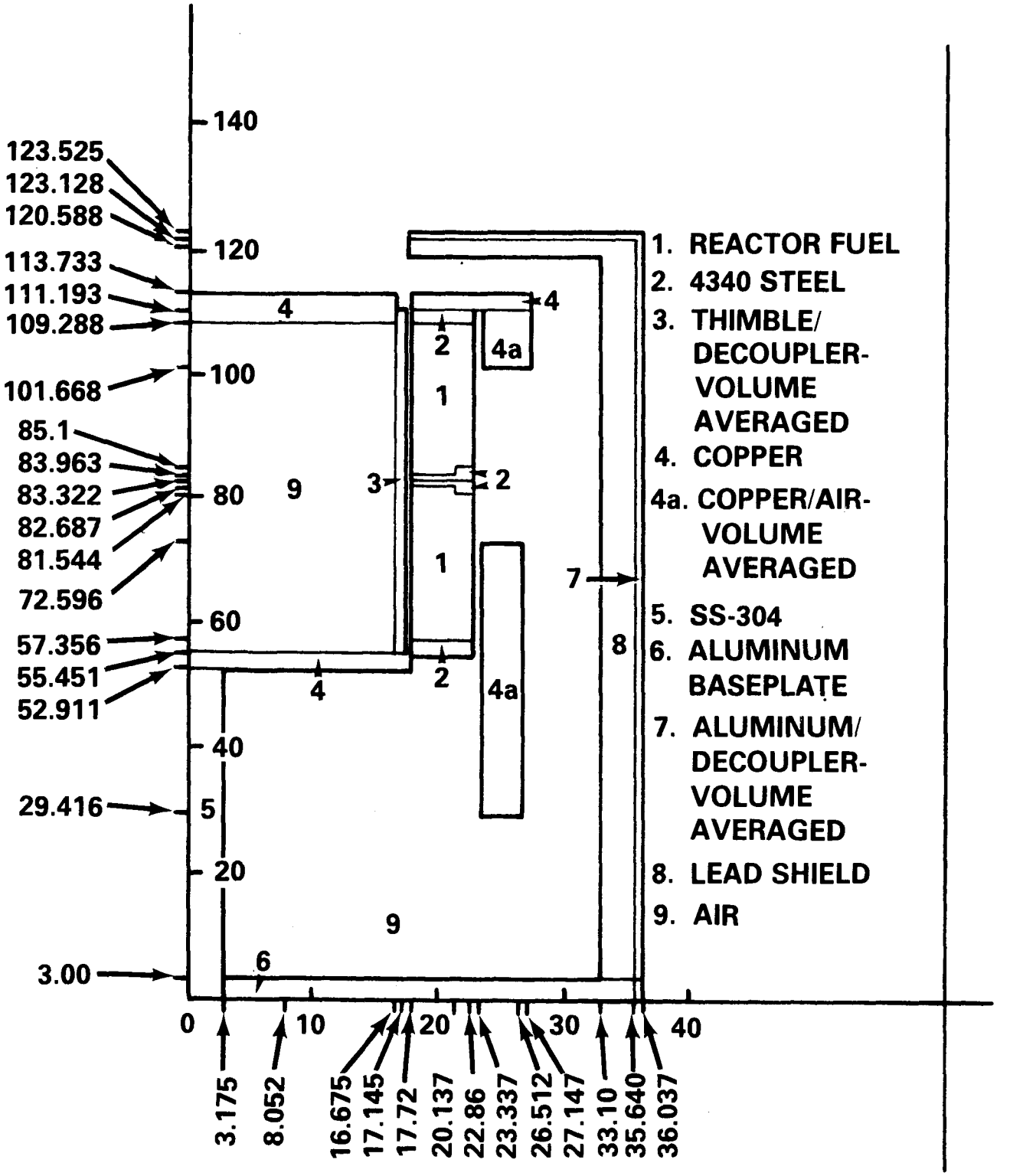

Figure 3.2-2
Coarse R-Z Model Of The SPR-IV Reactor

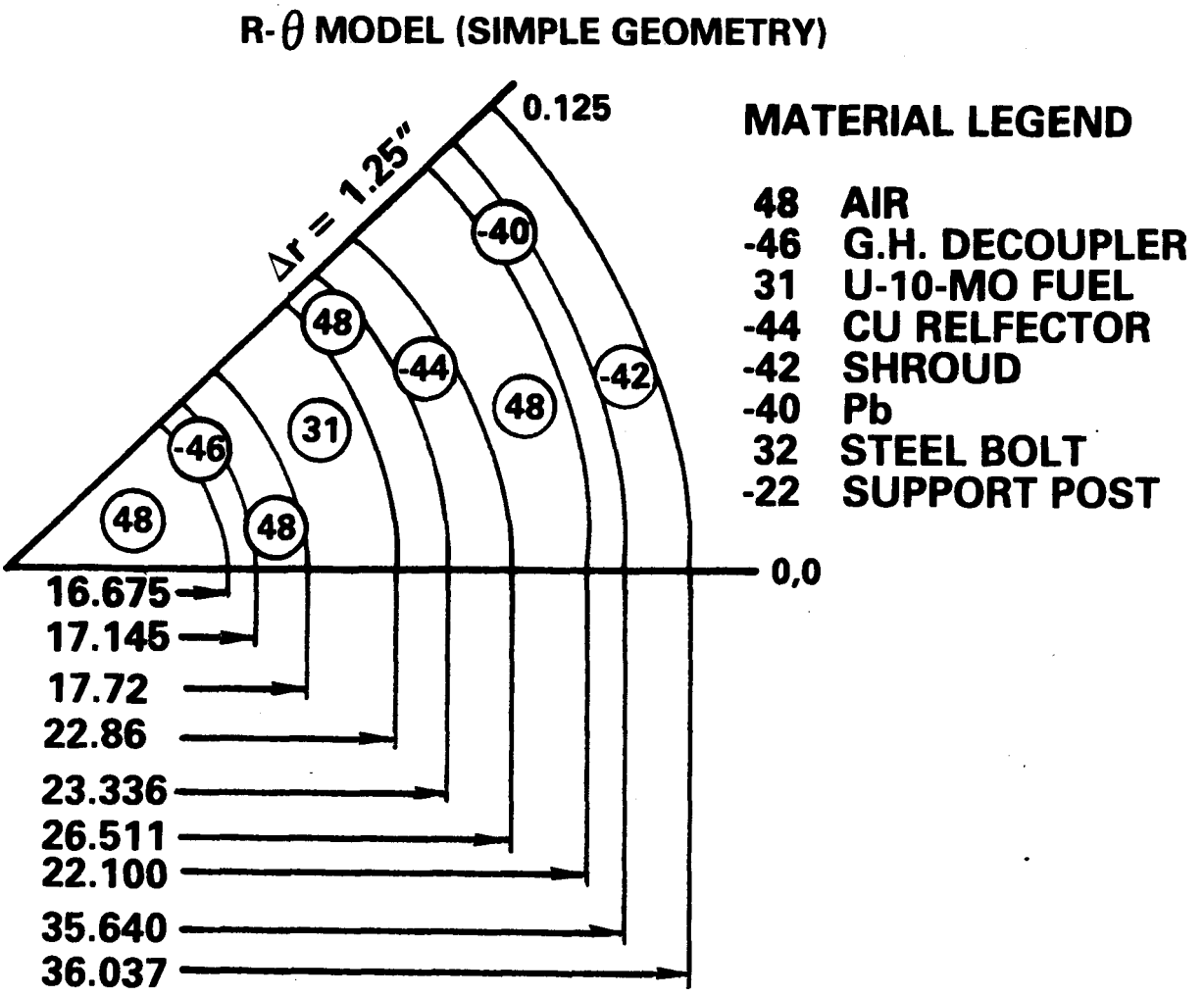

Figure 3.2-3A
Simple R-θ Model Of The SPR-IV Reactor

θ UNITS ARE FRACTIONS OF A REVOLUTION
(360° = 1.0)

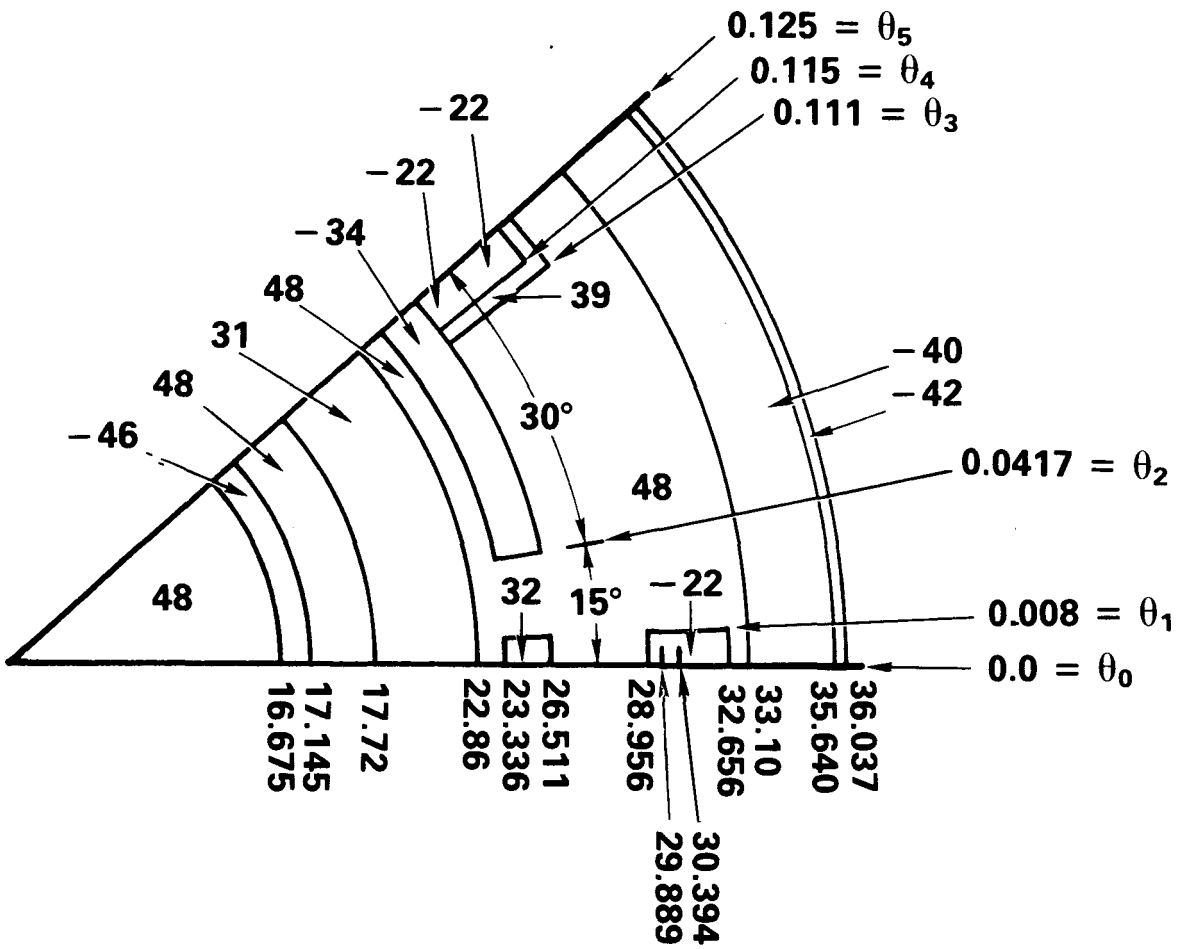

Figure 3.2-3B
Discrete R-θ Model Of The SPR-IV Reactor

homogeneous mixture of the reflectors and the clamping bolts. This is done because the bolts lie within the inner and outer cylindrical boundaries defined by the radial reflector surfaces. This geometry was used to determine the correct buckling height for the core and to serve as a basis for comparison of different reflector materials and shapes.

Figure 3.2-3B shows the discrete (non-continuous) radial reflector. The posts supporting the upper core half are shown here but in reality they only extend vertically to about the core midplane. By comparing the two R-θ models for a particular reference case--for example, with just the radial reflectors modeled in both cases--and by varying the volume fraction of the radial reflector in the simple model until k_{eff} agrees with the k_{eff} from the discrete model, an empirical volume fraction was derived for the simplified R-θ model. This type of analysis is illustrated in Figure 3.2-4. This new volume fraction, which may differ from the geometric volume fraction of the radial reflectors, 0.667, may then be used in the R-Z models as an approximation for the detail that cannot be explicitly modeled in the R-Z geometry. Thus, one can derive a transport corrected volume fraction for the radial reflectors in the homogenized R-Z model. This method can be extended to account indirectly for items like the support posts also. In the R-Z model the use of the empirically derived radial reflector volume fractions of 0.68 and 0.721 (see Figure 3.2-4) increased the reactivity of the system by 12¢ and 49¢, respectively, when the radial reflectors were modeled at their delayed critical position, four inches below the midplane. One could infer the difference between these worths, 37¢, to approximate a partial worth of the reflector guides and the upper core support posts.* This partial worth is consistent with other calculated values and with past experience, 63¢ = total worth of support posts and reflector guides.

---

*It is only a partial worth because the reflectors (whose empirical volume fraction includes an approximation for the support post and reflecter guides) in the R-Z model were only inserted to four inches below the midplane (dc position).

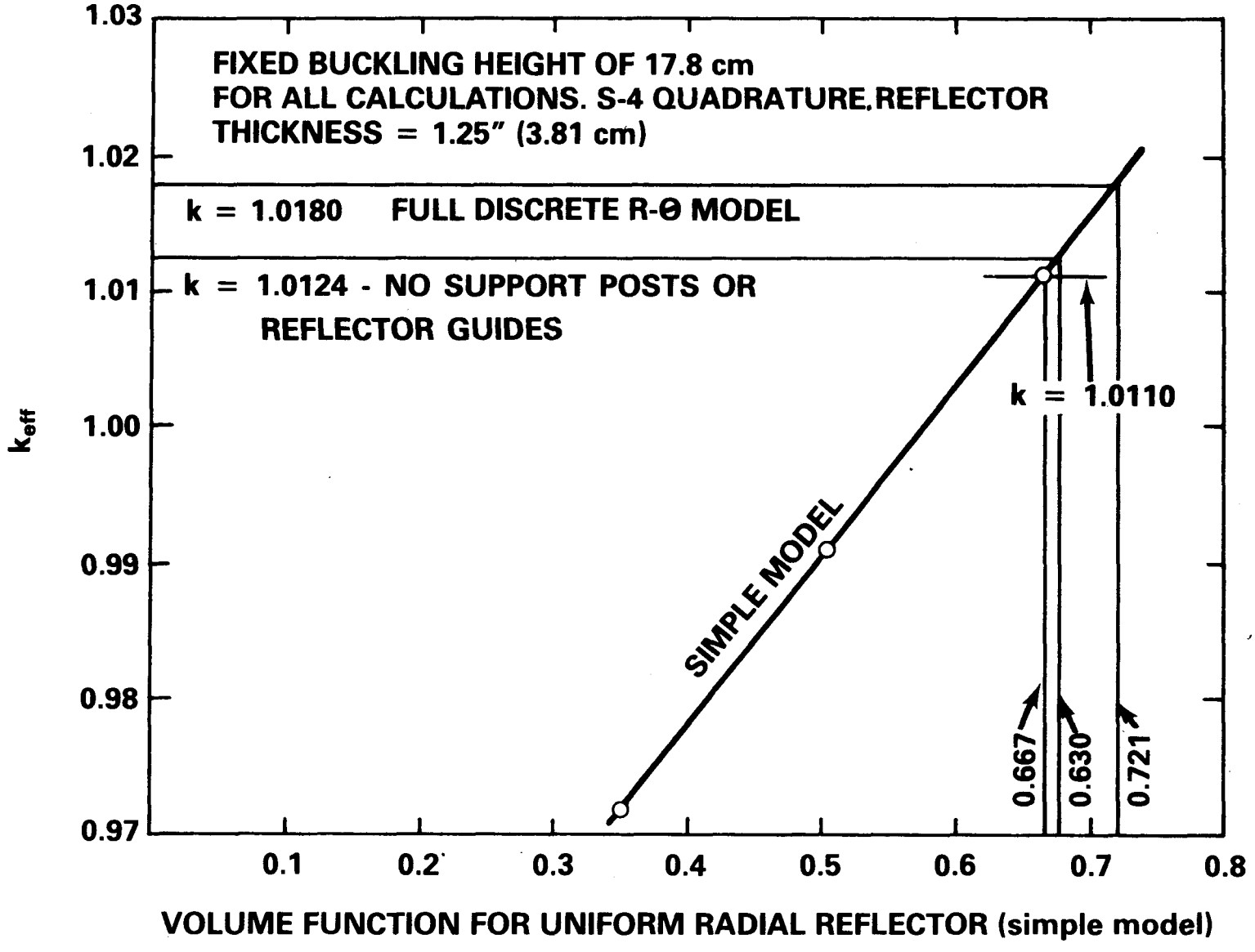

Figure 3.2-4
Evaluation of the Reflector Zone Homogenization Approximation

3.3 Calculational Results

The results can be divided into three categories of interest: criticality, performance, and component reactivity worths. The designer's most important task is to provide precise estimates on the critical dimensions of the fuel assembly since the core is difficult and costly to modify once it is fabricated. The more detailed bare core model was used to determine the final core dimensions. The S-16 TWOTRAN-II and KENO-IV results agreed within statistical uncertainty, $\pm$ 0.003.

The fission density and the flux profiles in the core as well as the majority of the reactivity worth calculations for components of the reactor were derived from numerous coarse-model R-Z runs and some discrete R-θ models--generally using S-8 or S-4 quadrature with TWOTRAN-II. KENO-IV was used to confirm some of the reactivity worth calculations and also to estimate the dimensions and reactivity worth of the storage pit. The average prompt-neutron generation time was calculated in KENO-IV as a by-product of the Monte Carlo tracking method.

3.3.1 Criticality

The purpose of the criticality calculations was to derive the design dimensions of the bare fuel assembly. A preliminary eigenvalue (or self-multiplication factor) for the bare core was estimated from the coarse R-Z model after the global system calculations had been made. Then final values were obtained from the more detailed bare core model using the same inside and outside diameter but a slightly taller assembly height to allow for the coolant gaps of 0.635 mm between the fuel plates.

The methods and data sets used in this design parallel those used by T. R. Schmidt in the design of SPR-III [3-5]. Benchmark evaluations of the data and calculational methods have been cited in that reference. For SPR-III the critical experiment resulted in approximately \$1.49 of excess reactivity compared to the simplified calculational model assuming the originally planned delayed critical positions of the control elements. The difference is partly attributable to extra reactivity from cooling tubes and other small parts that were not explicitly modeled. The reflectors were reduced in size to match the reactivity worths to

operational objectives. No fuel modifications were required.

The critical dimensions of the SPR-IV bare core are derived in Figure 3.3.1-1 by two different methods and for both S-8 and S-16 quadrature. Using the S-16 results and the integral (or global) reactivity method, the critical dimensions are: 13.95 inches (ID) and 18.0 inches (OD). The KENO-IV and S-16 TWOTRAN-II results for the bare core are in good agreement; the KENO-IV reactivity is more positive by only about $0.40. The final version of the complete reactor was only modeled for the TWOTRAN-II code, although earlier versions had been modeled for both codes with similar good agreement.

The relationship between the inside and outside critical diameters is a simple linear function as shown in Figure 3.3.1-2. The slope (ratio between a change in the inside and a change in the outside diameter) of the function is approximately 0.99.

3.3.2 Neutron Fluence Distribution

One of the major design criteria for SPR-IV was to provide a relatively flat flux profile within the exposure cavity of the reactor. Specifically the criteria for the peak-to-average flux in either the R-direction or the Z-direction is: $P/A \leq 1.15$. Since the bare reactor has a larger cavity diameter than previous models in the SPR series, it also tends to have a high leakage flux and the flux is skewed toward the lower half because the radial reflectors are positioned below the core midplane for most operations. To balance the axial flux better and also to reduce the reactivity worth of large experiments placed in the central cavity, axial reflectors for the cavity have been incorporated into the SPR-IV design.

Both the top and bottom reflectors are copper. The top reflector is 4.45 cm (1.75 in) thick and the bottom reflector is 2.54 cm (1.00 in) thick. The upper reflector is located inside the experiment tube. It is positioned vertically by a small cylindrical ledge that is at the same elevation as the interface between the fuel and the top fuel support ring. The bottom reflector is outside the experiment tube. Its top is slightly below the bottom of the lower fuel support ring. Additional fixed reflectors above and outside the fuel (the latter

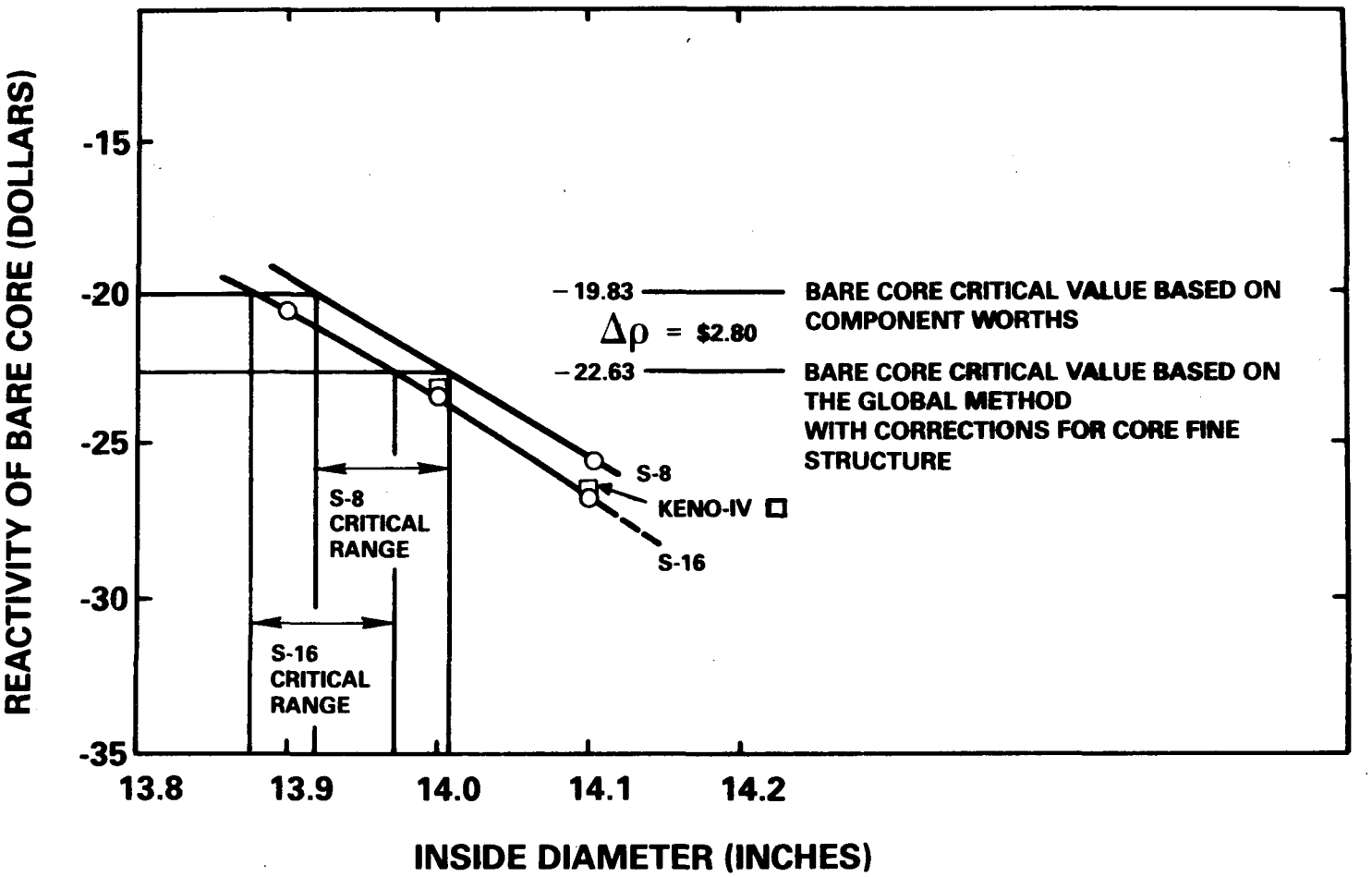

Figure 3.3.1-1
S-16 and S-8 Bare Core Critical Diameter Evaluation

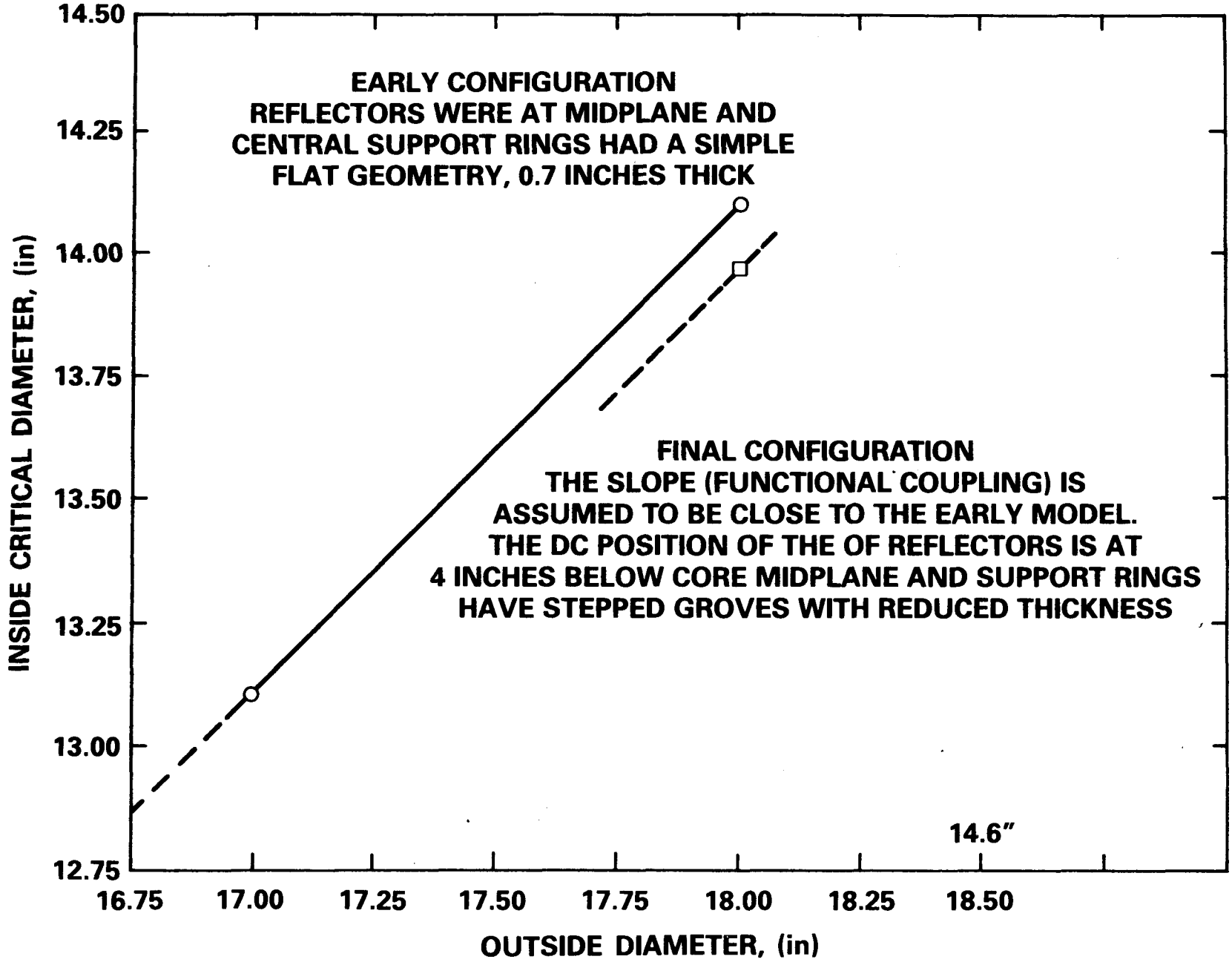

Figure 3.3.1-2
Relationship Between the Inside and Outside Critical Diameters for SPR-IV at at Fixed Height of 50.8 cm

are referred to as skirts or auxiliary radial reflectors) on the top half help to flatten the flux and make it more symmetric with respect to the axial midplane.

Figure 3.3.2-1 shows the improvement in axial flux symmetry that results from the addition of the fixed reflectors above and outside the fuel. The axial reflectors in the cavity are present in all three cases. The variations near the center and ends in these profiles are primarily the result of the steel support rings that bound the fuel in each core half.

A three-dimensional flux plot is given in Figure 3.3.2-2. This plot extends through the fuel and radial reflectors. The cavity is on the right side of the figure. The flux shape in the cavity region is smooth and uniform and resembles the seat-portion of a saddle. The peak-to-minimum ratios for the R-direction and the Z-direction are 1.07 and 1.25, respectively. The peak-to-average ratios are: $(P/A)_R = 1.02$ and $(P/A)_Z = 1.09$, both of which are within the design criteria of 1.15.

The relation between the centerline fluence in the cavity and the axial fluence at the peak radial location in the fuel is shown in Figure 3.3.2-3. The maximum fluence in the fuel is a factor of 1.43 larger than the peak fluence along the cavity centerline.

The peak centerline cavity fluence for a peak temperature increase in the core is shown in Figure 3.3.2-4. At 400°C ΔT maximum fuel temperature increase, the peak centerline cavity fluence is approximately 5.6×10^{14} nvt.

3.3.3 Fission Density Distribution

The fission density in the core is similar to the fluence distribution because the neutron spectrum and average fission cross-section are relatively constant throughout the core. Radial profiles of the fission density are shown in Figure 3.3.3-1 at axial peaks for the bottom and top core halves. The radial reflectors were positioned at their delayed critical elevation (10.2 cm or four inches below the core midplane).

Four axial fission density distributions are shown in Figure 3.3.3-2. The four curves illustrate the positive effect of adding fixed radial skirts and additional

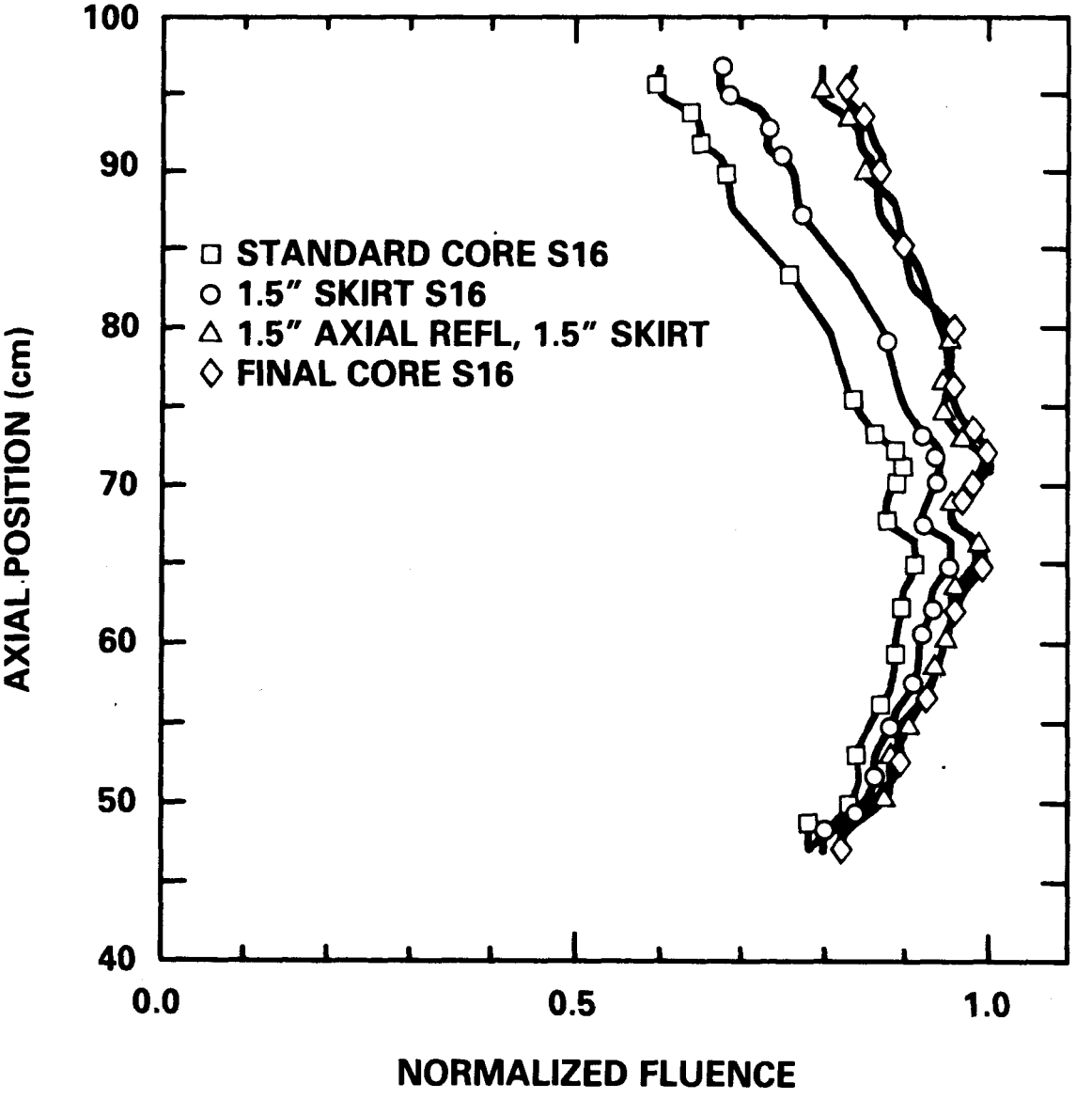

Figure 3.3.2-1

SPR-IV Axial Fluence Profile - Core Centerline

SPR–4 FLUX SHAPE

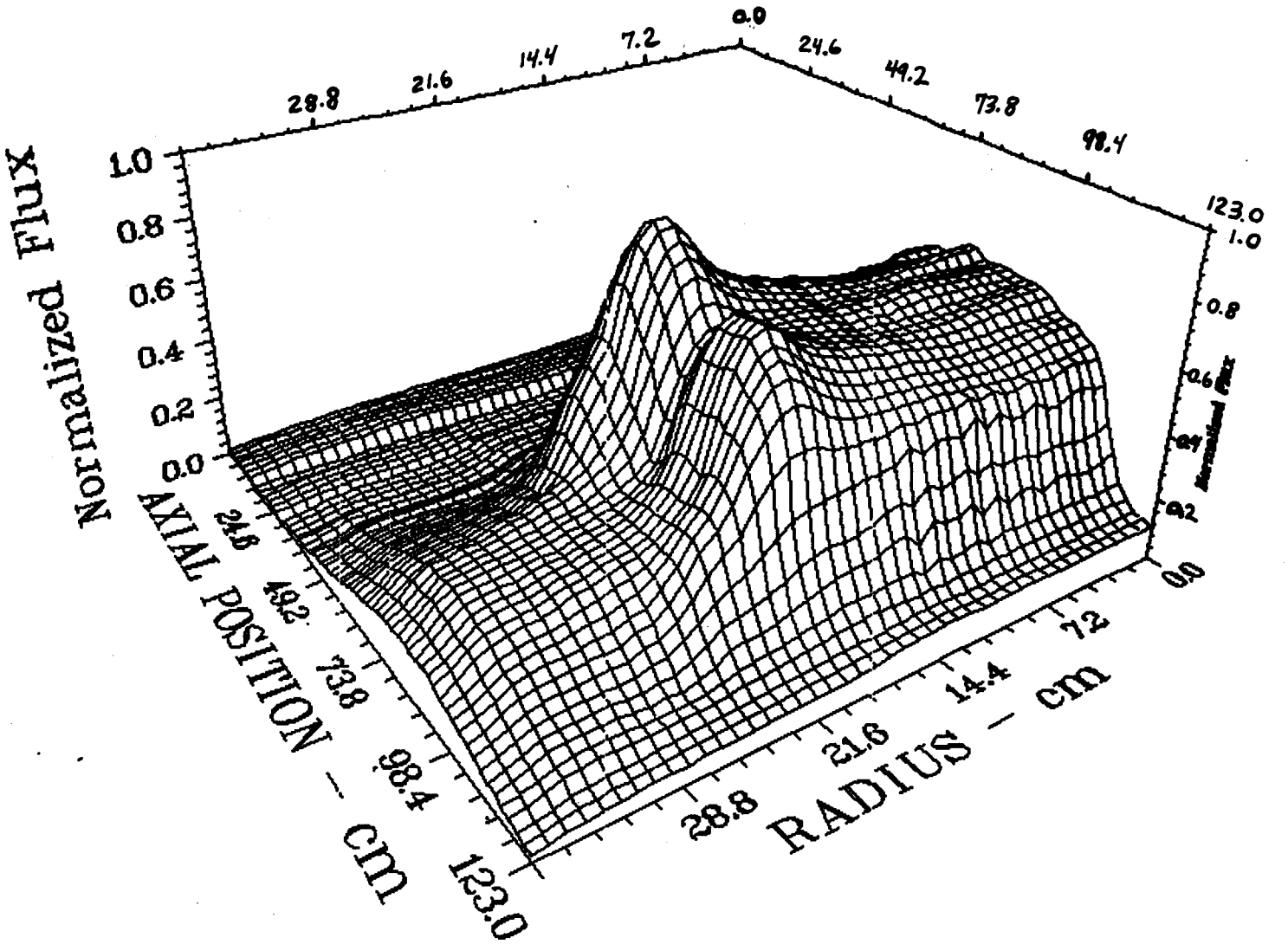

Figure 3.3.2-2

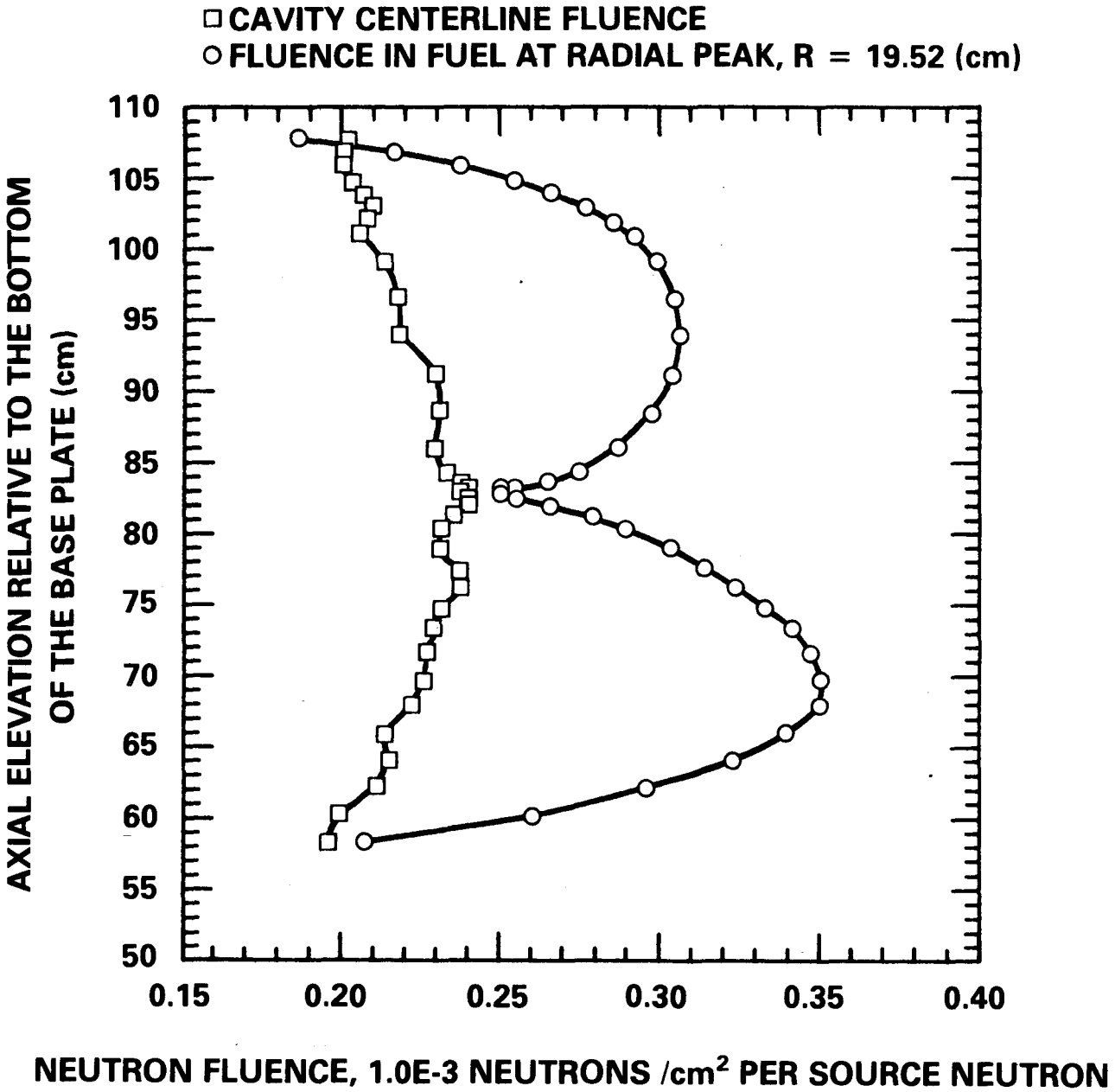

Figure 3.3.2-3

Axial Fluence Profiles for Cavity and Fuel

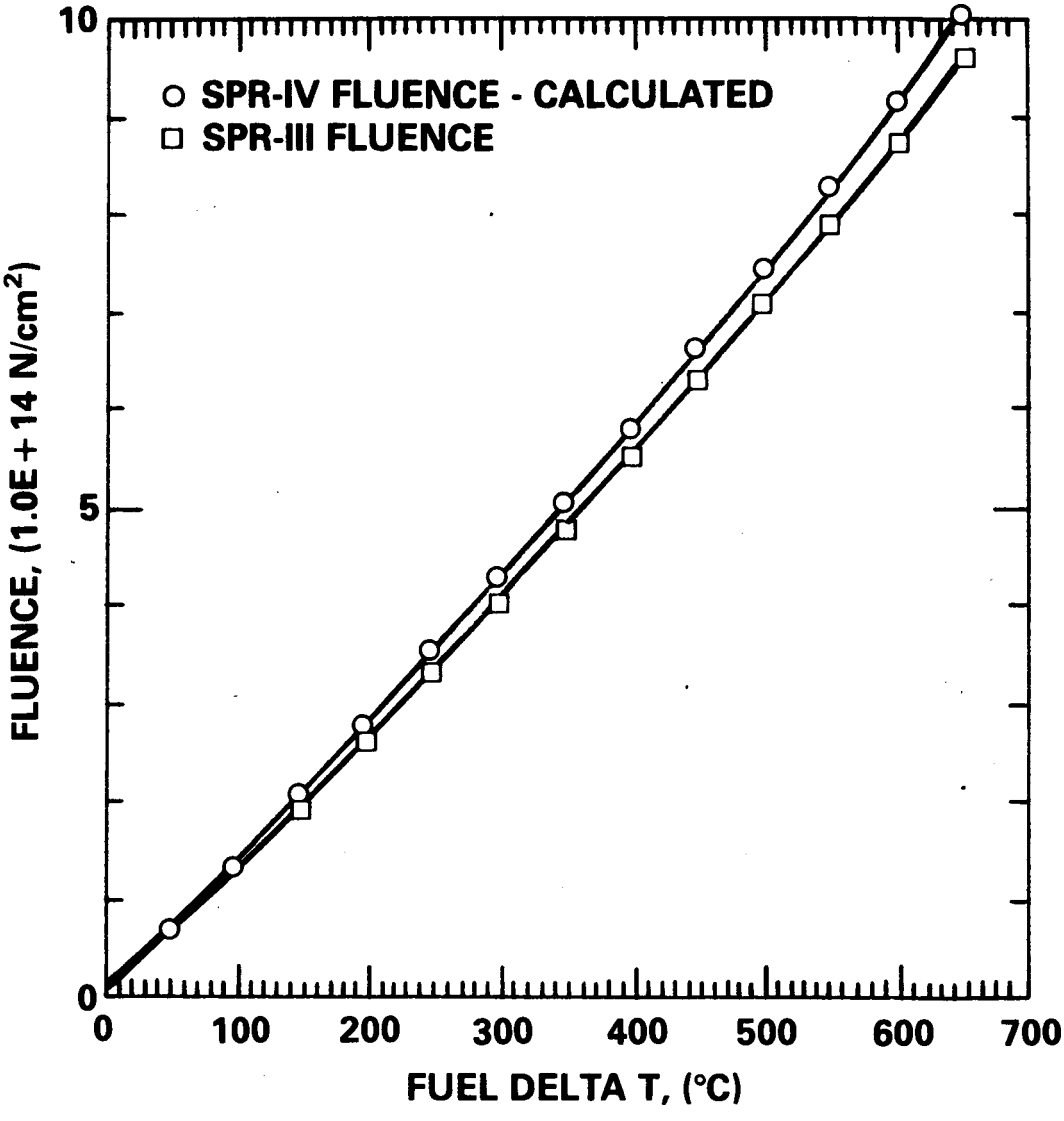

Figure 3.3.2-4

Peak Centerline Fluence in Cavity vs Peak Temperature Increase in Fuel

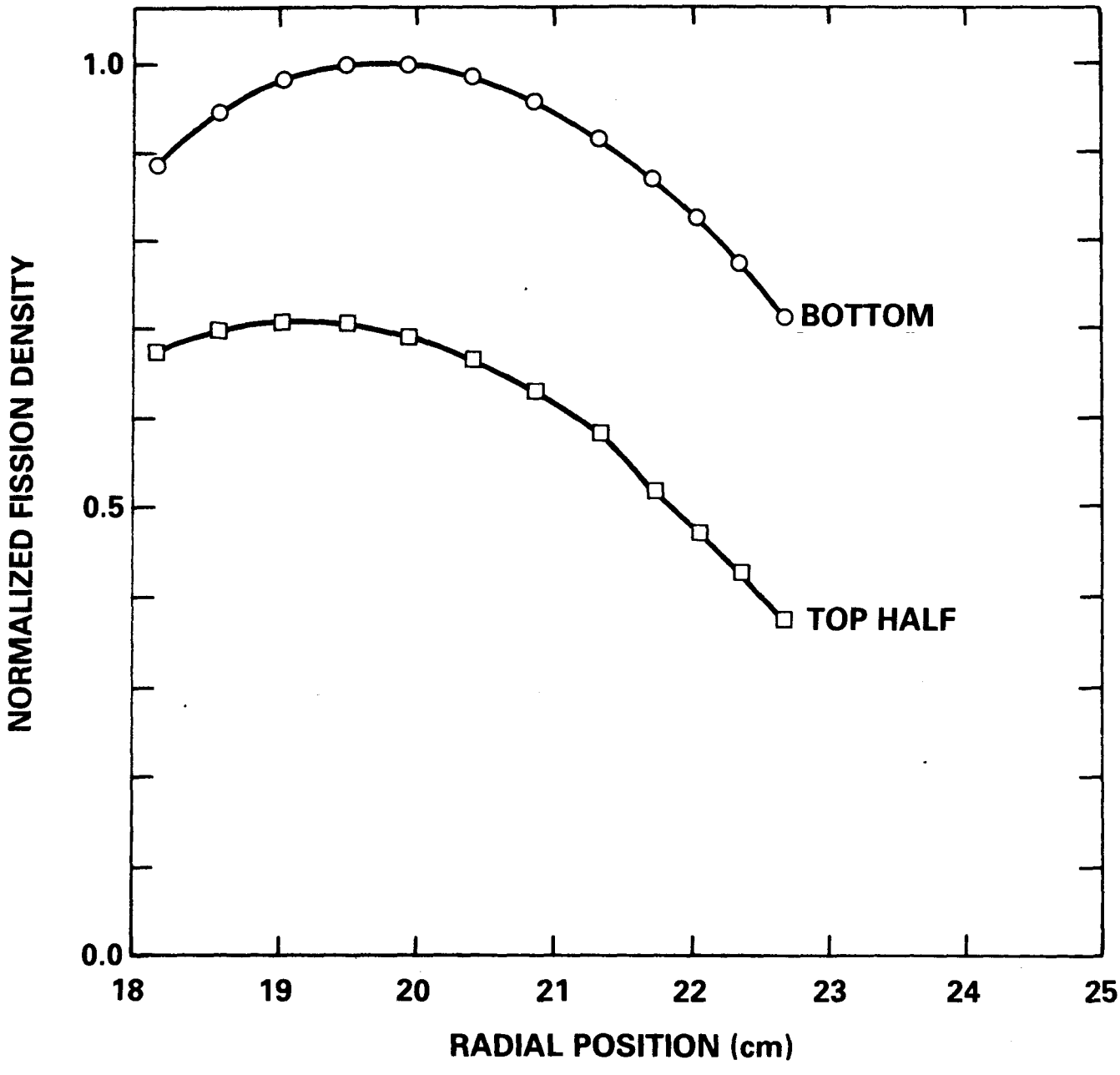

Figure 3.3.3-1

SPR-IV Radial Fission Density Plots

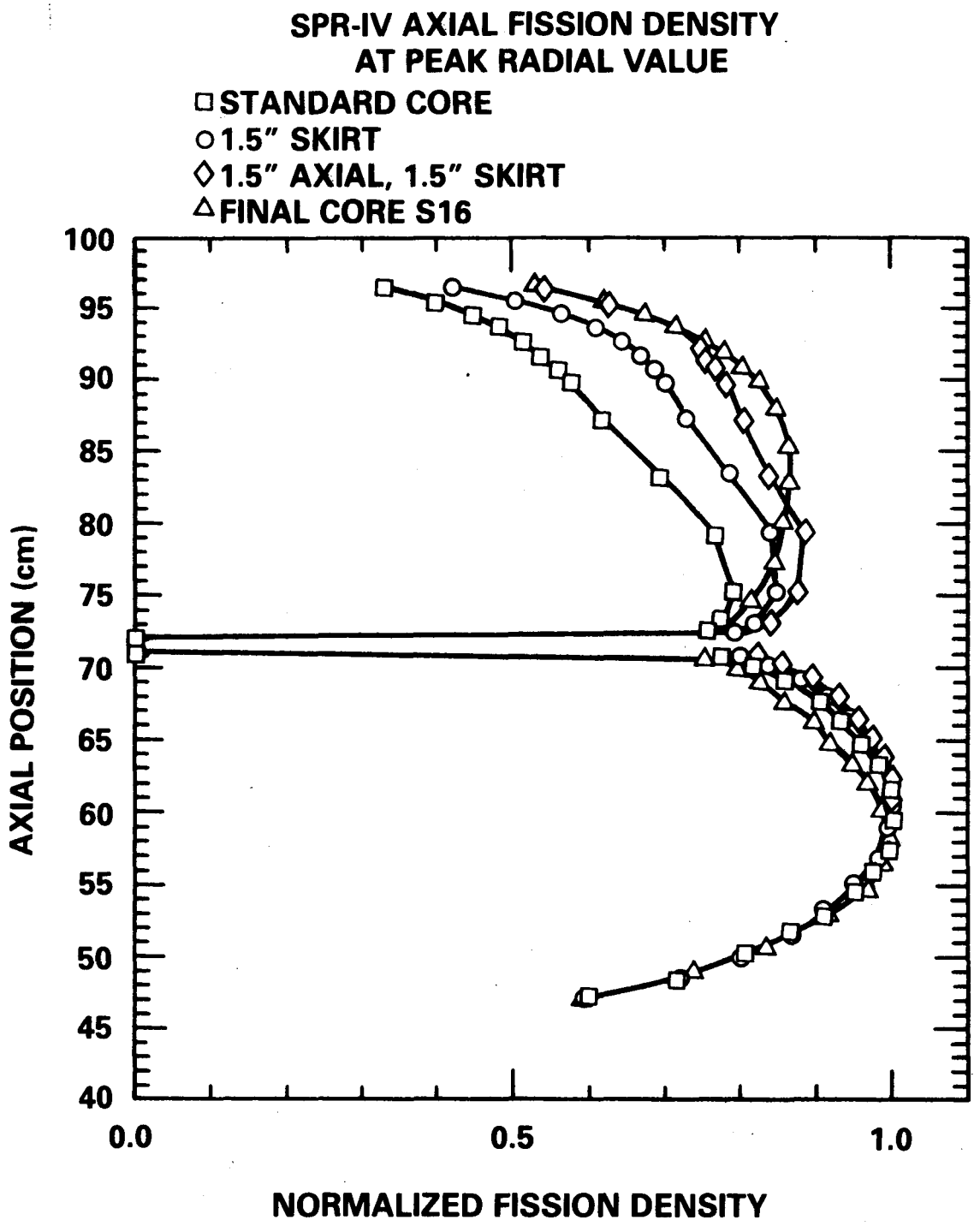

Figure 3.3.3-2

SPR-IV Axial Fission Density at Peak Radial Value

axial reflectors near the top of the core. These pieces offset the skewing influence of the movable radial reflectors which are positioned adjacent to the safety block (lower core half).

3.3.4 Neutron Spectrum

The group fluxes in the Hansen-Roach 16-group energy structure are shown in Figure 3.3.4-1 for SPR-IV and SPR-II. The normalized integral neutron spectrum is shown in Figure 3.3.4-2. The SPR-IV spectrum is similar but slightly softer than SPR-II (and SPR-III). There are virtually no neutrons at energy levels lower than E_n = 1 keV. For all practical purposes one could say that all but a small fraction of a percent are fast neutrons (E_n > 10 keV) in the absence of moderating materials. Spectral variations are rather small throughout the reactor. Schmidt [3-5] showed that the bare leakage spectrum from a fast pulse reactor is typically harder than the cavity spectrum because of the preferential leakage of high energy neutrons. The control elements adjacent to the fuel do soften the leakage spectrum slightly, but the Boron-10 loaded shroud absorbs the lower energy neutrons more efficiently, thus partially offsetting this effect. Polyethylene or other strong neutron moderators, however, can alter the spectrum considerably. Examples of the degree of spectral shift from this type of moderator has been reported previously by Bonzon and Philbin [3-6].

3.3.5 Reactivity Worth of Reactor Components

The reactivity worth of the reactor components was determined using both the simplified (coarse structure) R-Z and discrete R-θ models. The reactivity worths, dimensions of various components, and interaction between components are all evaluated simultaneously in the design process. The design process is an iterative process whereby changes are made and subsequently evaluated until design objectives are achieved.

The R-Z model was used, for example, to evaluate the reactivity worth of the control element bank as a function of the control element thickness, material type, stroke, and separation gap from the fuel. As another example, it was used to evaluate the reactivity worth of the safety block as a function of separation distance for different support plate thicknesses.

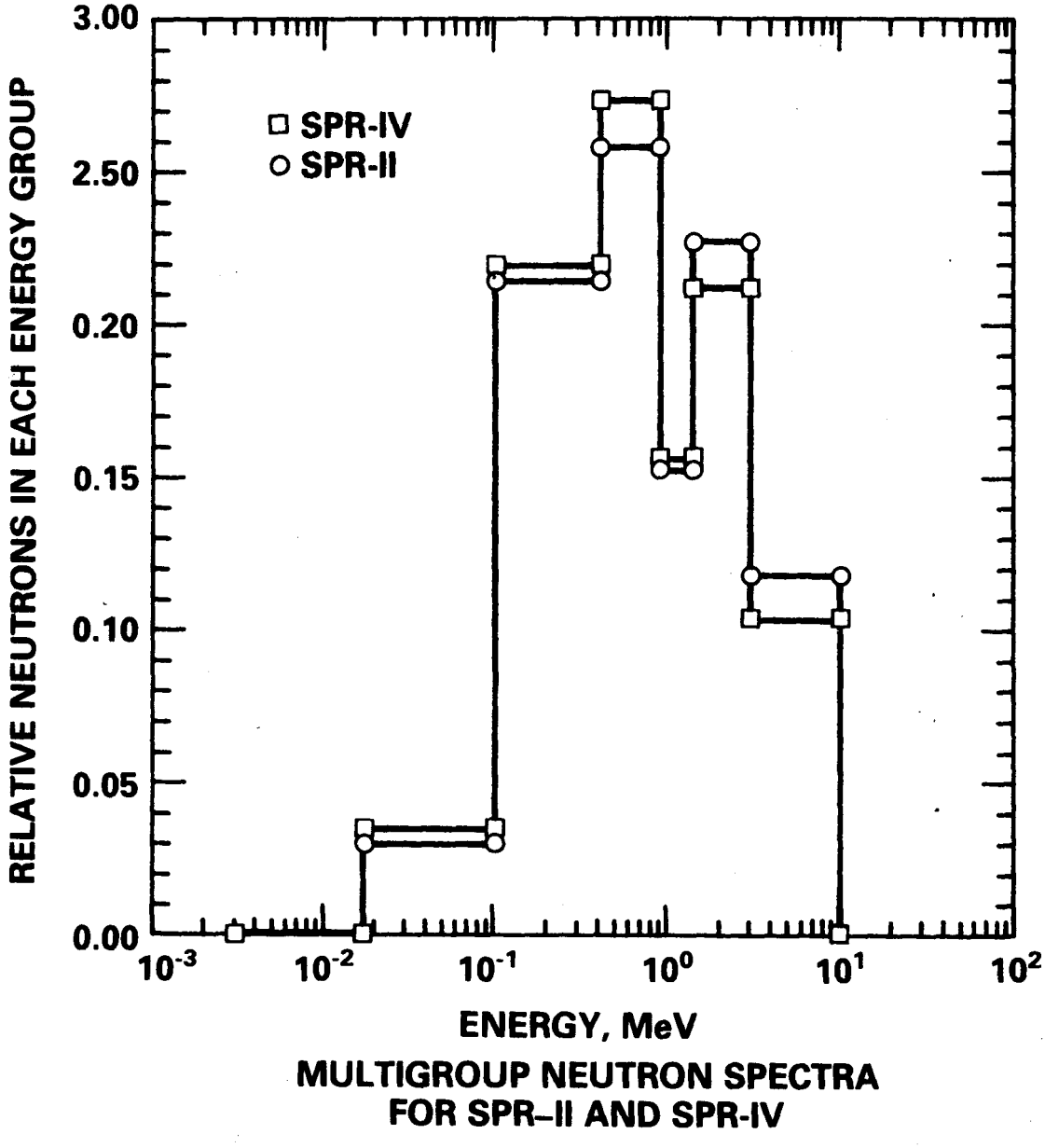

Figure 3.3.4-1

Multigroup Neutron Spectra for SPR-II and SPR-IV

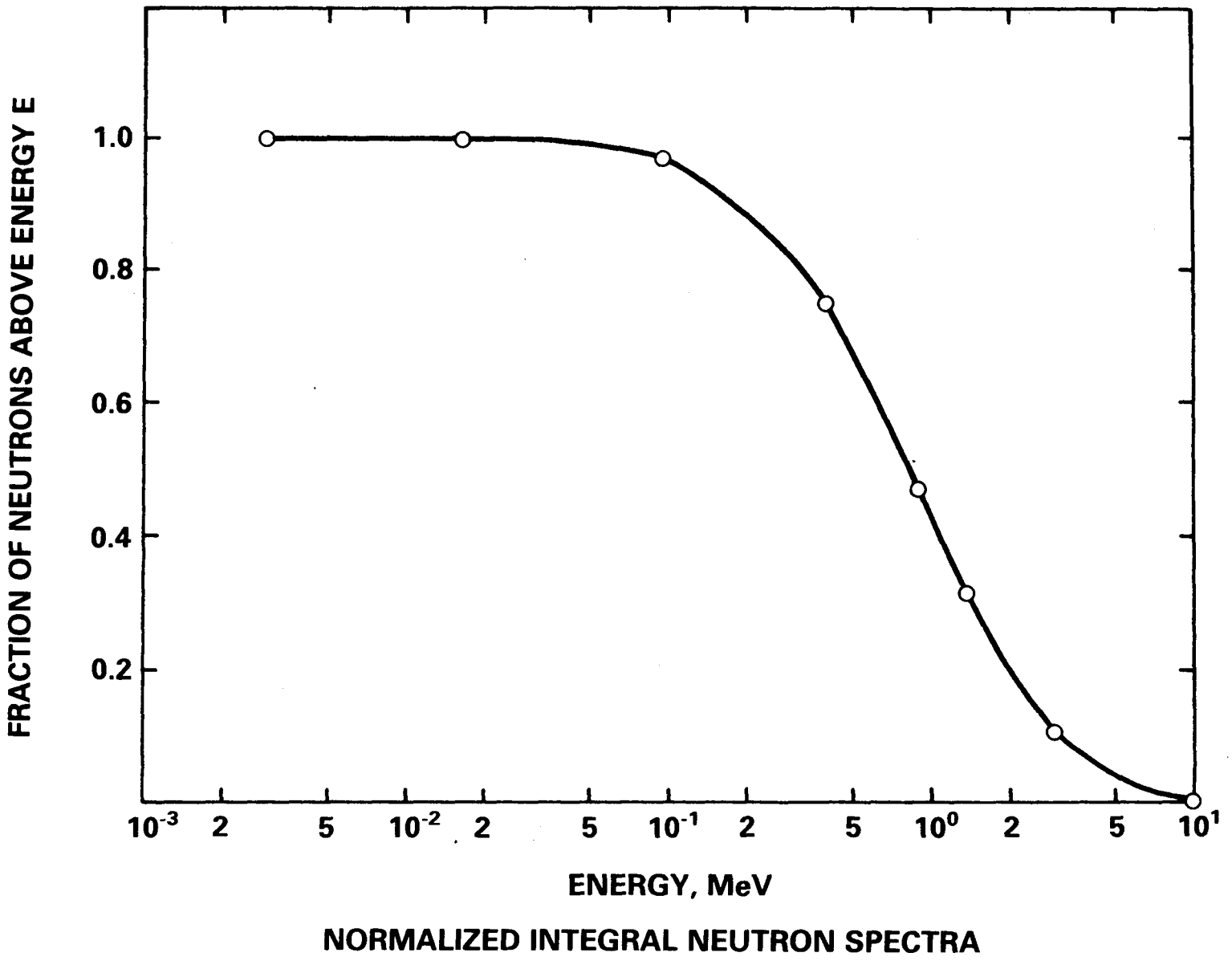

Figure 3.3.4-2
Normalized Integral Neutron Spectra

This model was also used to evaluate global reactivity effects that could be expected from uniform low fuel density or gaps purposely introduced for cooling channels. And finally, it was used to evaluate the reactivity worth of various components (the shroud, lead shield, cavity thimble, etc.) by comparing configurations (or models) with these components and without them.

The R-θ model was used to evaluate the reactivity worth and related influences of the upper core support posts, the core clamping bolts, and the reflector guides.

The derived reactivity response to changes in a variety of key design parameters is given in Table 3.3.5-1. These quantities were derived using reference dimensions for either a 43.2 cm (17 in) OD or 45.7 cm (18 in) OD core. The reference gap between the reflector and the fuel, for example, was 0.20 cm (0.08 in) which was taken from the SPR-III core design. Likewise, the radial reflector zone was simplified to a homogenized cylindrical annulus with uniform volume fractions of 0.667 for the copper reflectors, 0.056 of steel for the core clamping bolts, and void for the remainder. The negative reactivity afforded by full safety block separation (4 in or 8 in) is shown as a function of flat support rings (no steps) in Figure 3.3.5-1. One can see from this figure how additional shutdown can be achieved by making part of the support ring thinner. This was done in the final design. Many of the reference dimensions were refined as the design progressed. For example, the final radial reflector volume fraction is quadrant-dependent and additional axial reflectors and fixed skirts have been added. However, the sensitivities derived from the reference dimensions are useful guidelines and may be valuable in making future adjustments or modifications.

The reactivity balance for SPR-IV using the final configuration for the components and gaps is presented in Table 3.3.5-2. A 0.48 cm (3/16 in) gap was modeled between the fuel and the reflectors. The gap between the fuel plates (for cooling gas) was 0.064 cm (25 mils). Separate calculations using graphite in the radial reflector zone were made to design the stroke, 31.8 cm (12.5 in), and angular arc, 33.5°, of the burst element for a total reactivity worth of $1.20. Corrections have also been made to account for a smaller control element in the second quadrant. The total worth of the No. 2 element will be reduced to $2.00 by reducing the angular

Table 3.3.5-1

Derived Reactivity Responses

Description	17 Inch Core	18 Inch Core
Radial Reflector Worth $d\rho/dr$ (Δr = 0.5" to 1.5")		
Reflector at midplane elevation (gap = 0.08")	\$6.83/in*	\$6.97/in
Reflector full up (gap = 0.08")	\$8.44/in	
Reflector at midplane (gap = 0.5")	\$5.20/in	
Fuel-Reflector Air-Gap Worth, Radial Reflector (1") to Mid-Plane (0.0 to 0.5" gap)	\$5.18/in	
Fuel-Reflector Air-Gap Worth, Radial Reflector (1") Full In (0.0 to 0.5" gap)		\$5.84/in
Top Axial Reflector (1" to 1.5" thickness)	\$1.14/in	\$1.36/in
Reflector Solid Angle (Near 60° each)		\$0.58/degree
Fuel Density Effects	\$1.092/% Fuel Density	
Central Support Plates (Based on initial 100 mils of fuel replaced by steel)	-\$16.3/in	

*T. Schmidt's calculations for SPR-III give \$6.63/in.

Table 3.3.5-1 (Continued)

Description	17 Inch Core	18 Inch Core
Increased Fuel on Outside Diameter (Based on 1st 1/4")		+$9.54 per 1/4"
Increased Fuel on Inside Diameter (Based on 0.2" and normalized to 0.25" -- fine detail model)		+$7.73 per 1/4"
Safety Block Withdrawn 4" (0.7" support plates)		-$6.78**
Safety Block Initial Air-Gap (0.7" flat support plates)	0.35¢/mil†	

** The stepped support plate allows for closer fuel contact and larger safety block worth than shown here.

† For comparison SPR-II was 1.3¢/mil and SPR-III was 0.75¢/mil (pp. 85, SAND75-0657).

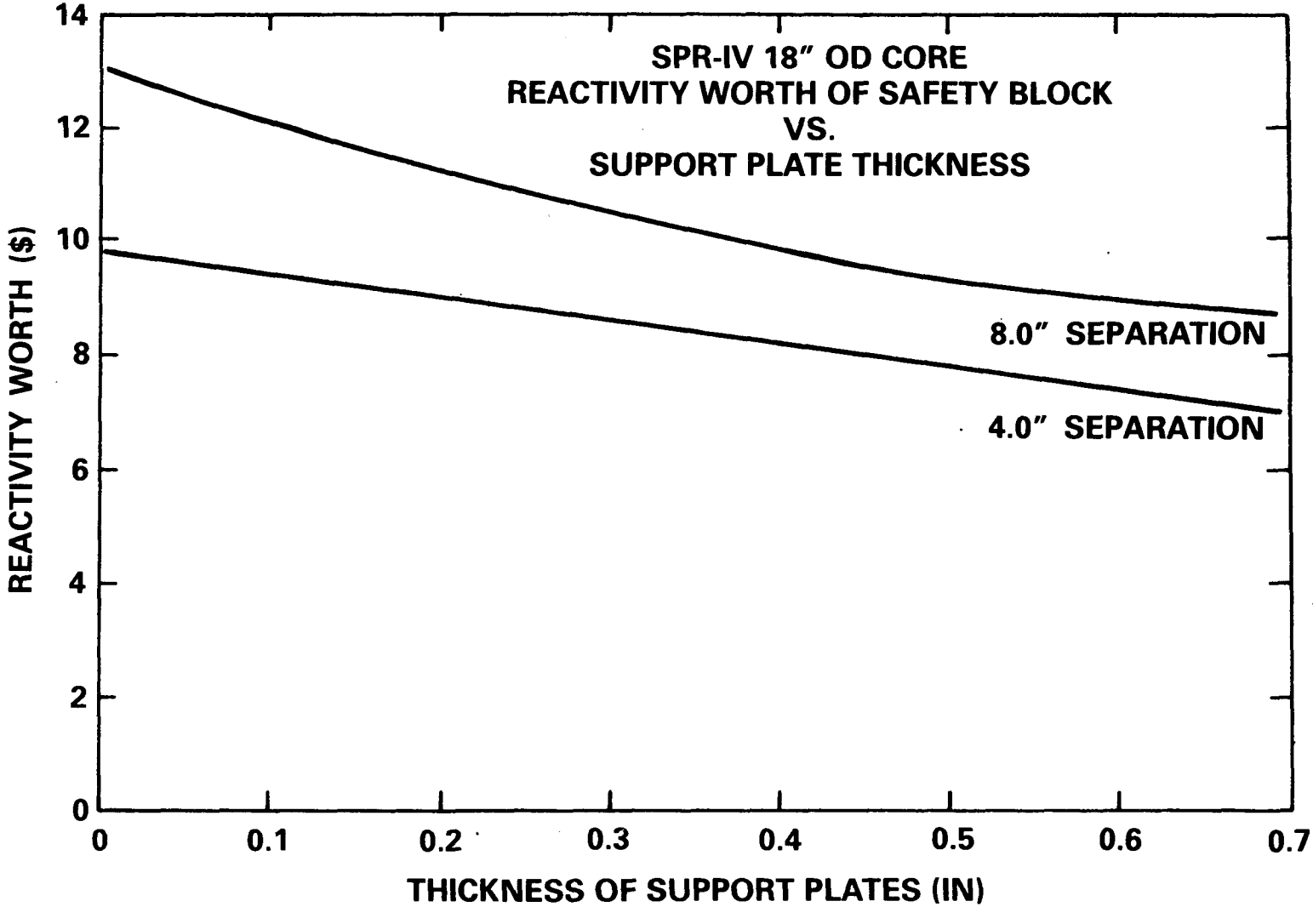

Figure 3.3.5-1
SPR-IV 18" OD Core, Reactivity Worth of Safety Block vs Support Plate Thickness

Table 3.3.5-2

Reactivity Balance for SPR-IV in the Delayed Critical Configuration

Reactivity of Bare Core (14.0" ID, 18.0" OD, 20.44 Height, S-16 TWOTRAN)[1]	-23.71
Experiment Tube	0.19
B-10 Loaded Thimble	0.22
Aluminum Table	0.18
Safety Block Support Post	0.12
Control and Burst Elements in Their Down Positions	0.24
Burst Element (33.5°) in its Shimmed (operational) Down Position[2]	0.70
Control Elements 1 and 3 (60°) at the DC Position[3]	2.42
Control Element 2 (30.6°) at the DC Position[4]	0.61
Upper Core Support Posts	0.20
Core Bolts	0.86
Reflector Guide Posts	0.43
Fixed Radial Skirts (3 of 4 Quadrants -- none on burst side)	0.91
Axial Reflectors in the Cavity ΔT - 1.75" Top ($3.26); ΔT = 1.0" Bottom ($2.51)	5.77
Top Axial Reflector Over the Fuel (1" thick)	0.75
Pb Shield and B-10 Decoupler on Outside of Shield	6.41
Miscellaneous	0.30
Difference Between This Method and the Global Model Method	2.80
	- 1.08

Table 3.3.5-2 (Continued)

Footnotes:

[1]Gaps are worth $3.10 (derived by filling in the gaps in the detailed model with fuel). Plate mass is 31^{+} kg for a typical B plate. There are 9 plates per core half.

[2]2.5 inches below core midplane. $\Delta\rho$ of the burst element over its 12.5 inch stroke is $1.20.

[3]$\Delta\rho$ of 1 and 3 from dc to full up is an additional $5.42.

[4]$\Delta\rho$ of 2 from dc to full up is $1.39. Total control element 2 worth = $2.00.

arc to ~30.6°. Control elements 1 and 3 are worth $3.92 each from full down to full up. The angular arc for control elements 1 and 3 is equal to 60° each. This arc is consistent with the homogeneous volume fraction of 0.667* used in the R-Z model for the copper in the radial reflector zone.

In the reactivity balance method the self-multiplication factor for the bare core was calculated with S-16 quadrature. The reactivity worth of the various components was derived by comparing the standard configuration (simplified model, S-8 quadrature) to another calculation where the component of interest was replaced with air. The reactivity worth of each component may be underestimated when eliminated individually from separate calculations. Synergistic effects will tend to increase the worth of some larger components by as much as 10 to 15 percent. Therefore, a $2.80 deficiency for $23.71 worth of components may be very close to the real error for this method.

An alternative method for evaluating the total system reactivity is the global method. In this method the bare core from the simplified model is normalized by means of a fuel density reduction factor to the fine structure bare core model. S-16 quadrature is used for both calculations. The density reduction factor accounts for gaps and other fine structure modeling that cannot be duplicated in the simple model. Then the complete system is recalculated (S-16) using the previously derived density reduction factor for the core fuel. Negative corrections can be made for the burst element, control element No. 2, and the fixed radial skirt that will not be used on the burst element side. Positive corrections can be made for the reflector guides and upper core support posts which were not modeled in the R-Z model.

The system reactivity analysis using the second method is presented in Table 3.3.5-3. One can see that this method predicts that the system is 1.08¢ below critical in the reference dc position, i.e., with the control elements at 10.2 cm (4 in) below the midplane. The discrepancy between the global (preferred) and

---

*Or 0.680 can be used as a bias factor to correct for homogenization.

Table 3.3.5-3

Reactivity Analysis of SPR-IV Preliminary Model
Using the Global Method

Density Reduction Factor for Fuel	0.9759*
Reactivity of the Density-corrected Simple R-Z Model (S-16)	$-0.32
k_{eff} = 0.9979 Fuel ID = 35.6 cm (14 in) Fuel OD = 45.7 cm (18 in) Assembled Fuel Height = 51.9 cm (20.4 in)	
Other Corrections:	
Reduced Worth of Burst Element (in down position)	-0.51
Reduced Worth of Control Element No. 2 (in dc position)	-0.58
Removal of Fixed Radial Skirt From Burst Element Quadrant	-0.30
Add Reactivity of Control Element Guides**	+0.43
Add Reactivity of Upper Core Support Posts**	+0.20
Corrected Total Reactivity (Global Method)	-1.08

*The geometric density factor or smear density factor is 0.9799.

**Worth of these components was derived from R-θ calculations.

component methods for the final reactivity of the complete reactor was $2.80. Since both methods predicted negative values, a final reactivity adjustment was made so the reactor would have a slightly positive reactivity based on the global method. This was done by reducing the inside fuel diameter from 35.6 cm (14.0 in) to 35.4 cm (13.95 in), thereby adding approximately $1.50. See Table 3.3.5-1. This raised the net reactivity from -$1.08 to about $0.40 above delayed critical (dc). Small parts like the cooling plena, not explicitly modeled, may add some additional reactivity, < $0.30. Final adjustments in the range of $1 can easily be made by adding or subtracting mass from the control elements or by modifying the reference dc position. These adjustments would obviate the need for any fuel modifications.

The overall dimensions of the fuel assembly, excluding the external but not the internal clamping rings, are 35.4 cm ID by 45.7 cm OD by 51.9 cm high (or 13.95 in ID by 18.0 in OD by 20.44 in high). For additional discussion on the selection of the critical fuel dimensions, see Section 3.4 at the end of this chapter.

The shutdown reactivity for the free field condition is about -$13.73 of which -$3.03 is the control margin of the control elements. A review of the reactivity margins available is shown in Table 3.3.5-4.

3.3.6 Reactivity Worth of Experiments

A variety of experiment geometries were calculated during the design evolution. Some of the experiments were evaluated both with and without axial reflectors. Results of these calculations are shown in Table 3.3.6-1. The benefit of the axial reflectors in the cavity is dramatic for all cases tested. The reactivity worth of the experiments was reduced by $4.00 to $5.00.

A special calculation was done to evaluate SPR-IV inside the SPR-II reactor storage pit. The SPR-IV reactor (in the scrammed configuration) was calculated to be only $1.00 (or less) subcritical. This situation was a factor in the decision to build a new reactor building for the SPR-IV reactor. The new building will have a much larger reactor storage pit.

Table 3.3.5-4

Control Margins for SPR-IV -- Free Field

Shutdown Reactivity Available	Reactivity From DC
Safety Block Up, All Elements Down	-$ 3.03
Safety Block Reactivity (Stepped Support Ring and 4-Inch Stroke)	- 10.70
Total Shutdown	-$13.73

Element	Total Reactivity in Stroke	Excess Reactivity From DC
Control Element 1	$ 3.92	$ 2.71
Control Element 2	2.00	1.39
Control Element 3	3.92	2.71
Burst Element	1.20	1.20
Total	$11.04	$ 8.01 excess

Fuel Plate	Reactivity Worth
Top Plate	$ 1.82
Bottom Plate	$ 2.17

Table 3.3.6-1

SPR-IV Experiment Reactivity Worths

	Without End Reflector	With End Reflectors
Poly (17 cm OD x 20 cm H Cylinder)	-$8.90*	-$ 4.50*
Graphite (17 cm OD x 20 cm H Cylinder)	- 5.61*	- 0.77*
Lead Shield (17 cm OD x 20 cm H Hollow Cylinder With ID 3.2 cm)	- 6.08*	- 1.31*
Steel (6.4 cm OD x 20 cm H)	------	- 0.55*
Poly (6.4 cm OD x 20 cm H)	------	- 0.94*
(6.4 cm OD x 28 cm H)	------	- 0.82
Fuel (U-10 w/o Mo) (6.4 cm OD x 20 cm H)	------	+ 1.23*
Hollow Pu Cylinder (19.7 cm ID x 20.0 cm OD x 19.5 cm H)		+ .95
Hollow Pu Cylinder (as above) Plus External Mock HE Cylinder (OD of Mock HE Cylinder 24 cm)		+ 1.36
SPR-II Reactor Pit Reactivity Worth The pit is 91.4 cm x 91.4 cm wide x 216 cm high; walls are 15.2 cm thick of concrete; sliding door over reactor is 22.9 cm of lead (8") and steel (two plates each 1/2" thick). There are quarter-inch thick sheets of 60 w/o B_4C-loaded silastic on 3 of the 4 walls.		+$10.00 to $11.00

*These calculations were made with early models. There were no fixed auxiliary radial reflectors in these early models. Also axial reflectors--where indicated--were only 2.5 cm (1") thick. Later models increased the top axial reflector to 4.5 cm (1.75"). Significant additional reduction in reactivity worth is not expected from the additional axial reflector thickness.

3.3.7 Performance Summary

The performance of the reactor is similar to the other SPR reactors. The effective neutron lifetime is 22 nanosec (which is 50 percent greater than SPR-III) giving a pulse width at half maximum power of 125 μsec for a 400°C temperature increase in the fuel. The peak fluence in the cavity is 5.6×10^{14} n/cm^2. The energy release for the core is about 30 MJ. Nominal steady state power will be 22 kW providing a flux of 4×10^{11} n/cm^2-sec in the cavity. Higher steady state power and flux may be possible depending on the efficiency of the cooling system. Table 3.3.7-1 gives a summary of SPR-IV performance characteristics.

3.4 Independent Review of the Nuclear Design

An independent design review of SPR-IV was made by General Atomic Co. (GA) using KENO-IV and the MICROX [3-7] cross-sections. A comparison of the results is given in Table 3.4-1. Sandia's KENO-IV calculations agreed favorably with the S-16 TWOTRAN-II bare core results, -$23.31 and -$23.71, respectively, but are higher than the GA KENO-IV results by $2.73. The 16-group Hansen-Roach cross-sections were used for the Sandia results. Traditionally, the Hansen-Roach cross-sections have been sufficient for calculating bare fast reactor critical dimensions.

Despite differences introduced by the independent cross-section data and models, the results indicate that the reactivity of the 35.6 cm (14 in) ID system was probably too low. A correction, based primarily on the global method, was made by reducing the inside diameter of the fuel to 35.4 cm (13.95 in). This increased the reactivity of the system from -$1.08 to about $0.40 (above dc). This correction finalized the dimensions of the bare core.

Table 3.3.7-1

SPR-IV Performance Characteristics

Nominal Pulse	
Temperature Increase	400°C
Effective Neutron Lifetime	22 nsec
Initial Period	35 μsec
Full Width Half Maximum Power	125 μsec
Neutron Fluence	5.6×10^{14} n/cm^2
Peak Neutron Flux	4.5×10^{18} n/cm^2-sec
Gamma Dose	1.3×10^{5} rads (Si)
Peak Gamma Dose Rate	1.0×10^{9} rads (Si)/sec
Peak Power	240,000 Mw
Energy Release	30 MJ
Steady State	
Power	22 kW
Neutron Flux	4×10^{11} n/cm^2-sec
Gamma Dose Rate	1.0×10^{2} rads (Si)/sec
Fuel Temperature	$T_{max} < 300$°C

Table 3.4-1

Benchmark Evaluation of a Preliminary SPR-IV Model with a 35.6 cm (14 in) ID and a 45.7 cm (18 in) OD.

	Reactivity ($)	
	Bare Core	Complete Core
GA KENO-IV MICROX	-26.04*	-3.07**
GA KENO-IV Hansen-Roach Estimate	-24.30*	-1.52
Sandia KENO-IV Hansen-Roach	-23.31	----
Sandia TWOTRAN-II Hansen-Roach (S-16)	-23.71	-1.08
Sandia TWOTRAN-II Hansen-Roach Bare Core (S-16) Plus Component Worths (S-8)	----	-3.88***

---

*Corrected to remove the worth of the experiment tube and the boron-loaded thimble.

**Generalized geometry was used to model the heterogeneous graphite and copper radial reflectors. Corrections were made to approximate the additional worth of the large steel core bolts which were not included in the model.

***Approximately $2.00 of this amount is considered to be due to synergistic effects, however.

Chapter 3 References

3-1 K. D. Lathrop, F. W. Brinkley, TWOTRAN-II: An Interfaced Exportable Version of the TWOTRAN Code for Two-Dimensional Transport, LA-4848-MS, Los Alamos National Laboratory, Los Alamos, NM (July 1973).

3-2 L. M. Petrie, N. F. Cross, KENO-IV, An Improved Monte Carlo Criticality Program, ORNL-4938, Oak Ridge National Laboratory, Oak Ridge, TN (November 1975).

3-3 G. E. Hansen, W. H. Roach, G. I. Bell, J. J. Devaney, C. B. Mills, and L. C. Connolly, Los Alamos Group-Averaged Cross Sections, LAMS 2941, Los Alamos Scientific Laboratory (September 1963).

3-4 The Vitamin C Library, DLC-41C, from the Radiation Shielding and Information Center (RSIC) in Oak Ridge, TN.

3-5 T. R. Schmidt, Sandia Pulsed Reactor-III (SPR-III): Neutron Physics Core Calculations, Sandia National Laboratories, Albuquerque, NM (January 1974).

3-6 L. L. Bonzon and J. S. Philbin, Absorbed Dose and Kerma for Reactor Neutron Spectra, SLA-73-0414, Sandia National Laboratories, Albuquerque, NM (June 1973).

3-7 D. Mathews and P. Koch, MICROX-2 -- An Improved Two-Region Flux Spectrum Code for the Efficient Calculation of Group Cross Sections, GA-A15009, Vol. 1 (Dec. 1979)

4.0 Thermomechanical Analysis

The extremely short pulse widths characteristic of fast burst reactors such as SPR-IV gives rise to thermally induced propagating stress waves within the core fuel plates. The rapid thermal shocking of the core plates requires a thermomechanical analysis to assure that maximum stresses will not result in damage to fuel plates, core bolts, or plate support rings. In the following sections, the modeling and calculations for stressed reactor components are discussed.

4.1 Fuel Plate Thermomechanical Response

Calculations of the mechanical response of a 3.81 cm* (1.5 in.) thick SPR-IV plate (14 in. i.d., 18 in. o.d.) due to pulse heating were made using the STEALTH [4-1] two-dimensional code. Models have been compared to experimental results obtained for the mechanical behavior of U-10 w/o Mo during rapid heating [4-2, 4-3]. The results of the comparisons indicated that oscillatory behavior and permanent damage of U-10 w/o Mo can be predicted with acceptable accuracy.

4.1.1 Properties

The mechanical properties of concern in the analysis are Young's modulus, Poisson's ratio, yield strength, and the thermal expansion coefficient. These mechanical properties of U-10 w/o Mo are shown in Figure 4.1-1 as a function of temperature.

4.1.2 Heating Rate and Profile

The heating rate curve was obtained from the temperature ramp curve presented in reference 4-3 for symmetric power pulses,

$$Q = C_v T_{max} \gamma e^{-\gamma (t-t_p)} / (e^{-\gamma (t-t_p)} + 1)^2$$

*3.81 cm was a reference thickness for this study but the final plate thickness is 2.75 cm. The final fuel plate ID is 35.4 cm (13.95 in) rather than 35.6 cm (14 in).

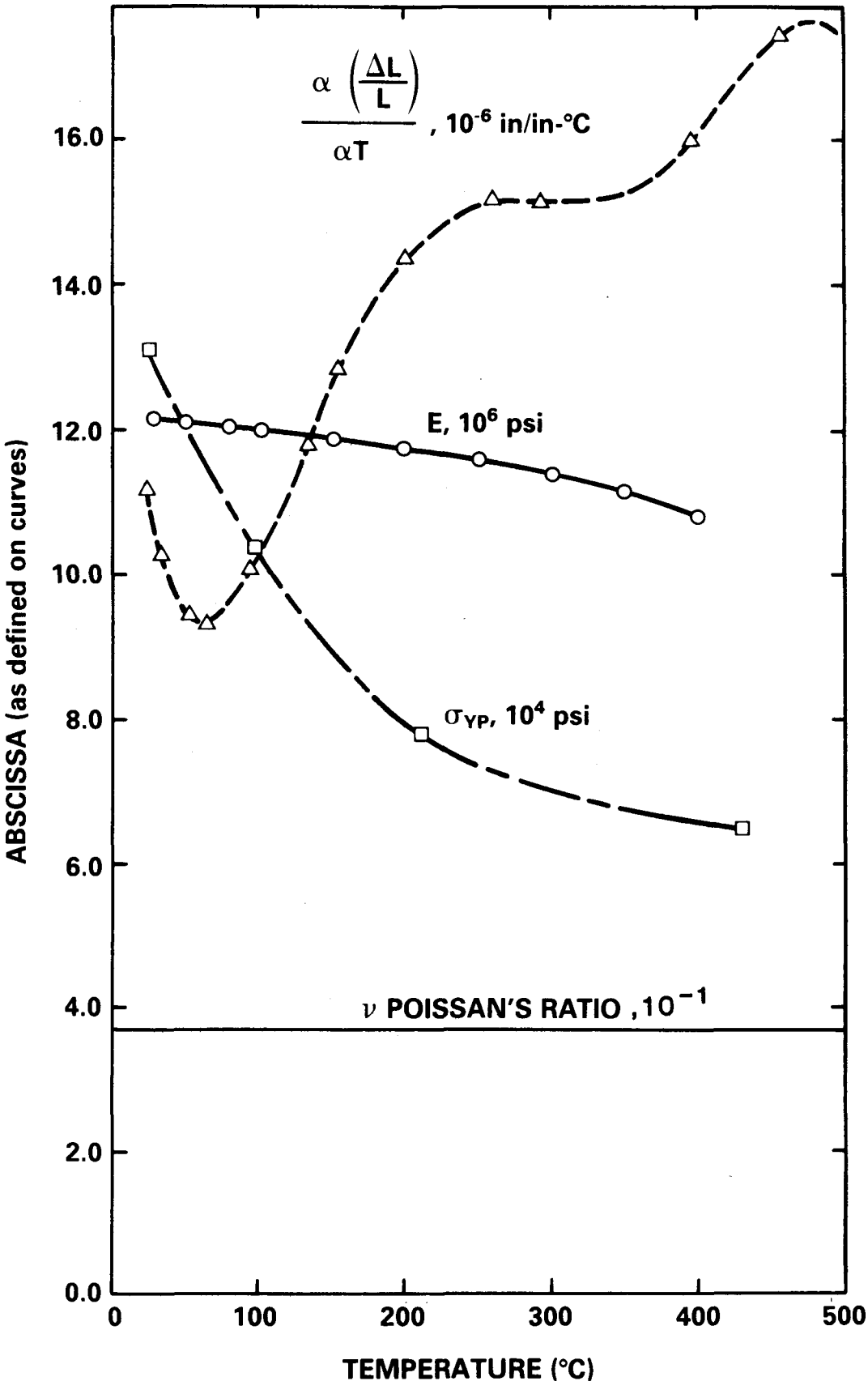

Figure 4.1-1
Mechanical Properties for U-lo w/o Mo

where

γ = 3.52/pulse width

t_p = time for beginning of pulse

T_{max} = maximum temperature rise

C_v = specific heat (2.504 J/cm^3-°C)

t = time

Pulse widths for the SPR-IV core material and geometry have been estimated from neutronic calculations and knowledge of SPR-II and SPR-III core behavior. The range of pulse widths used in the analysis is shown in Figure 4.1-2, along with those of other SPR cores.

The radial fission density profile was obtained from a TWOTRAN-II edit at the location of the peak axial fission density (slightly below the core midplane). A plot of the normalized fission distribution is shown in Figure 4.1-3.

4.1.3 Material Equation of State

The U-10 w/o Mo was modeled using an incremental pressure function to account for the nonlinear behavior of Young's modulus and the thermal expansion coefficient,

$$p^{N+1} = p^N - K^{N+1/2} \cdot \dot{}^{N+1/2} \Delta t + 3.0 \; \alpha^{N+1/2} (T^{N+1} - T^N)$$

where

p^N = pressure at time t^N

$K^{N+1/2}$ = bulk modulus at $t^{N+1/2}$

$\dot{}^{N+1/2}$ = volumetric strain rate at $t^{N+1/2}$

$\alpha^{N+1/2}$ = instantaneous thermal expansion coefficient at $t^{N+1/2}$

T^N = temperature at t^N

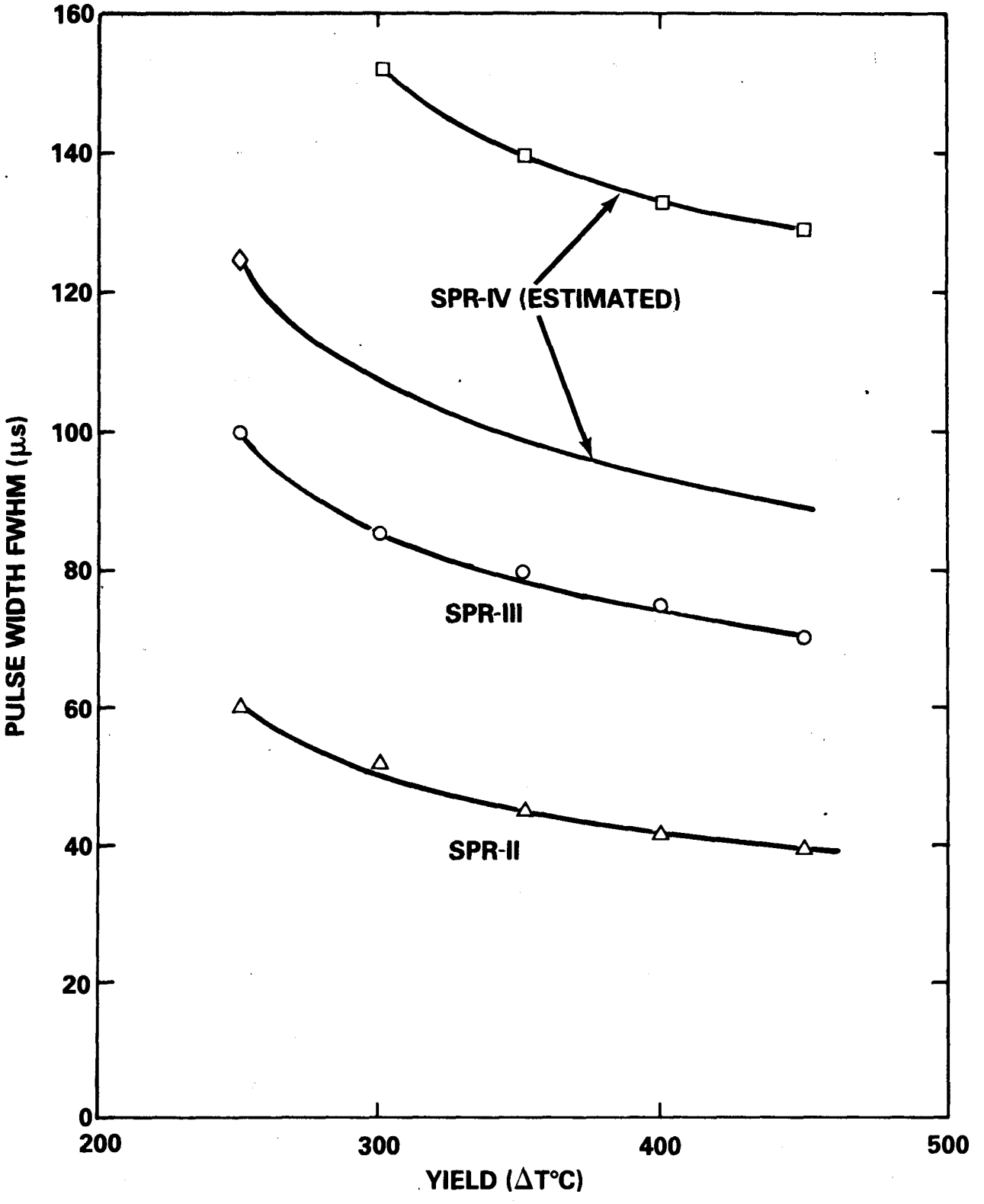

Figure 4.1-2
SPR Pulse Width at Half Maximum Power vs Temperature Rise (pulse yield) Free Field

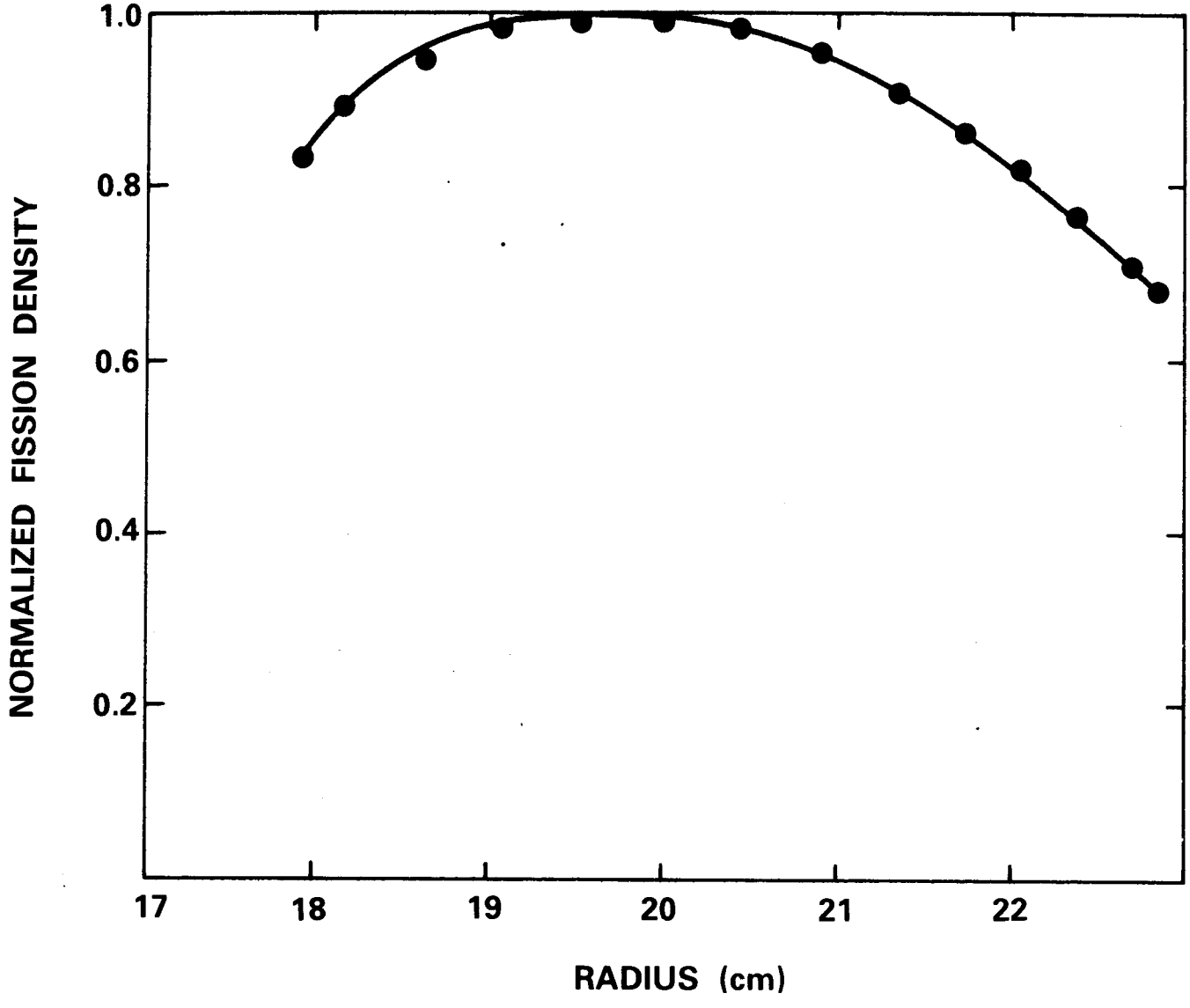

Figure 4.1-3

SPR-IV Radial Fission Distribution

4.1.4 Results

Shown in Figure 4.1-4 is the grid structure of the SPR-IV plate. Typical time behavior of maximum hoop stress, equivalent stress and design margin (equivalent stress/yield stress) at the inner and outer surface of the fuel ring are shown in Figures 4.1-5 to 4.1-7, for a temperature rise of 300°C and a pulse width of 125 sec. Radial movement of the inner and outer surfaces of the plate is also shown in Figure 4.1-8. A tabulated compilation of results is presented in Table 4.1-1. The design margin important for establishing operating limits is shown as a function of temperature rise in Figure 4.1-9.

From this figure the maximum pulse yield is seen to be 400 - 450°C. At this yield the R at the inner surface ranges between .18 - .21 cm (71-82 mils), and at the outer surface between .20 - .23 cm (78-91 mils). For the equivalent temperature rises, the ratio of equivalent-to-yield stress is approximately the same in SPR-III and SPR-IV, and the radial displacements in SPR-IV are about twice those of the smaller SPR-III core.

4.2 Core Support Bolts

An approximate stereomechanical (spring-mass) model [4-4] was used to estimate maximum bolt stresses for SPR-IV during pulse operation. This calculation is conservative in the sense that the heating throughout the core is taken to be uniform. The stress equations are

$$\sigma = (E_1 E_2)^{1/2} \alpha \; T_o \; (p_1/p_2 + A_2/A_1)^{1/2} \; (1 - T_p/2T_f)$$

$$\text{for } T_p/T_f < 1$$

and

$$\sigma = (E_1 E_2)^{1/2} \; T_o \; (p_1/p_2 + A_2/A_1)^{1/2} \; (T_f/2T_p)$$

$$\text{for } T_p/T_f \geq 1$$

where

T_f (fundamental period of oscillation) = $2L/C$

L = assembly length
C = wave propagation speed

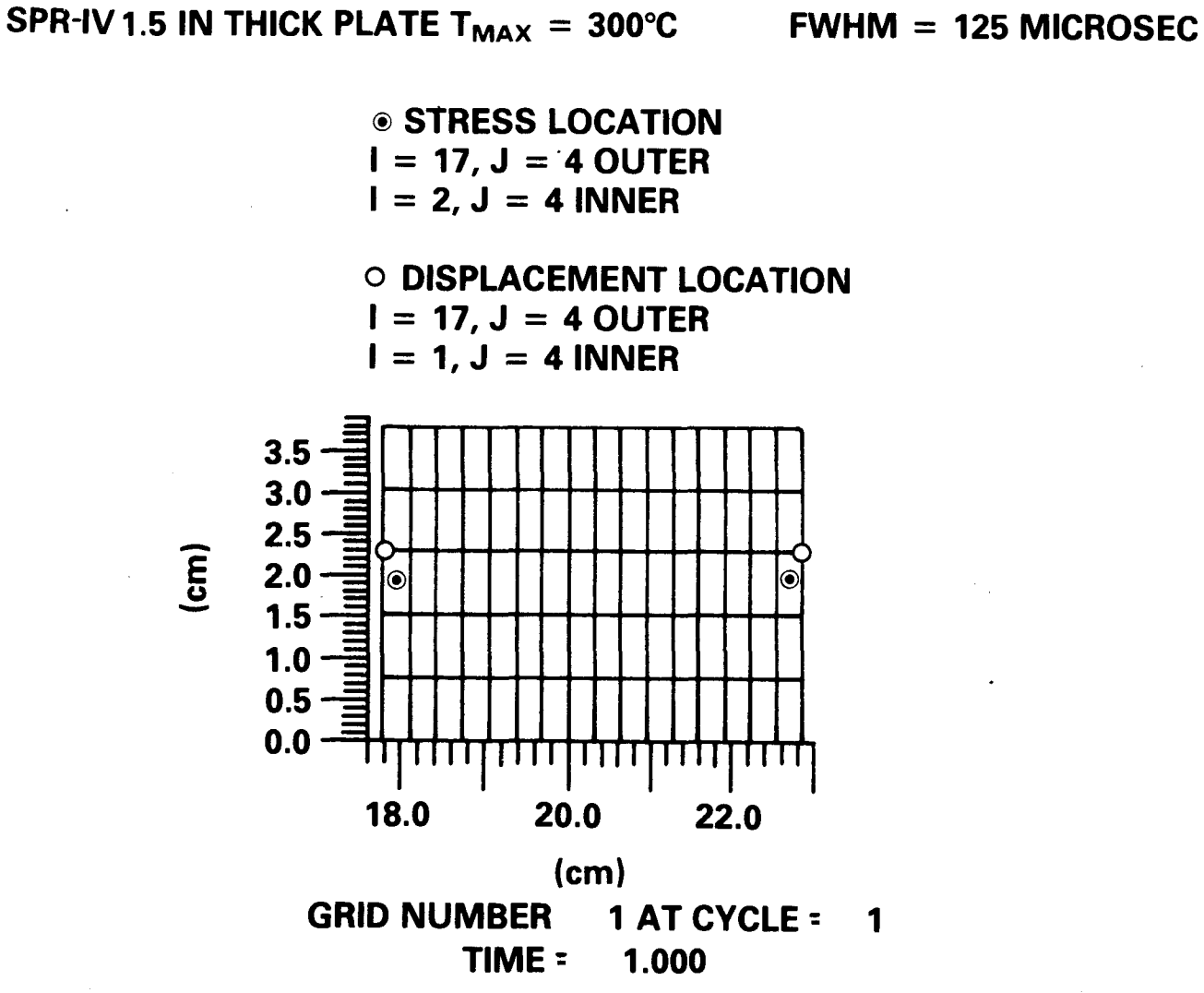

Figure 4.1-4

SPR-IV Fuel Plate Grid Structure

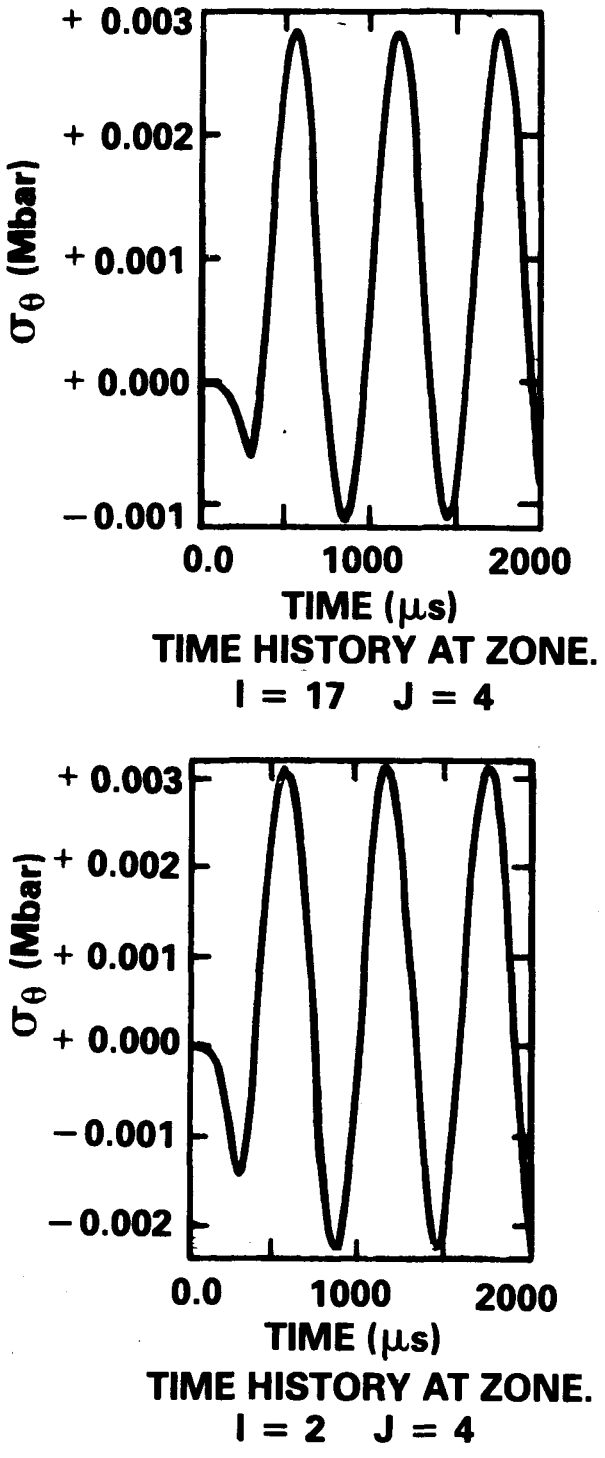

Figure 4.1-5
Hoop Stress Time History for SPR-IV Fuel Plate
(300°C ΔT, 125 μs burst width)

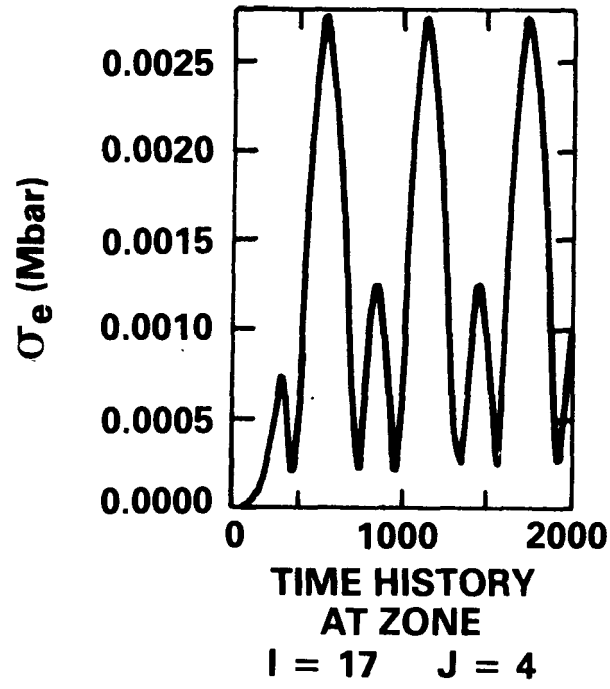

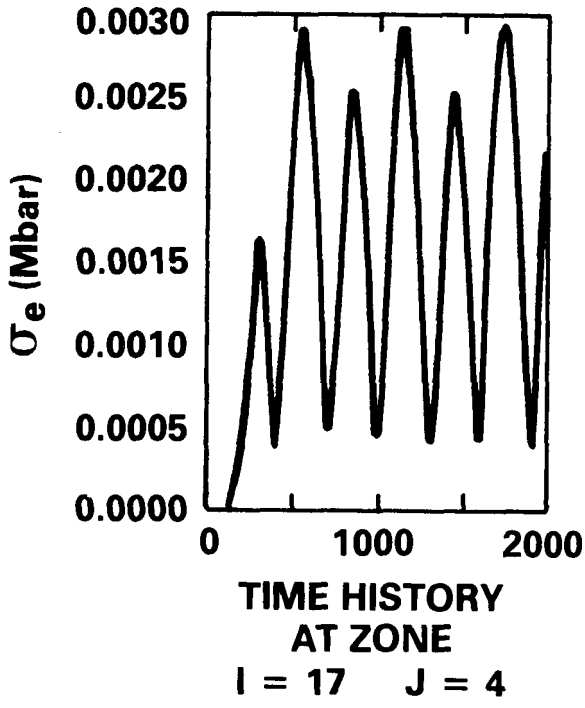

Figure 4.1-6

Equivalent Stress Time History for SPR-IV Fuel Plate (300°C ΔT, 125 μs burst width)

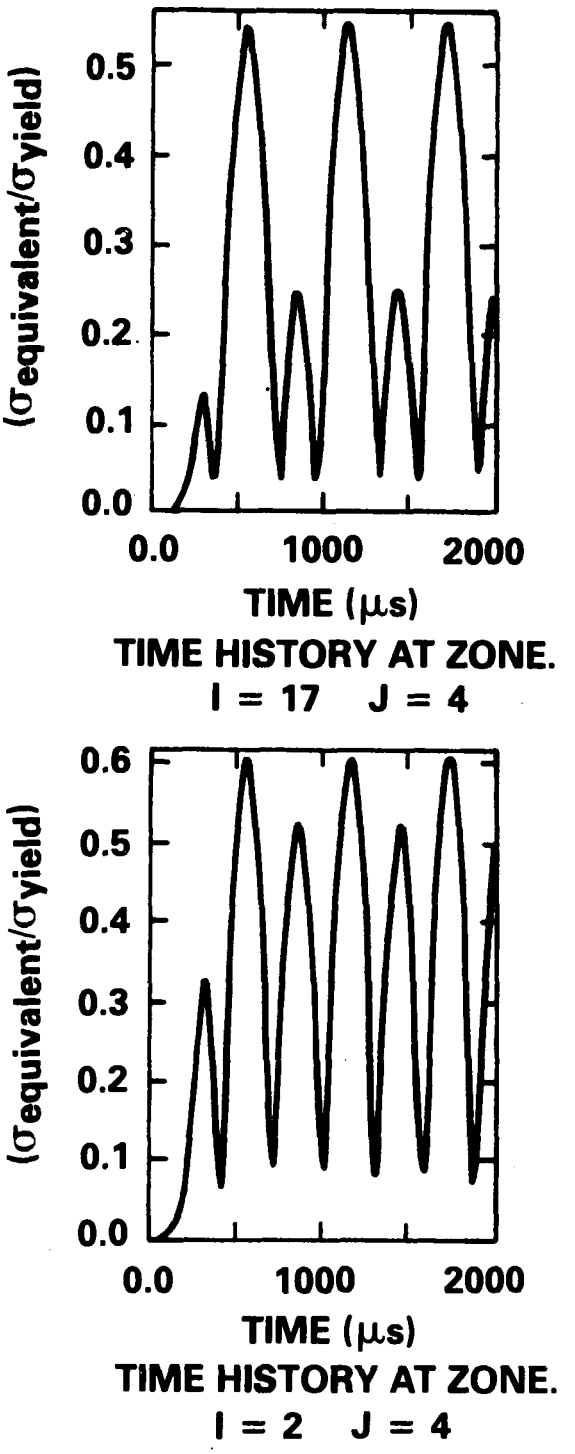

Figure 4.1-7
Design Stress Ratio (equivalent/yield) Time History for SPR-IV Fuel Plate (300°C ΔT, 125 μs burst width)

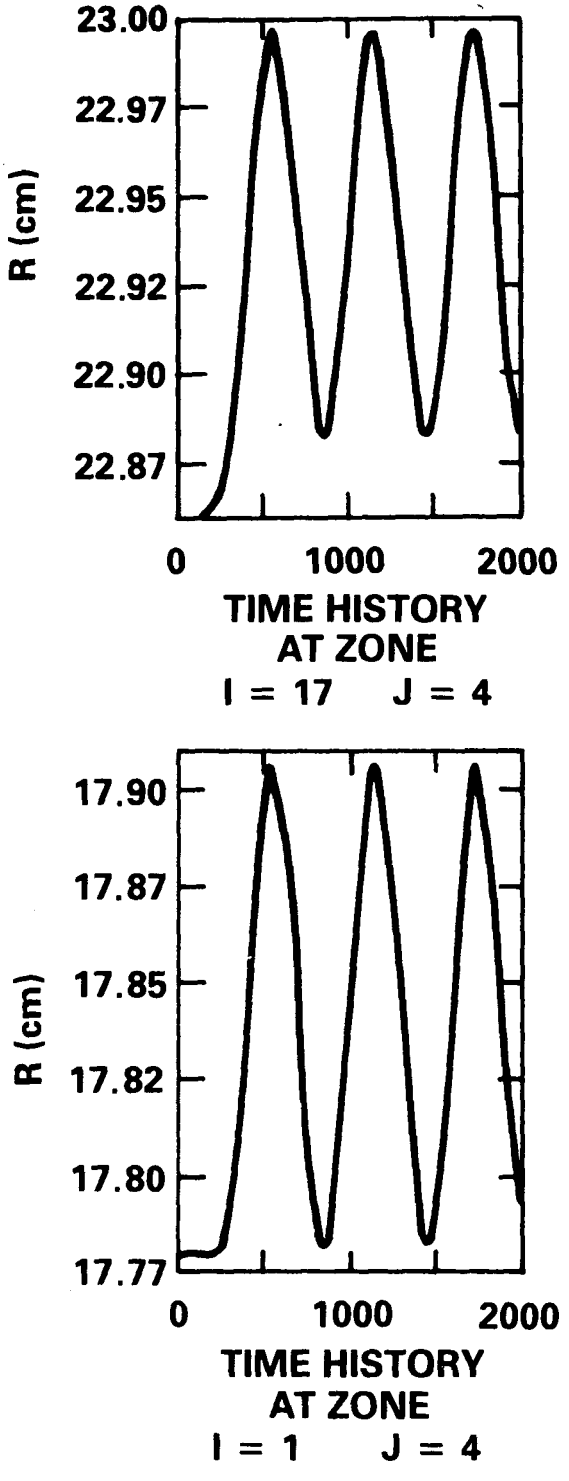

Figure 4.1-8

Radial Displacements for SPR-IV Fuel Plate
(300°C ΔT, 125 μs burst width)

Table 4.1-1

SPR-IV Mechanical Behavior

Parameter (maximum)	Maximum Temperature Rise (°C) 300	350	400	450
(ksi)				
$(\sigma_\theta)_{in}$ tensile (compressive)	42.08 (29.02)	52.24 (37.73)	62.4 (44.98)	72.56 (50.79)
$(\sigma_\theta)_{out}$	38.45 (13.79)	47.80 (18.86)	58.04 (23.2)	68.2 (26.12)
$(\sigma_e)_{in}$ (ksi)	39.18	48.61	58.04	68.2
$(\sigma_e)_{out}$	37.73	49.34	55.87	65.3
$(\sigma_e/\sigma_y)_{in}$	0.56	0.72	0.875	1.03
$(\sigma_e/\sigma_y)_{out}$	0.51	0.65	0.82	0.975
ΔR_{in} (mils)	47.24	59.06	70.81	82.68
ΔR_{out}	52.36	62.99	77.8	90.55
FWHM (μs)	152	140	133	129

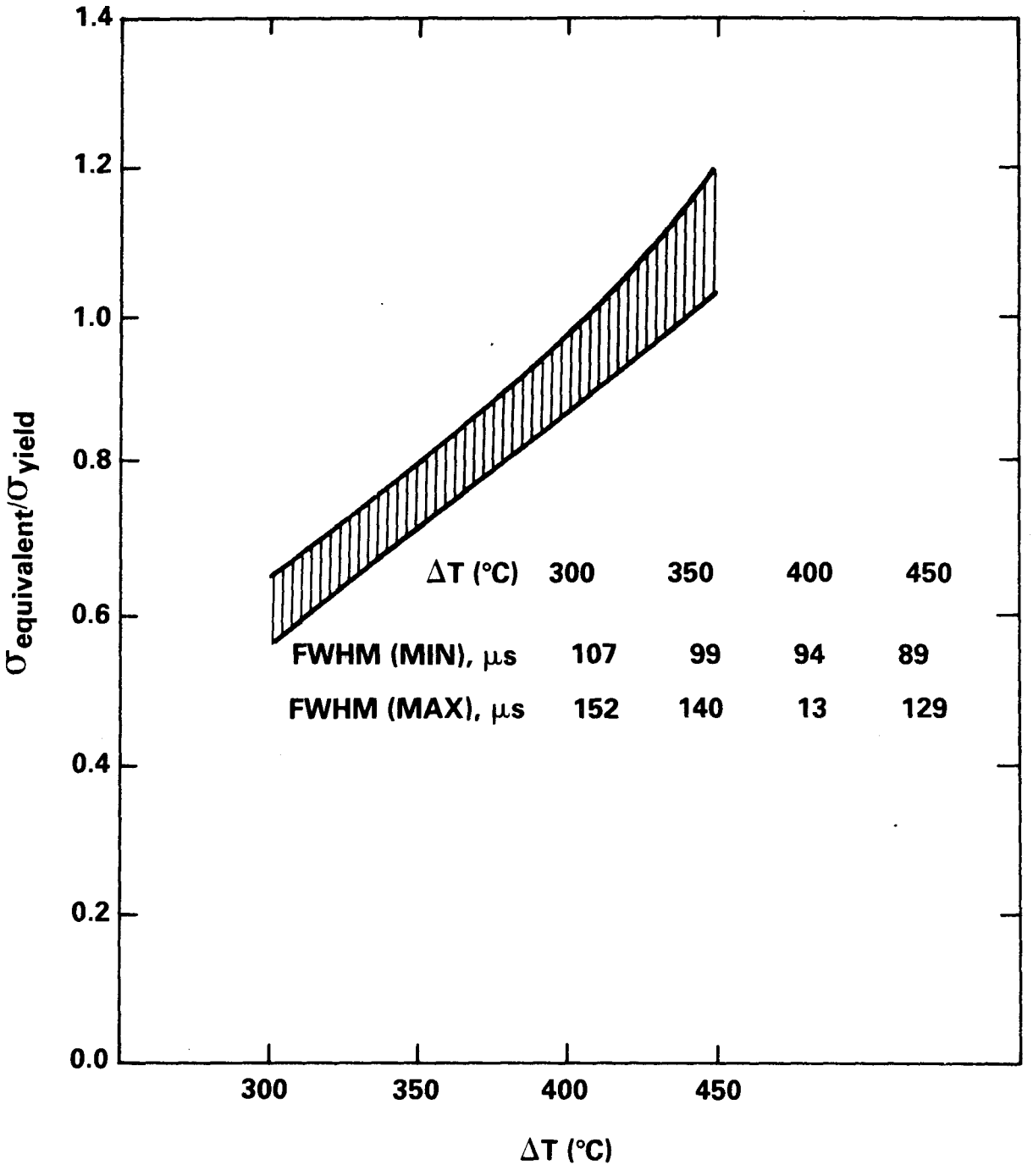

Figure 4.1-9

SPR-IV Plate Mechanical Response to Pulse Heating

T_p = pulse period

E = Young's modulus

α = thermal expansion coefficient

T_o = maximum assembly temperature

p = density

A = contact area

plates	material #2
bolts	material #1

These equations were used with material properties for SPR-IV plates and bolts.* Equivalent pulse periods for a linear heating ramp were determined based on fits to the heating curves for a symmetric power pulse, Figure 4.2-1. Shown in Figure 4.2-2 are maximum bolts stresses for assemblies with a range of contact areas which are indicated by plate contact thickness and bolt diameter. With a anticipated SPR-IV burst width of 125 s, bolts of 2.54 cm (1 in.) diameter can be used provided the ring thickness in 1.27 cm (0.5 in.) and the working stress of the bolt is $\sim$1.03 (10) dyne/cm^2 (150 ksi).** As a matter of design, a bolt of 3.18 cm (1.25 in.) diameter should be given preference for the SPR-IV assembly with a working stress limit no less than 1.03 (10) dyne/cm^2.

4.3 Core Support Ring

Shown in Figure 4.3-1 is a drawing of the SPR-IV core, indicating support bolt, rings and fuel plates. The dynamic-structural analysis of bolts and support rings followed a two-step approach which was used to conservatively estimate maximum stresses produced in these members during pulsing. In the first step the plates were held together by four support bolts with complete rigidity assumed for the support rings. The axial oscillations and resulting stresses in the bolts

*A-286 steel properties were used in this analysis, but 4340 steel may be the final design choice.

**Interpret 1.03 (10) dynes/cm^2 as 1.03 x 10^{10} dynes/cm^2. The number in brackets is the power to which 10 is raised. This convention is used throughout Chapters 4 and 5.

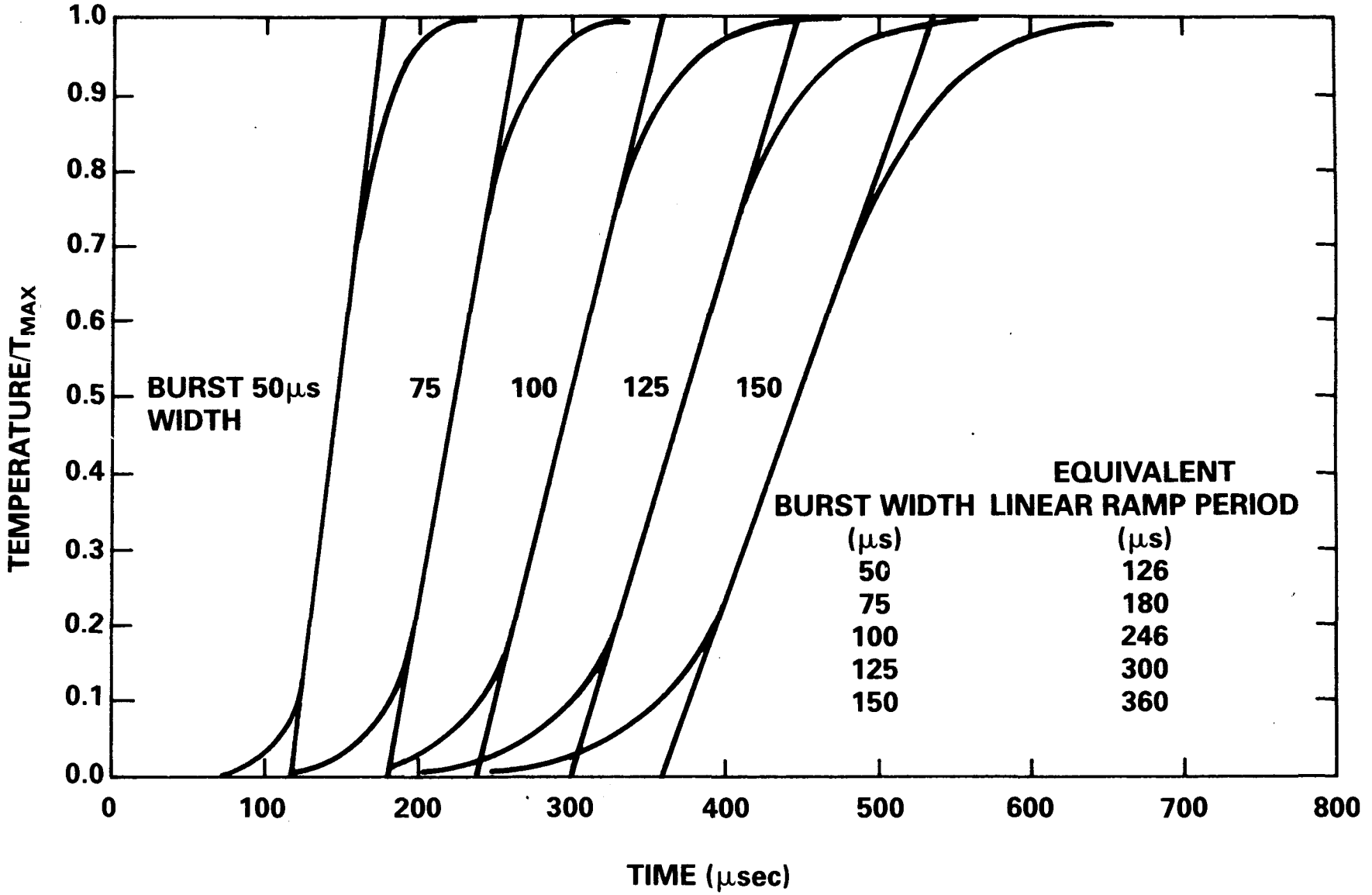

Figure 4.2-1
Temperature Rise Functions for Various Pulse Widths

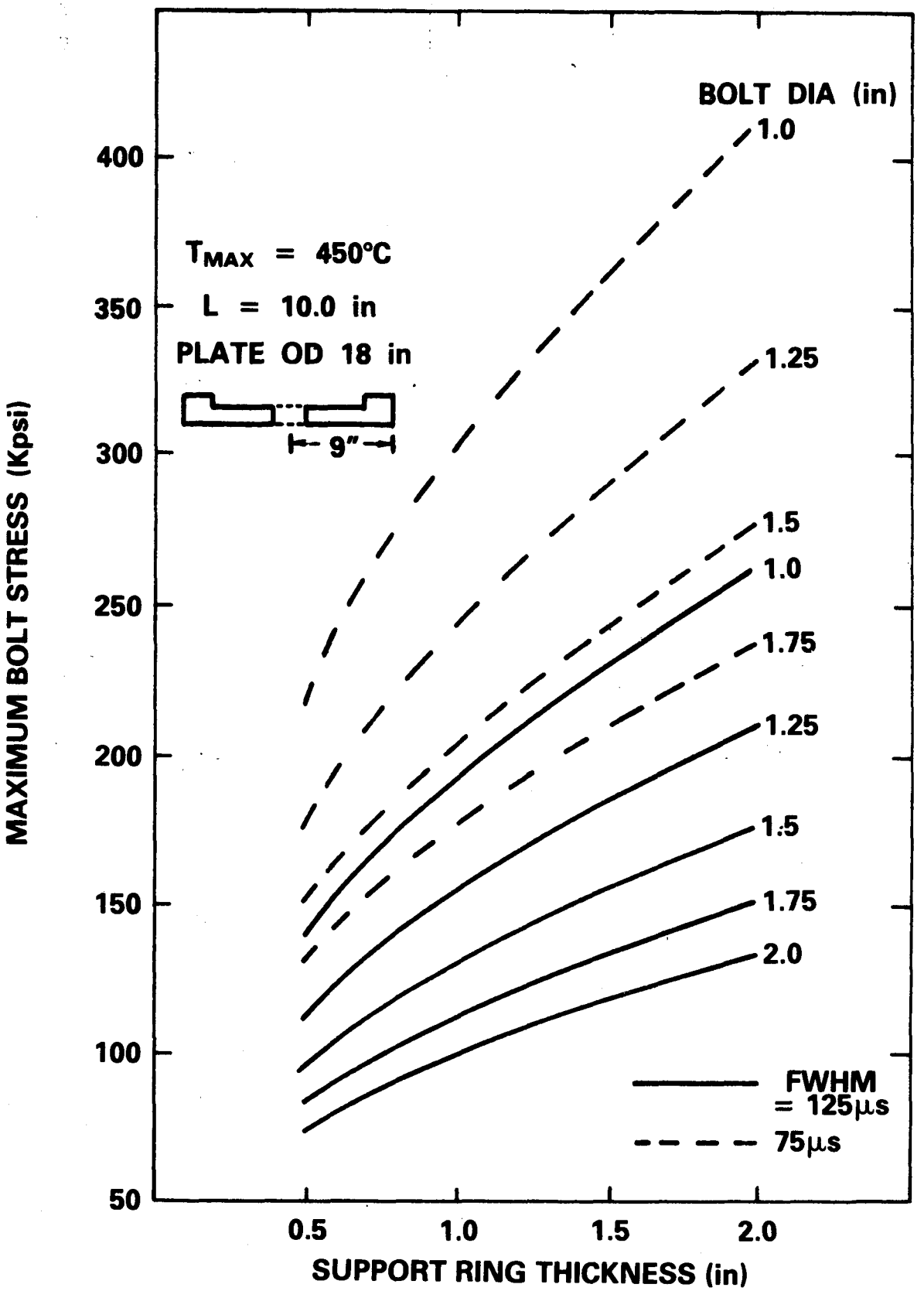

Figure 4.2-2
Bolt Stress for SPR-IV

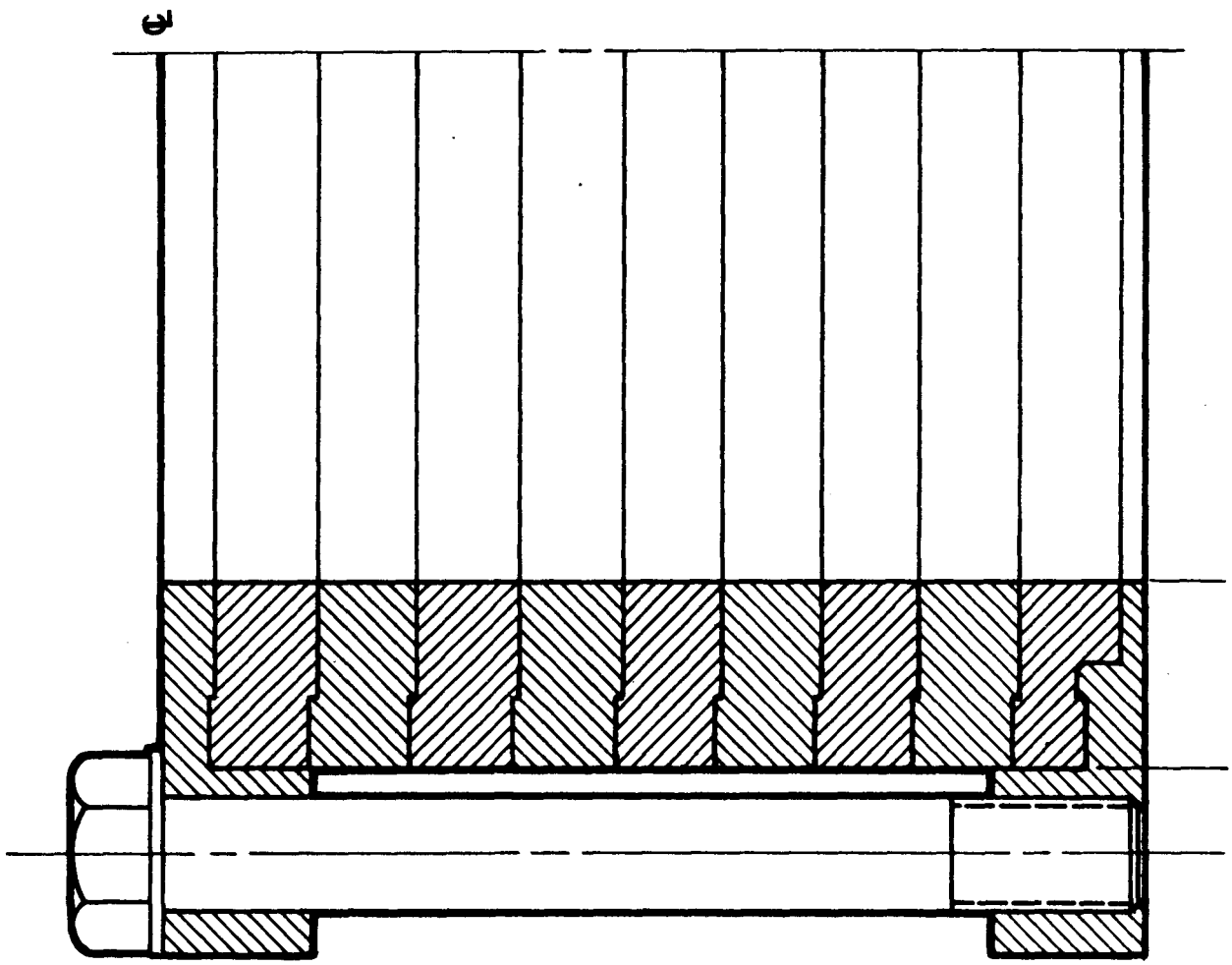

Figure 4.3-1

SPR-IV Core Half Showing Plate and Structure Support Members

were calculated according to reference 4-4. The maximum stresses in the support rings were then determined from a static analysis of the rings using the maximum loading amplitude previously calculated for the bolts. The equivalent static loading method of analysis is applicable to the support rings since the dynamic response of the rings is significantly greater than that of the bolt/plate assembly. The model for the support rings is discussed below; results are given for both analytic and numerical calculations.

4.3.1 Ring Model

The support ring was designed such that the only load-bearing surface is at each of the four core support bolts. The model shown in Figure 4.3-2 was used to approximate the ring as an elastic beam, with the loading based on an axial core restraint which is provided by a support surface which is circumferentially continuous. This manner of loading is consistent with the model used to calculate the axial response of the core assembly. The reduction of axial response of the assembly due to a discontinuity of the circumferential support is not addressed here.

4.3.2 Analytical Results

Using the beam dimension of Figure 4.3-2, the maximum tensile stress at location "A" is determined from the beam flexure formula,

$$\sigma = \frac{MC}{I}.$$

Shown in Figure 4.3-3 is the maximum tensile stress at "A" as a function of beam load conditions. Since there is a discontinuity at location "A", the nominal stresses must be corrected by a stress concentration factor, K_t. A curve of K_t is represented in Figure 4.3-4 for a geometry similar to that of the support ring model. With a minimum corner radius, the stress concentration is estimated to be 2.0; and for a corner ratio of $r/h = 0.58$, the concentration factor is reduced to 1.3. The effect of stress concentration at "A" is indicated in Figure 4.3-3 for the concentration factors discussed here.

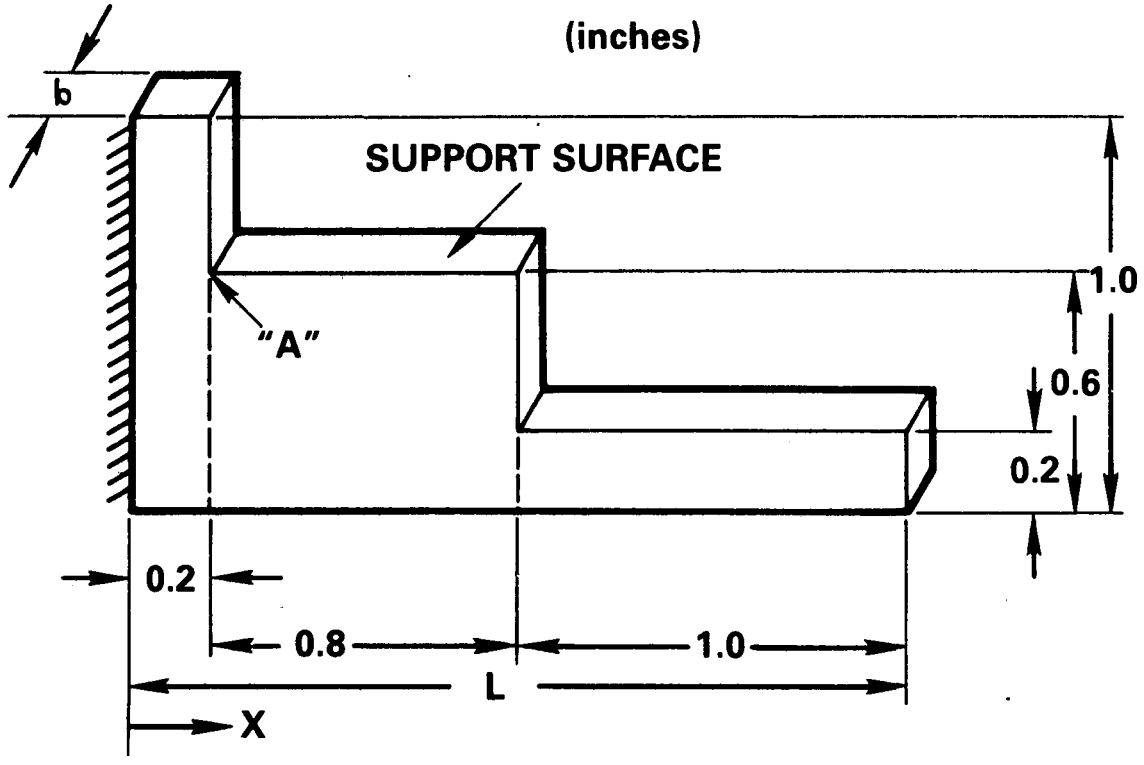

Figure 4.3-2

Simplified Model of a Candidate Support Ring

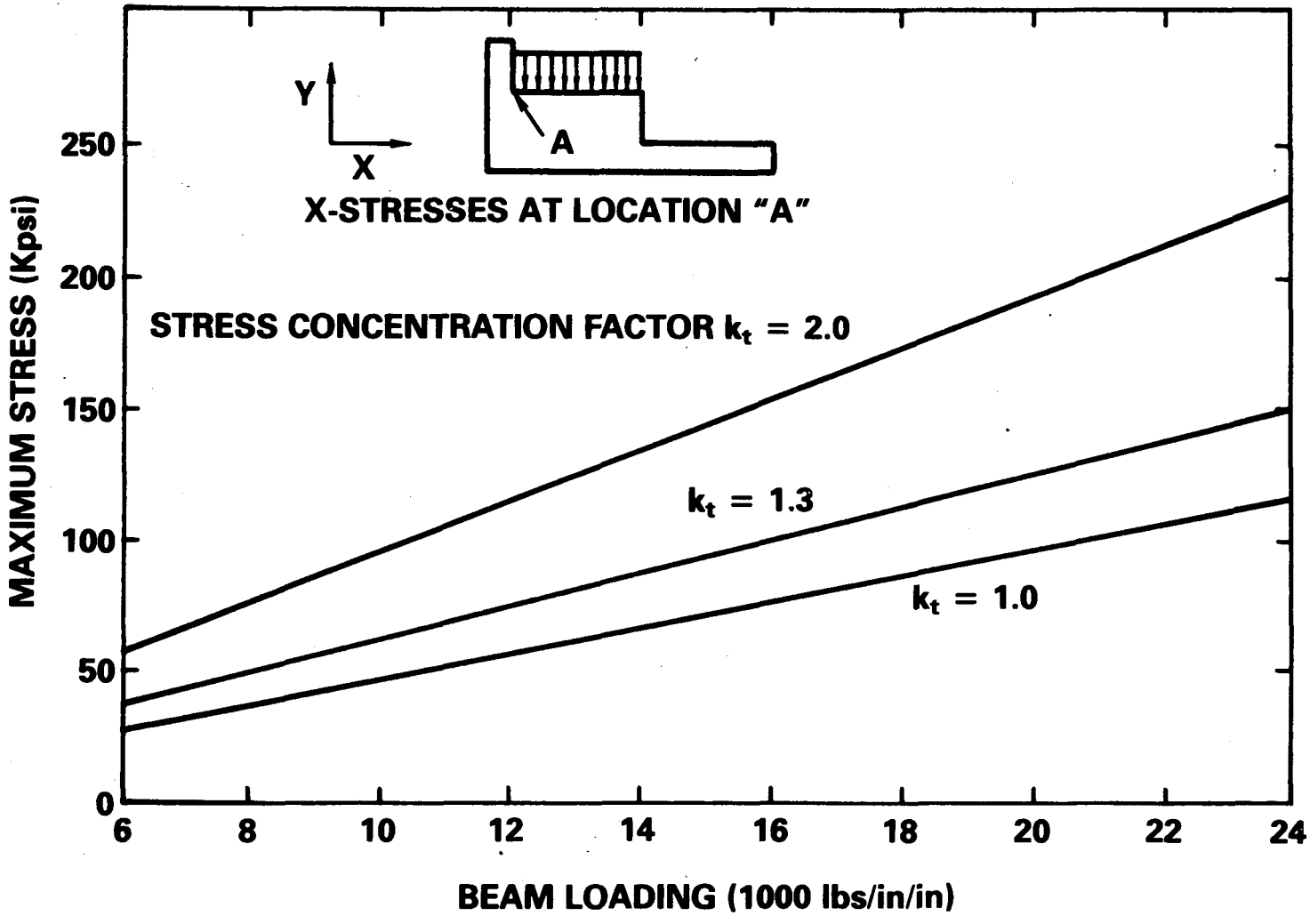

Figure 4.3-3

Maximum Beam Stress Due to Uniform Loading

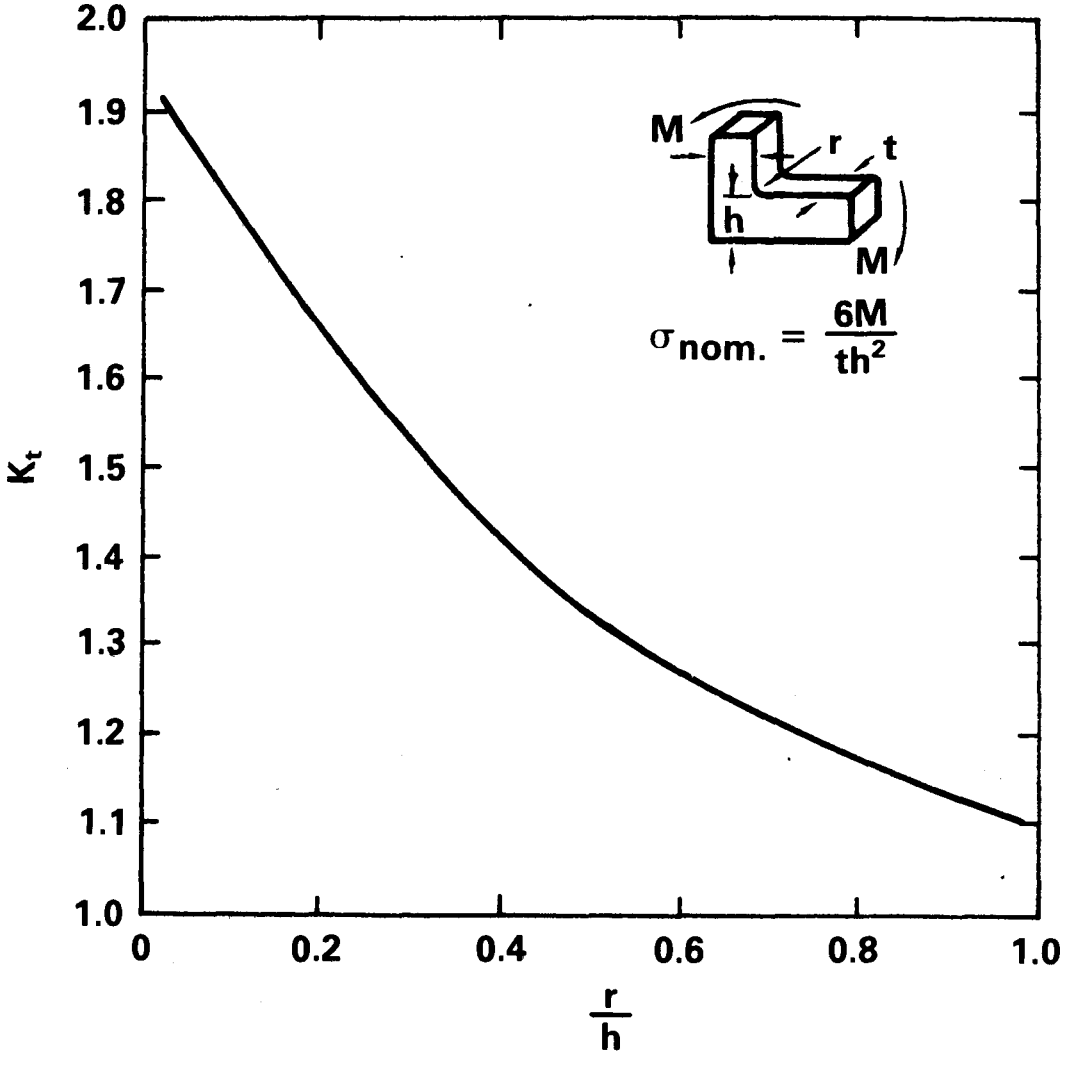

Figure 4.3-4

Stress Concentration Factor for L Section Bending (Ref. 4-5)

Scaling the bolt stresses to the projected loading surfaces of the support rings is made according to

$$\text{Ring (beam) loading} = 4.0 * A_{(\text{bolt})} * \sigma_{(\text{bolt})}/A_{(\text{ring})}$$

where

$A_{(\text{ring})}$ = support surface area

$A_{(\text{bolt})}$ = cross-sectional area of bolt

σ = maximum axial stress in bolt

For a 3.18 cm (1.25 in.) bolt diameter with a working stress of 1.03 (10) dyne/cm^2 (150 ksi), the loading is 1.36 (9) dyne/cm/cm (19.7 (3) lbs/in/in)). For this loading the maximum stress ranges from 9.65 (9) dyne/cm^2 (140 ksi) for K_t = 2.0 to 6.27 (9) dyne/cm^2 (91 ksi) for K_t = 1.3. These results indicate that a high strength alloy should be used for the ring material, and special attention should be given to reducing the stress concentrations at geometric discontinuities as represented by location "A".

4.3.3 Numerical Model of the Support Ring

The calculation of stresses for the ring model by a finite element method was used to investigate ring geometry effects on maximum stresses. The basic numerical models are shown in Figure 4.3-5. With a loading of 4.6 (8) dyne/cm/cm (6.667 (3) lbs/in/in)) on the support surface of the beam, the maximum stress contours are shown in Figure 4.3-6. As indicated in this figure, the maximum stress occurs at the point of geometric discontinuity, referenced previously as location "A". The effect of the treatment of the beam as a narrow member was investigated by repeating the above plane stress calculation by a plane strain and an axisymmetric approximation. The results in terms of the Von Mises (equivalent stress) were

σ_e("A")	boundary approximation
3.47 (9) dyne/cm^2 [50.3 ksi]	plane stress (narrow beam)
3.05 (9) [44.3]	axisymmetric
2.94 (9) [42.6]	plane strain

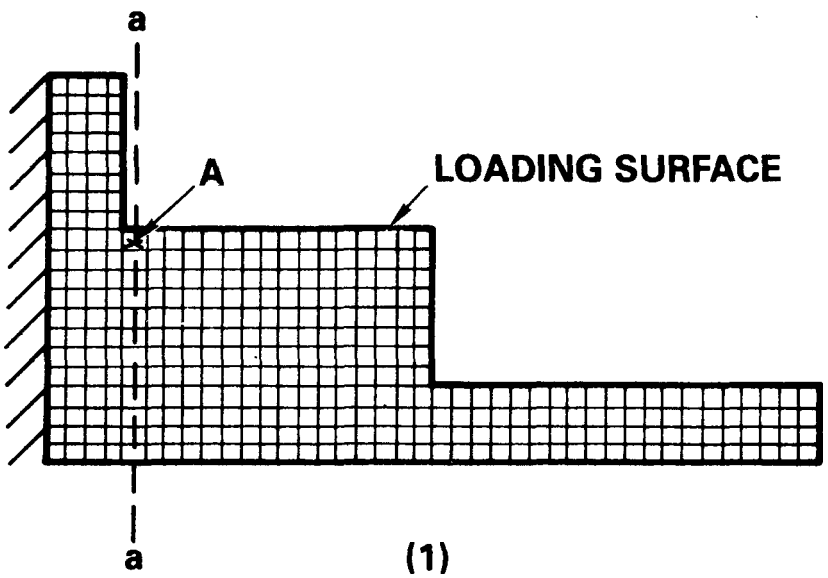

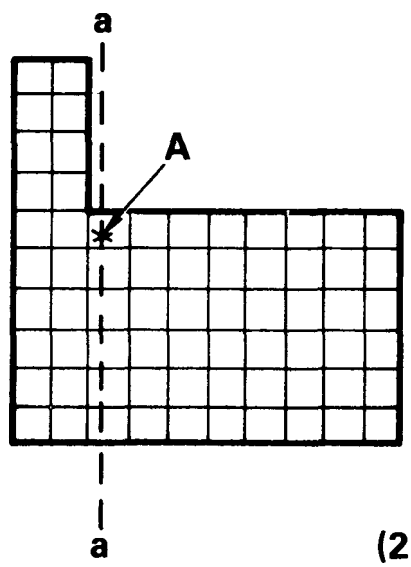

Figure 4.3-5

Numerical Models of the Support Ring Structure

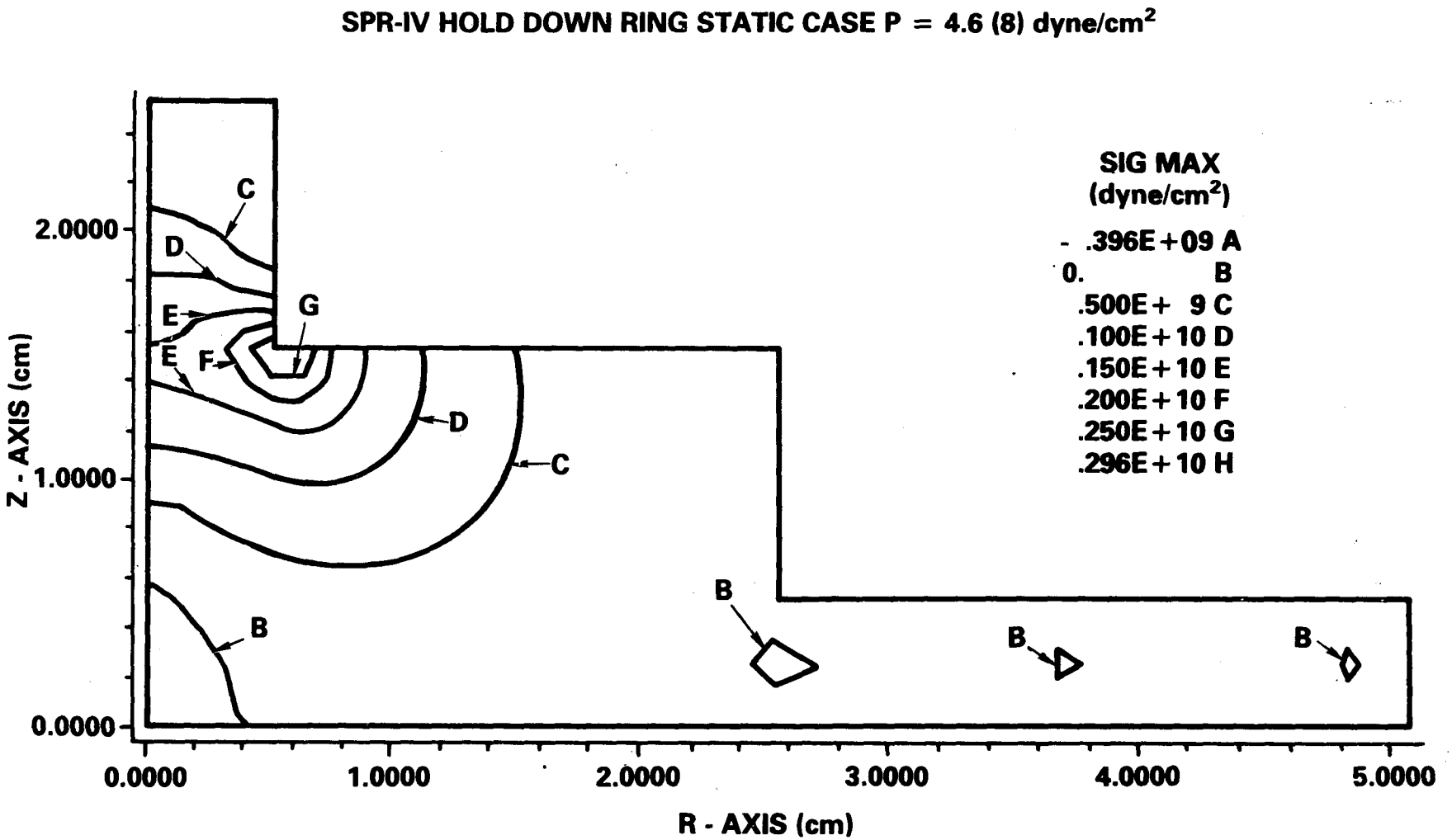

Figure 4.3-6
Stress Contours for the Support Ring as Calculated Using SASL, Ref. 4-6 (Young's Modulus = 2.1E+12 dyne/cm)

The plane stress calculation is considered to be an appropriate approximation for the ring, and one which reflects a conservative approach.

Shown in Figure 4.3-7 is a plot of the stress distribution profile through the beam for two numerical models represented in Figure 4.3-5 along with the values predicted using the beam flexure formula. The effect of stress concentration is evident from this figure. A table of equivalent stresses at "A" for various beam geometries, Figure 4.3-8, is shown in Table 4.3-1. A comparison of the tabulated values indicate that increasing the depth of the beam at the load plane by 1/3 will reduce maximum stress by $\sim$1/3. With proper design of the beam at the transition location "A" ($r/h \sim 0.6$), a stress reduction of 1/3 is also possible.

4.3.4 Summary

The support ring design for SPR-IV has been a compromise between mechanical compatibility, structural strength, and core operational requirements. The structural analysis has been limited to approximate techniques. However, the methods and approximations have been applied in a manner which have resulted in conservative design decisions. Comparing the results of both analytical and numerical models, it has been determined that the support ring is capable of withstanding pulse loading (ΔT=400 to 450°C) providing the structural material is a high strength alloy having a yield strength greater than 6.9 (9) dyne/cm^2 (100 ksi).

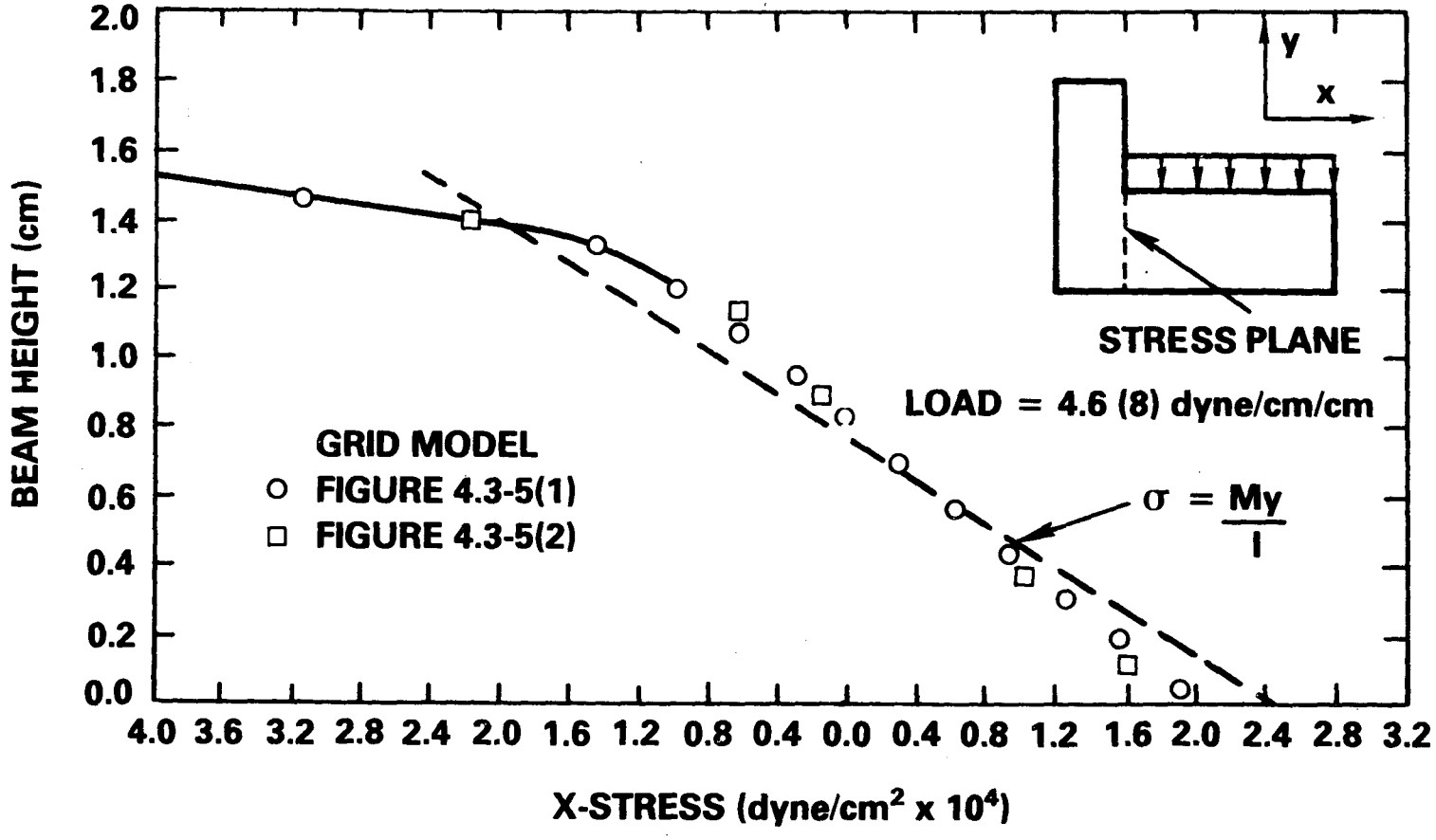

Figure 4.3-7

X-Stress Distribution through Support Ring Model at Point of Discontinuity

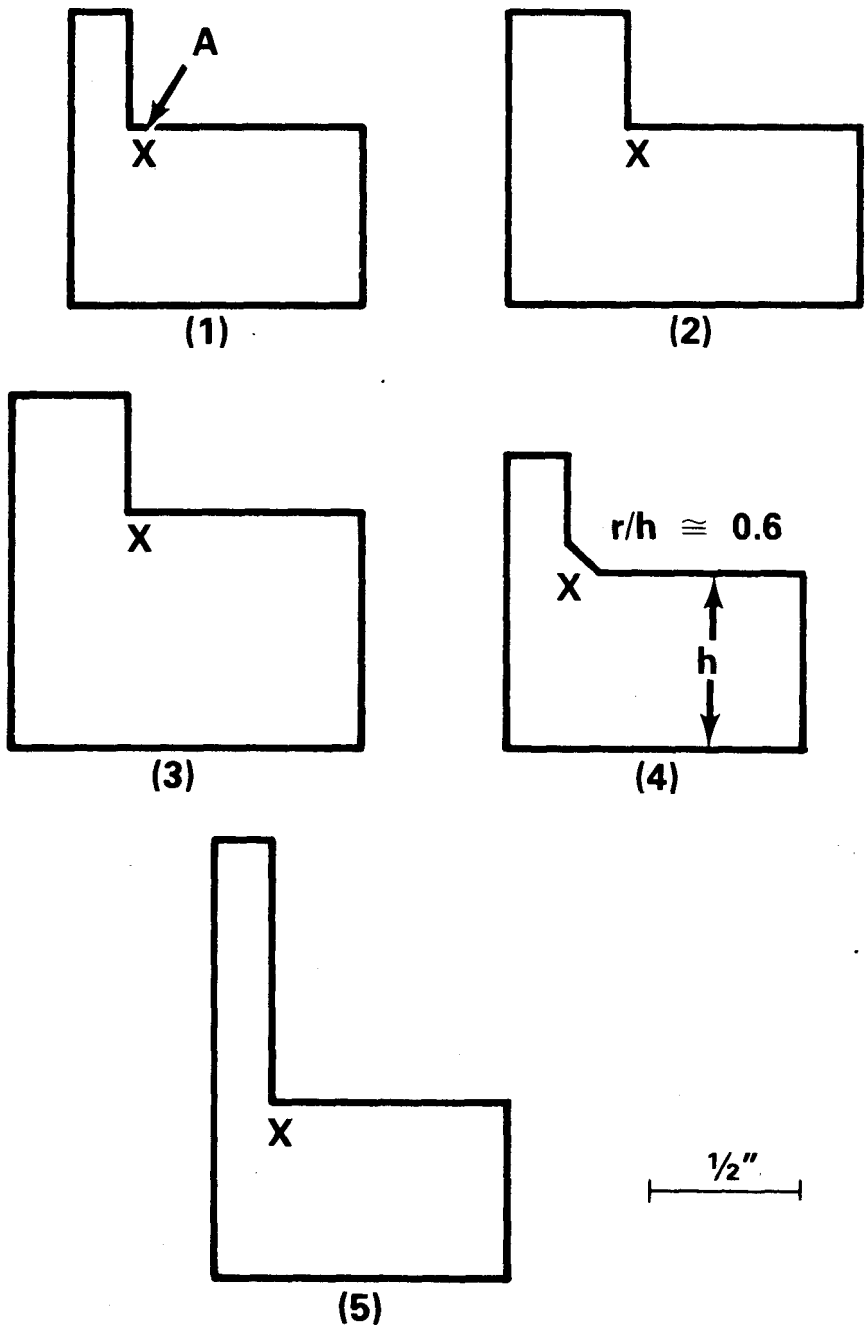

Figure 4.3-8

Beam Geometry Variation for Support Ring Model

Table 4.3-1

Maximum Equivalent Stresses for Various Beam Geometries

(loading = 4.5 (8) dyne/cm/cm)

Geometry (Figure 4.3-8)	Stress (dyne/cm^2)
1	2.522 (9)
2	2.762 (9)
3	1.776 (9)
4	1.788 (9)
5	2.779 (9)

References

4-1 "STEALTH," A Lagrange Explicit Finite Difference Code for Solids, Structural and Thermohydraulic Analysis, EPRI NP-260.

4-2 Reuscher, J. A., and Schmidt, T. R., Nucl. Tech., 28, 57 (1976).

4-3 Reuscher, J. A., Nucl. Engr. Design, 18, 213 (1972).

4-4 Burgreen, D., Nucl. Sci. & Engr., 30, 317 (1967).

4-5 Lipson, C. and Juvinall, R. C. "Handbook of Stress and Strength," Maxmilliam (1963).

4-6 SASL: A Finite Element Code for the Static Analysis of Axisymmetric and Plane Solids Subjected to Axisymmetric and Plane Loadings, SCL-DR-72-0061, Sandia National Laboratories, Livermore, CA. (1972).

5.0 Cooling System Design

The cooling system for SPR-IV consists of two subsystems. One is external and the other is internal to the reactor stand. All equipment associated with supply of low temperature nitrogen gas to the reactor stand is considered the external cooling system. At the reactor stand the configuration of gas plenum and gas flow path for plate cooling is referred to as the internal reactor cooling system. The design philosophy for an overall system has been to first satisfy requirements for plate cooldown time as they impact the internal system, and to then use that design as input specifications for the external system. An analysis of the current SPR cooling system was made to establish reasonable bounds on expected system performance, even for a highly modified cooling system.

The maximum cooldown period established for pulse operation was based on a desire to operate the reactor in an efficient fashion, that is, maximize the number of pulses that could be run in an eight hour shift. Between pulses, the reactor must be cooled to near ambient temperature conditions (20°C) before the reactor can be set for further pulsing. The present cooldown period for SPR-III is between 45 minutes to an hour. This means that between four to five pulses are possible in an 8 hour shift. The design goal for the SPR-IV cooling system was not to exceed this cooldown time period, and hopefully to reduce this time somewhat. What makes sense for a minimum cooldown time is primarily a practical consideration, depending to a certain degree on the time that must be allowed from an operational and neutronic standpoint. In this regard it did not seem to be beneficial to reduce cooldown time to less than approximately 30 minutes. The design goal, therefore, for SPR-IV cooldown time was set at a maximum of an hour with a preferred time of 30 minutes.

It is also expected that the reactor will be run to some extent in the steady state mode. The cooling system, however, has not been specifically designed for optimal performance in this mode, except for requirements placed on the external cooling system which would provide continuous low temperature gas flow for extended periods of operation (4-5 hours). It is believed, however, that an efficient internal cooling system for pulsing can also provide a good steady state performance.

In Section 5.1 - 5.3, the design procedure for the internal cooling system is presented. These efforts

involved both numerical and experimental methods to characterize pulse cooldown behavior. From the analysis and design presented in these first sections, specifications were formulated for the external system. Section 5.4 is devoted to a description of this system, which is an upgrade of the current cooling system for SPR-III. This upgrade will provide an external cooling system which will meet the design needs of SPR-IV, and will also function to enhance the performance of SPR-III. The external system was designed by the BDM Corporation on contract to SNL.

5.1 Reactor Cooling System Configurations

The cooling surfaces available for a SPR type core consisting of stacked plates are the:

- exterior radial
- interior radial
- interior axial

surfaces as shown in Figure 5.1-1. The areas associated with these surfaces for various plate dimensions are given in Figure 5.1-2. There are two basic cooling configurations that utilize such surfaces or combinations thereof. The current SPR-III method of cooling utilizes the exterior radial geometry. External cooling tubes with holes along the tube length are used to direct nitrogen gas at the plate's radial surfaces, producing a nitrogen jet cooling configuration. Combining the interior radial and axial surfaces requires an interior plenum with a plate flow-through design. These two cooling geometries are shown in Figure 5.1-3. The interest in the external tube configuration is primarily due to the fact that this cooling scheme has been used in the past and it's performance is matter of record. However, this configuration does not make optimum use of all potential cooling surfaces. In fact, only a fraction of the exterior radial plate surface is available for cooling as a result of space taken up by the core bolts and radial reflectors. The interior plenum concept represents a significant change in cooling geometry, which is both simple and efficient.

5.2 External Cooling Tubes

In order to model the external cooling tube geometry for predicting cooldown performance of SPR-IV, a

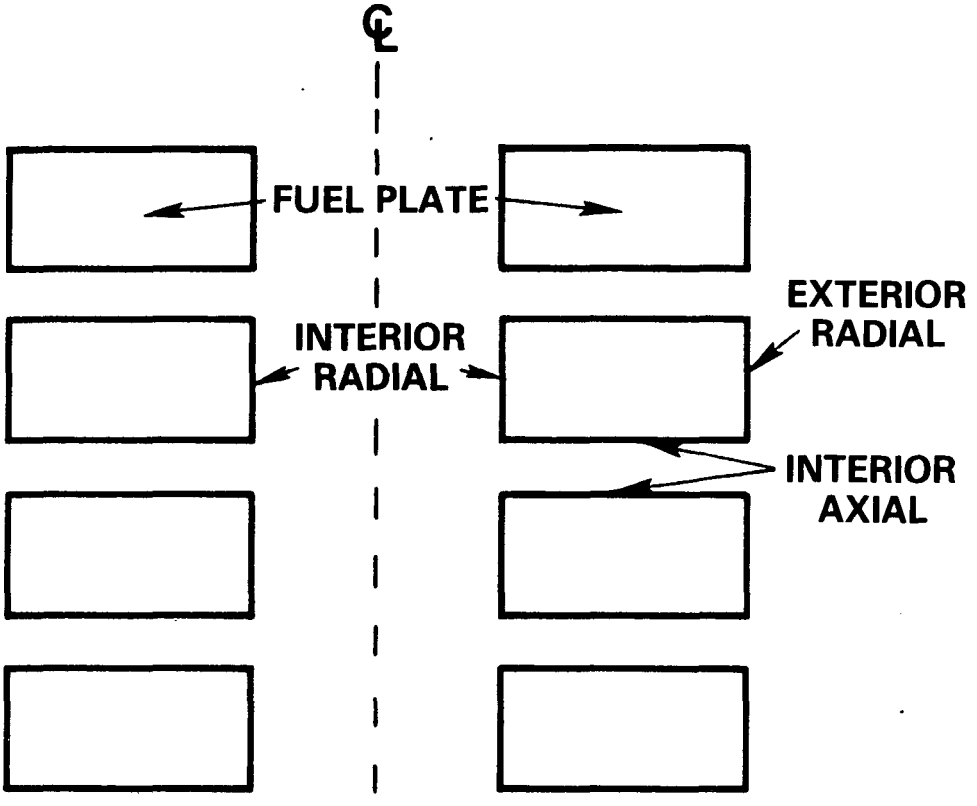

Figure 5.1-1

SPR Core Cross-Section Indicating Potential Heat-Transfer Surfaces

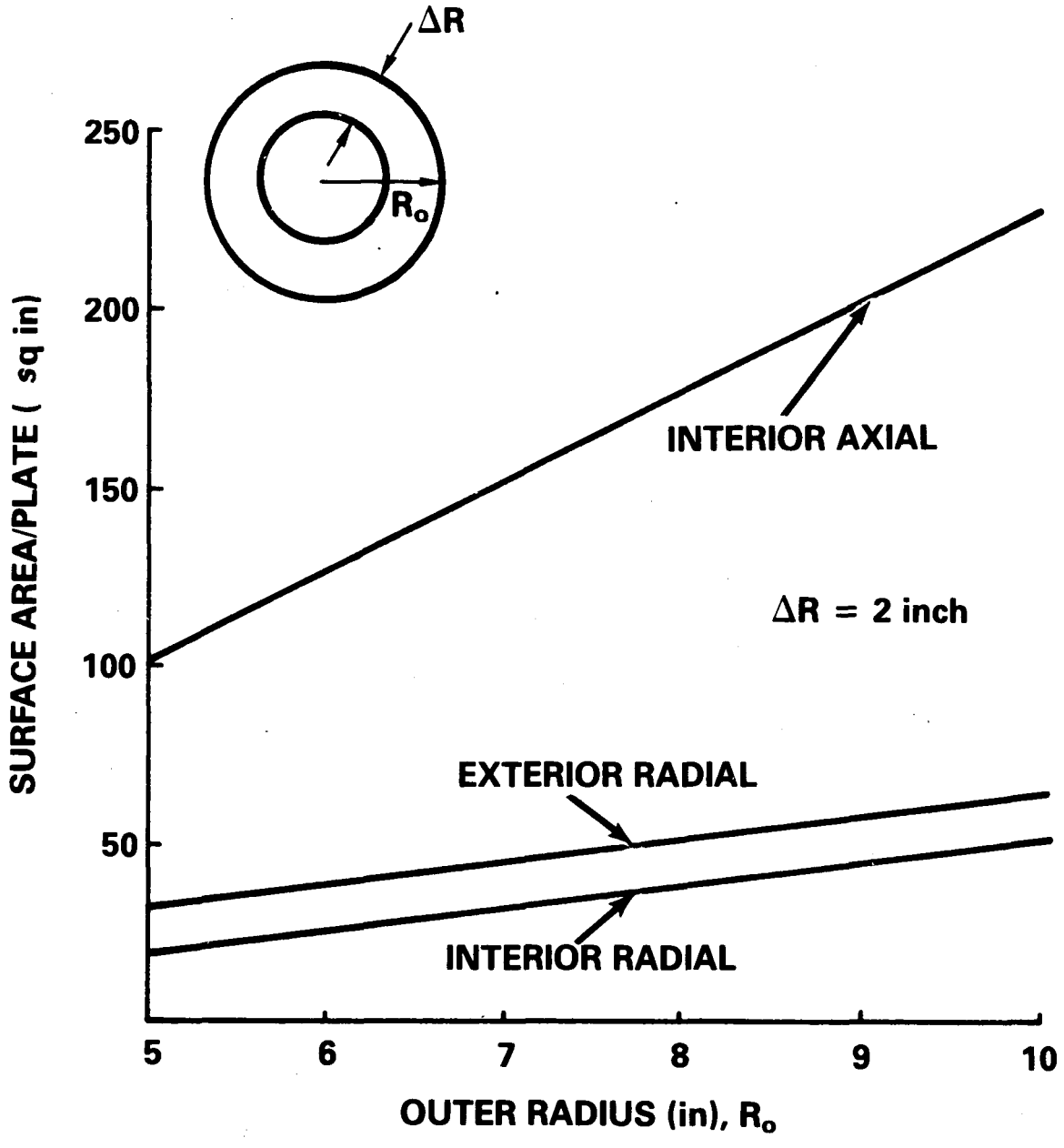

Figure 5.1-2

Heat Transfer Areas for SPR Plate

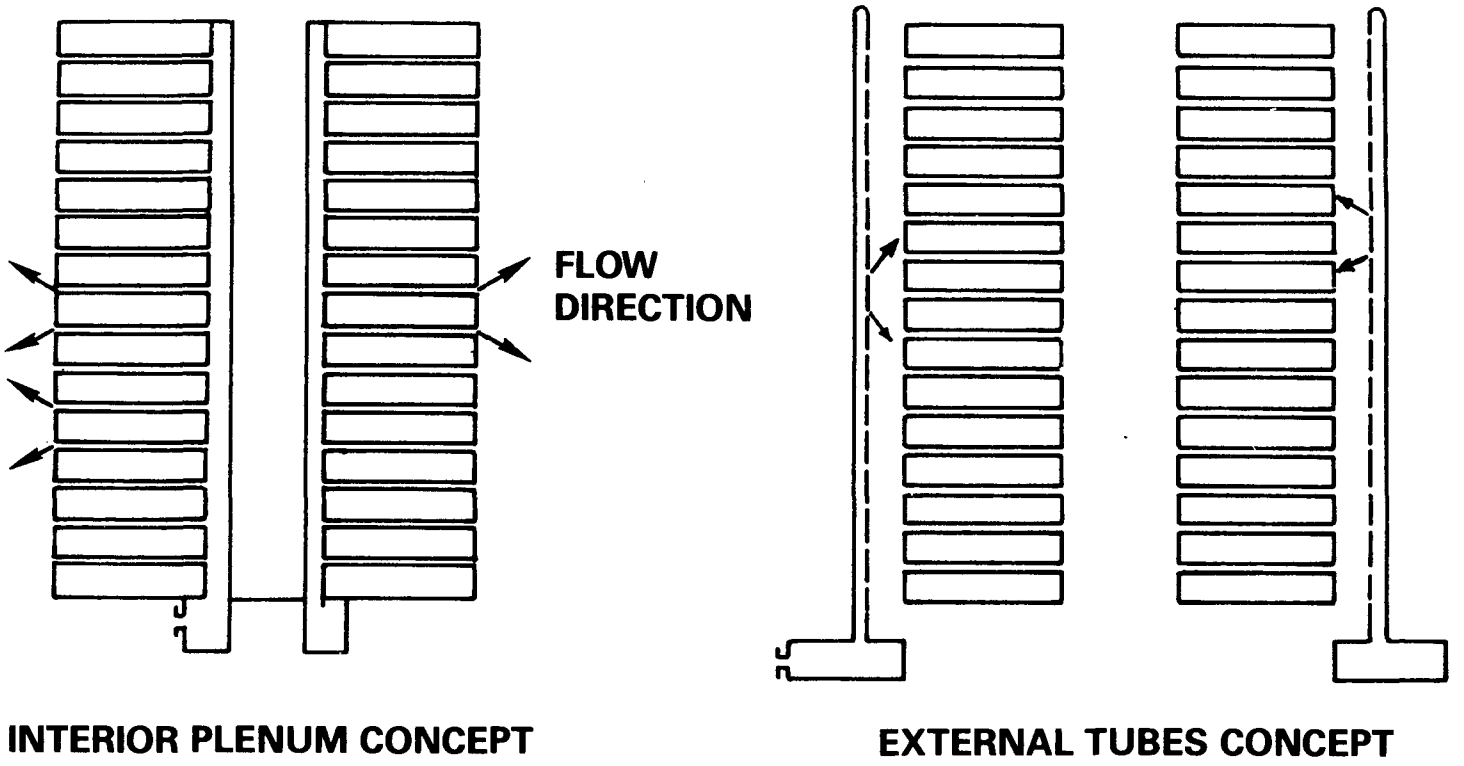

Figure 5.1-3

Candidate SPR-IV Cooling Concepts

calculational model was first set up for SPR-III and results were compared to core cooldown temperature measurements in a reference pulse experiment. For the transient analysis, the inlet gas temperature (nitrogen jet temperature) and fuel surface temperature were measured with thermocouples. The fuel surface temperature was measured near the upper core-half midplane, centered azimuthally between cooling tubes as shown in Figure 5.2-1. With the development of the SPR-III model, a comparison between SPR-III and SPR-IV cooldown was calculated for external cooling system operation to determine if cooling by external tubes would be practical for SPR-IV.

5.2.1 SPR-III Model

The thermal response at the SPR fuel plate was modeled in 2-D R-theta geometry using the TAC2D heat transfer code [5-1]. The model is shown in Figure 5.2-2. The cooling surface was divided into three regions which reflected general flow patterns. The cooling in each region was determined with a separate heat transfer coefficient. The analysis consisted of matching the measured plate surface temperature history with a TAC2D calculation using the measured inlet coolant temperature. Unknown parameters were the three heat transfer coefficients and the adiabatic maximum temperature for the plate. A radial fission profile, from the SPR-III SAR [5-2], was used in obtaining initial plate temperature profiles.

Initially it appeared that a reasonable model would be difficult to obtain due to the number of unknown parameters. The cooldown history, however, has information which can be used in a time sequence to approximate each parameter separately. For example, the maximum surface temperature measured in the first minute of cooling is strongly influenced by thermal relaxation in the fuel with weak dependence on the surface cooling. The initial surface temperature decline is a local effect dependent on the heat transfer coefficient in the immediate region of the thermocouple. The tail of the temperature history just prior to coolant shut off and the equilibrium fuel temperature after shut off are sensitive to the heat transfer coefficient for the overall plate. By combining all of these aspects into the analysis, a model can be structured in an acceptable manner.

Two SPR-III pulse runs were analyzed. Each had approximately the same yield, but differed in the external cooling evaporative coil setup which governs the inlet temperature and the gas flow rate, Figure 5.2-3. The inlet temperature corresponding to coil configuration A

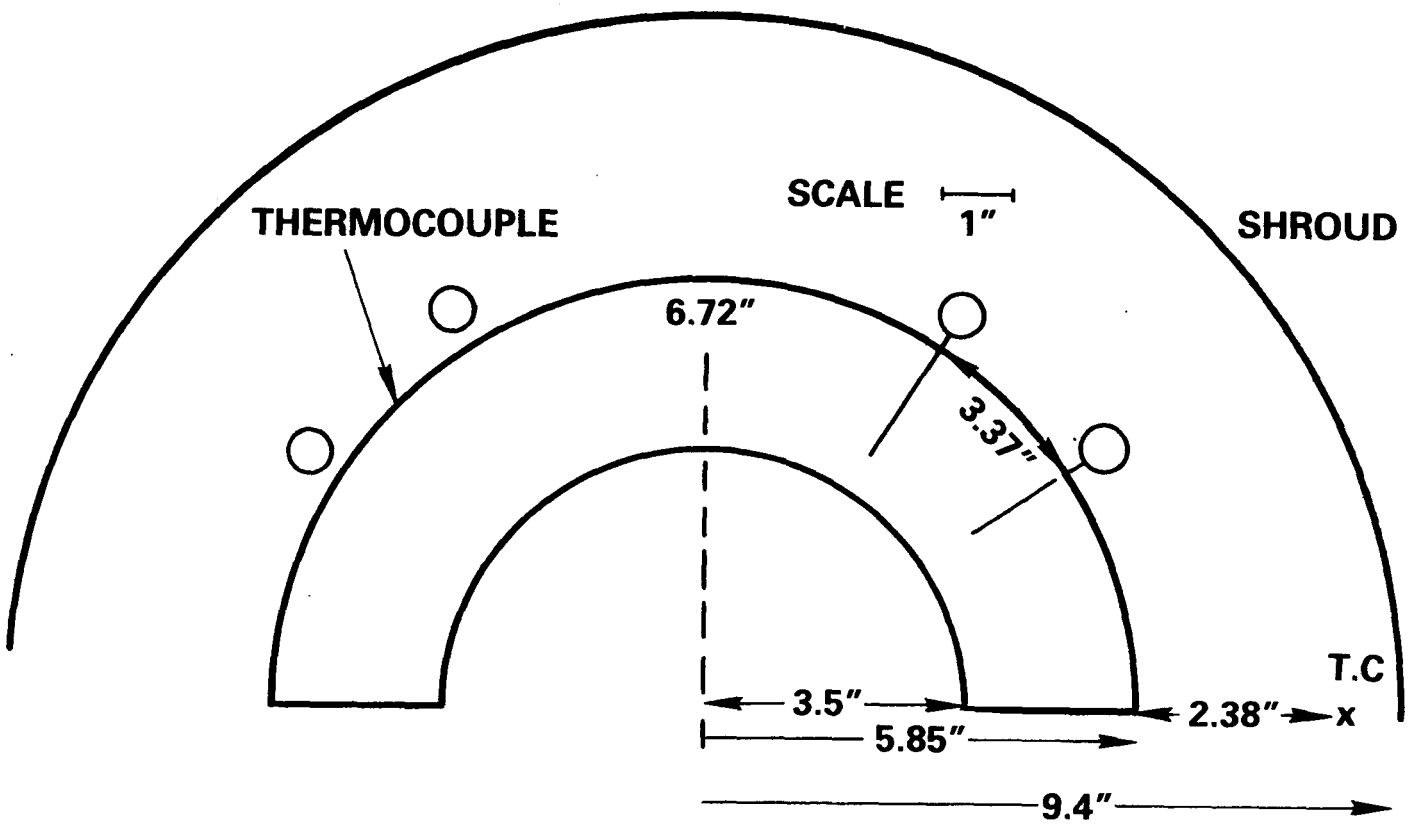

Figure 5.2-1

SPR-III Plate and Cooling Geometry

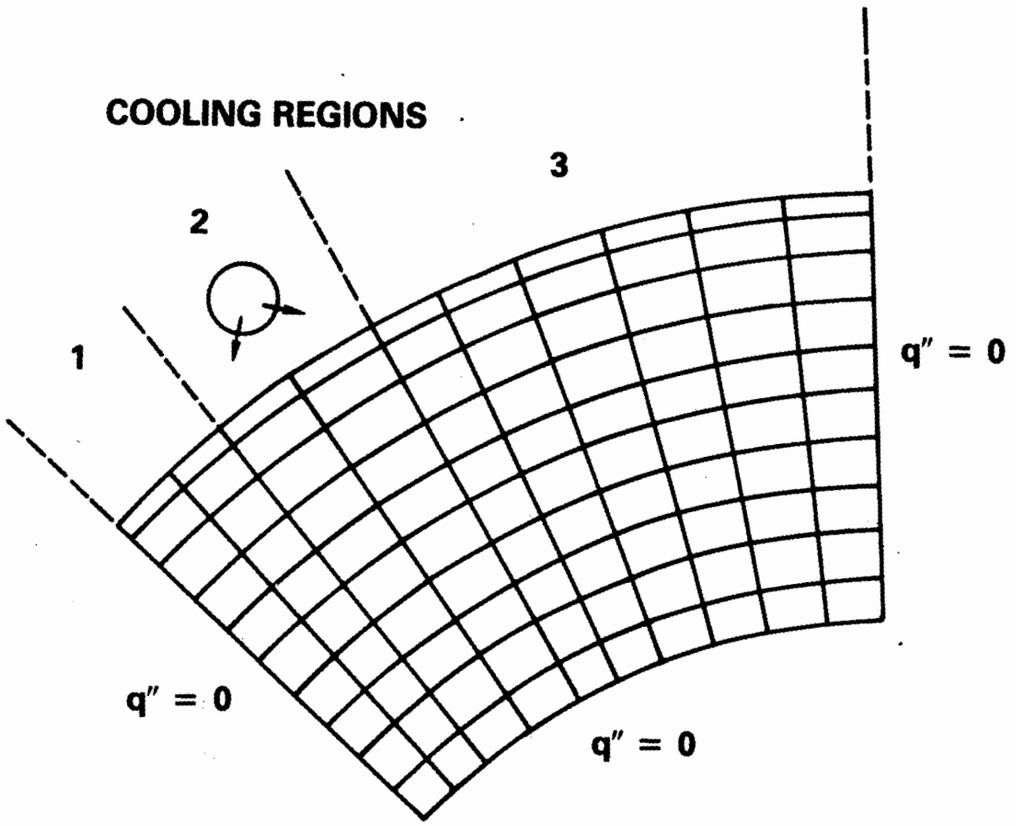

Figure 5.2-2

Thermal Model for SPR-III Fuel Plate

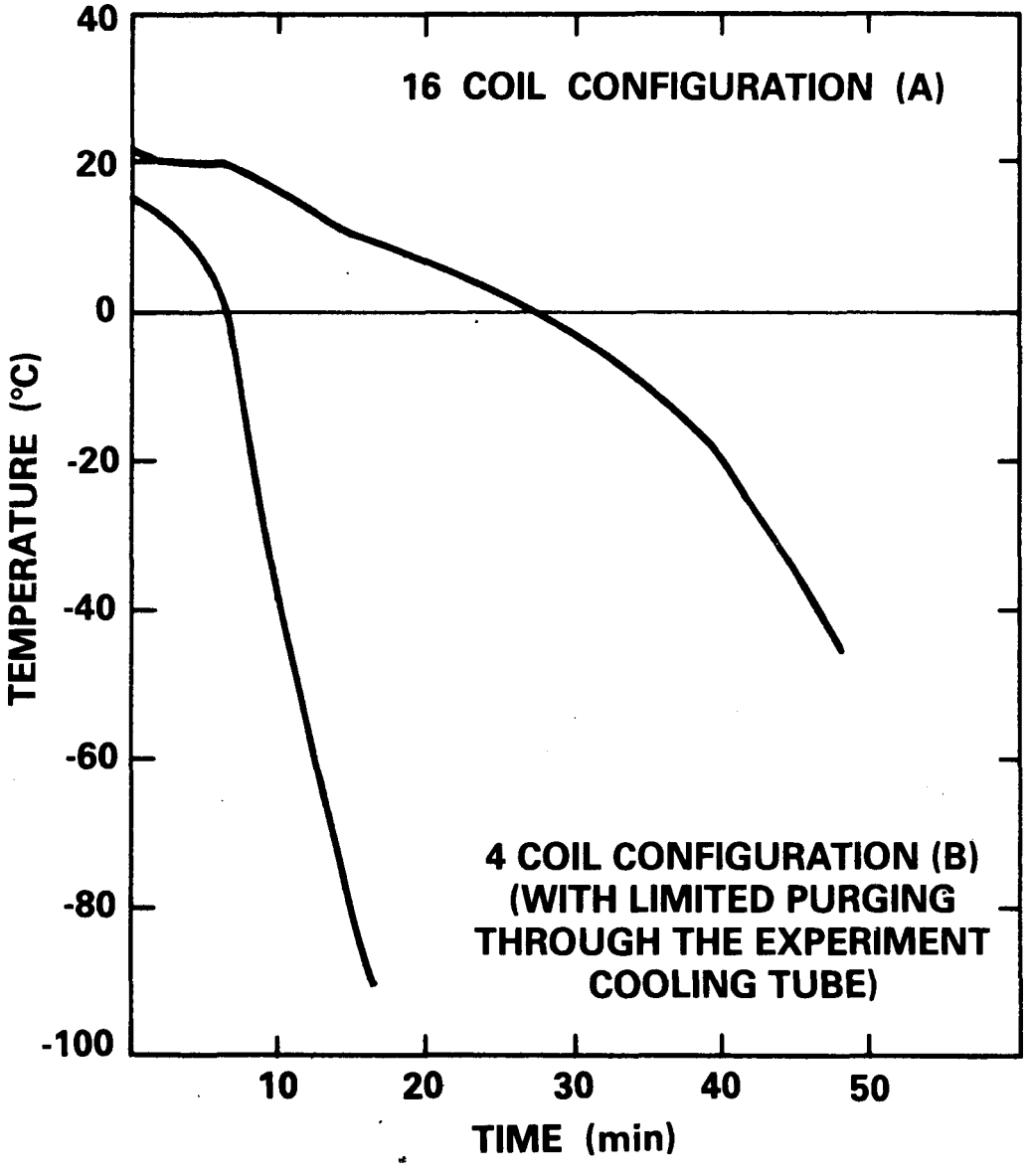

Figure 5.2-3

Reactor Stand Inlet Nitrogen Temperature for Pulse Operation

corresponds to the normal operational mode for SPR-III. Configuration B, with a minimum of coils operative, employed a partial system chilldown prior to pulsing. This produced rapid gas temperature drops at a slightly higher flow rate than coil configuration A.

Shown in Figures 5.2-4 and 5.2-5 are the measured and calculated surface temperatures for SPR-III. The maximum adiabatic temperature at the axial plane of the measurement was determined to be ~270°C. Tabulated heat transfer coefficients are presented in Table 5.2-1.

5.2.2 SPR-IV Model

The purpose of evaporative coil configuration B was to investigate probable optimum performance of an external cooling system to reduce core cooldown time. From measurements it was determined that minor changes in the external system would make it possible to obtain -100°C gas on demand. For this inlet gas temperature a SPR-IV model was formulated using initial temperature profiles as determined from SPR-IV neutronic calculations and scaled heat transfer coefficients based on the previous SPR-III model. The heat transfer coefficients were scaled according to the increased surface area dimensional changes for SPR-IV as compared to SPR-III, Table 5.2-2. Shown in Figure 5.2-6 are estimated cooldown rates for SPR-IV. Compared to calculated SPR-III cooldown rates, SPR-IV requires cooldown times of about twice those of SPR-III. The estimated 55 minute cooldown time for SPR-IV is within the bounds set for maximum allowable cooldown time. However, this estimated time requires an improved or an optimum external cooling system operation. With "routine" operation of the current external cooling system, the external tube cooling concept would not be acceptable from the standpoint of excessive cooldown time.

5.3 Interior Gas Plenum

An important quantity required for assessing the cooldown rate of the SPR-IV core using an interior gas plenum design is the mass flow rate of the gas. For an estimate of the gas flow capable of being delivered by the current external cooling system, gas temperature at the inlet and exit of the SPR-III reactor stand was measured during steady state operation. Using the known neutronic power (neutronic), the flow rate was determined. As a cross-check on this method, the average rate of

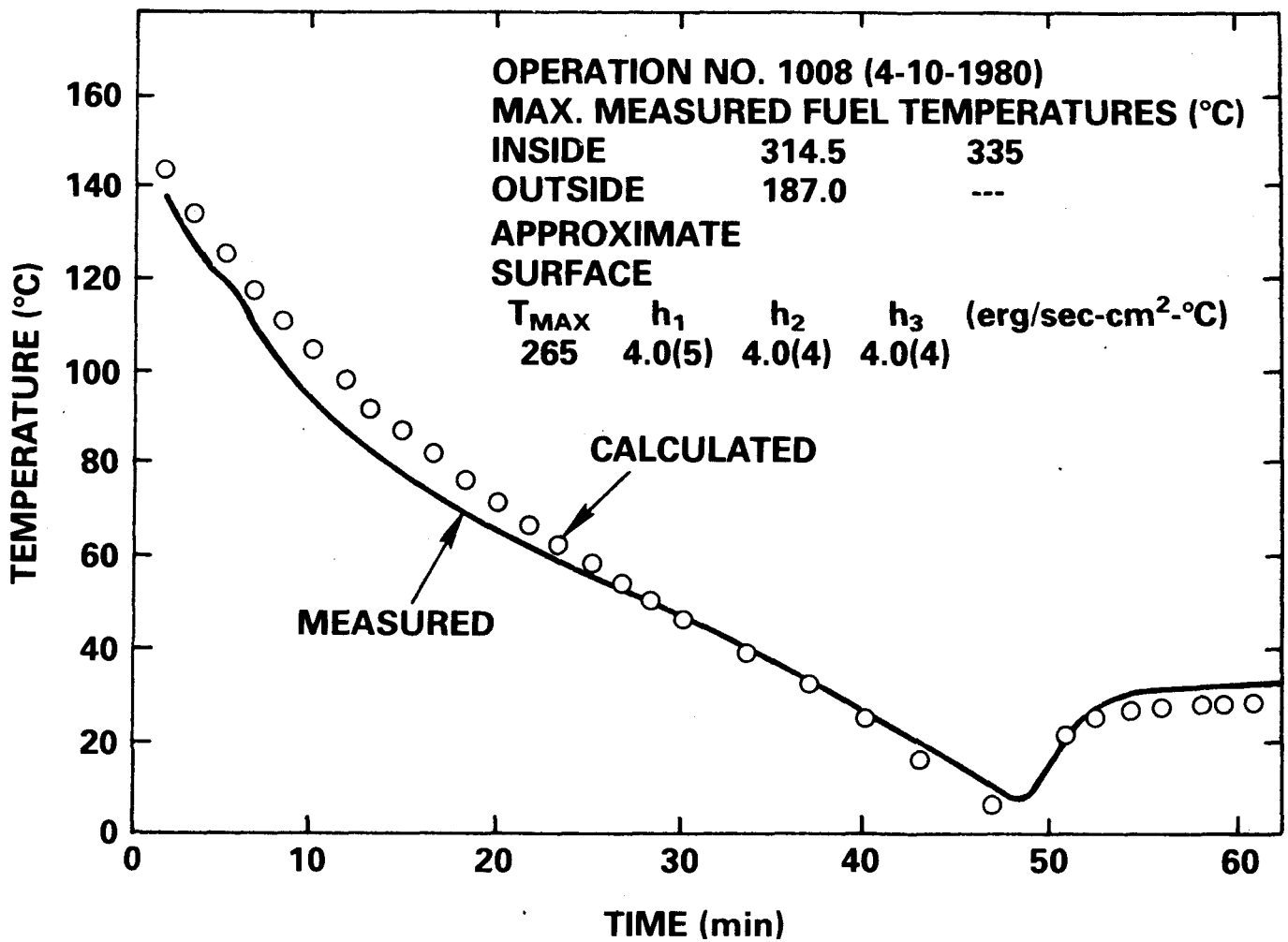

Figure 5.2-4

Surface Cooldown for the SPR-III Core,
Coil Configuration A (16 coils)

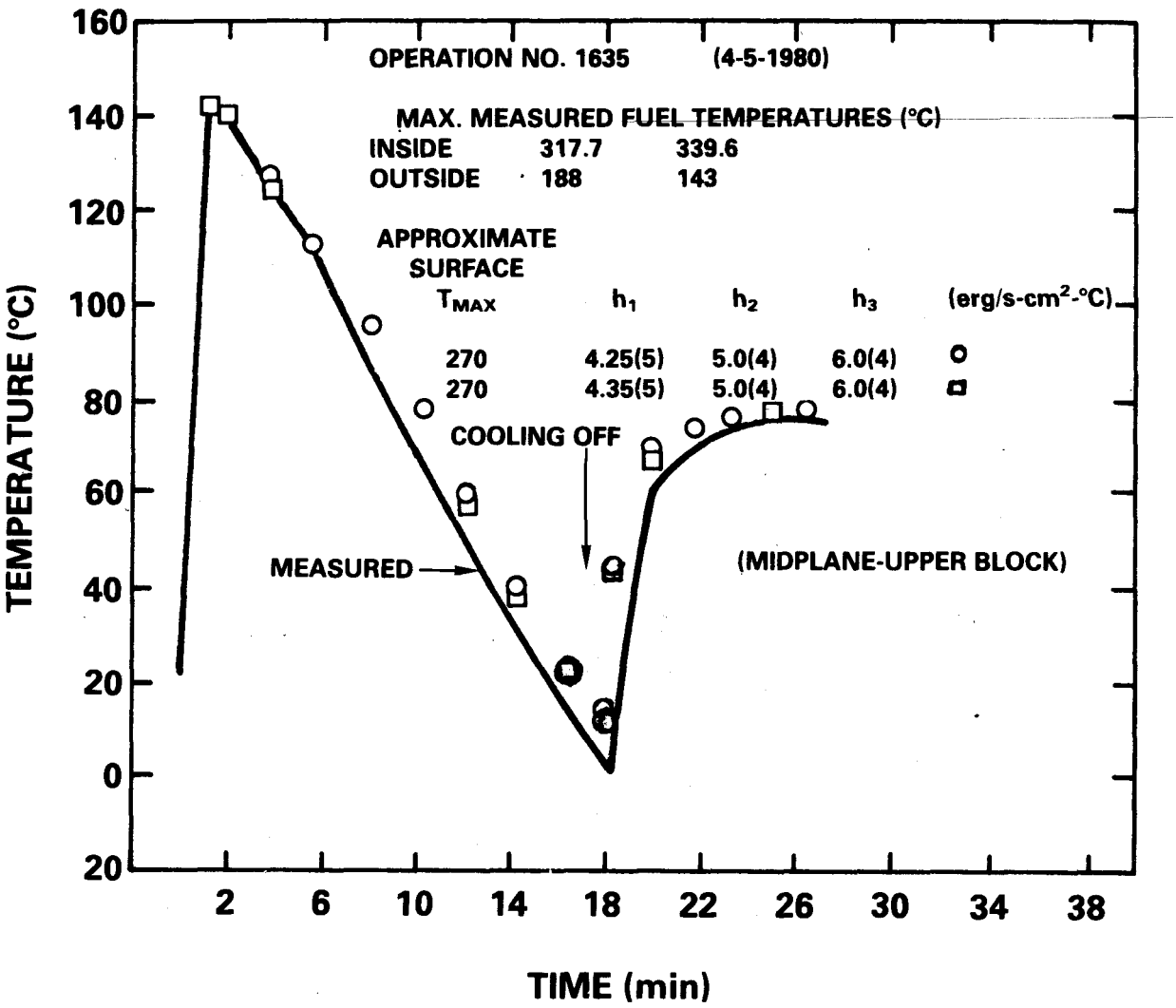

Figure 5.2-5

Surface Cooldown for SPR-III Core,
Coil Configuration B (4 coils)

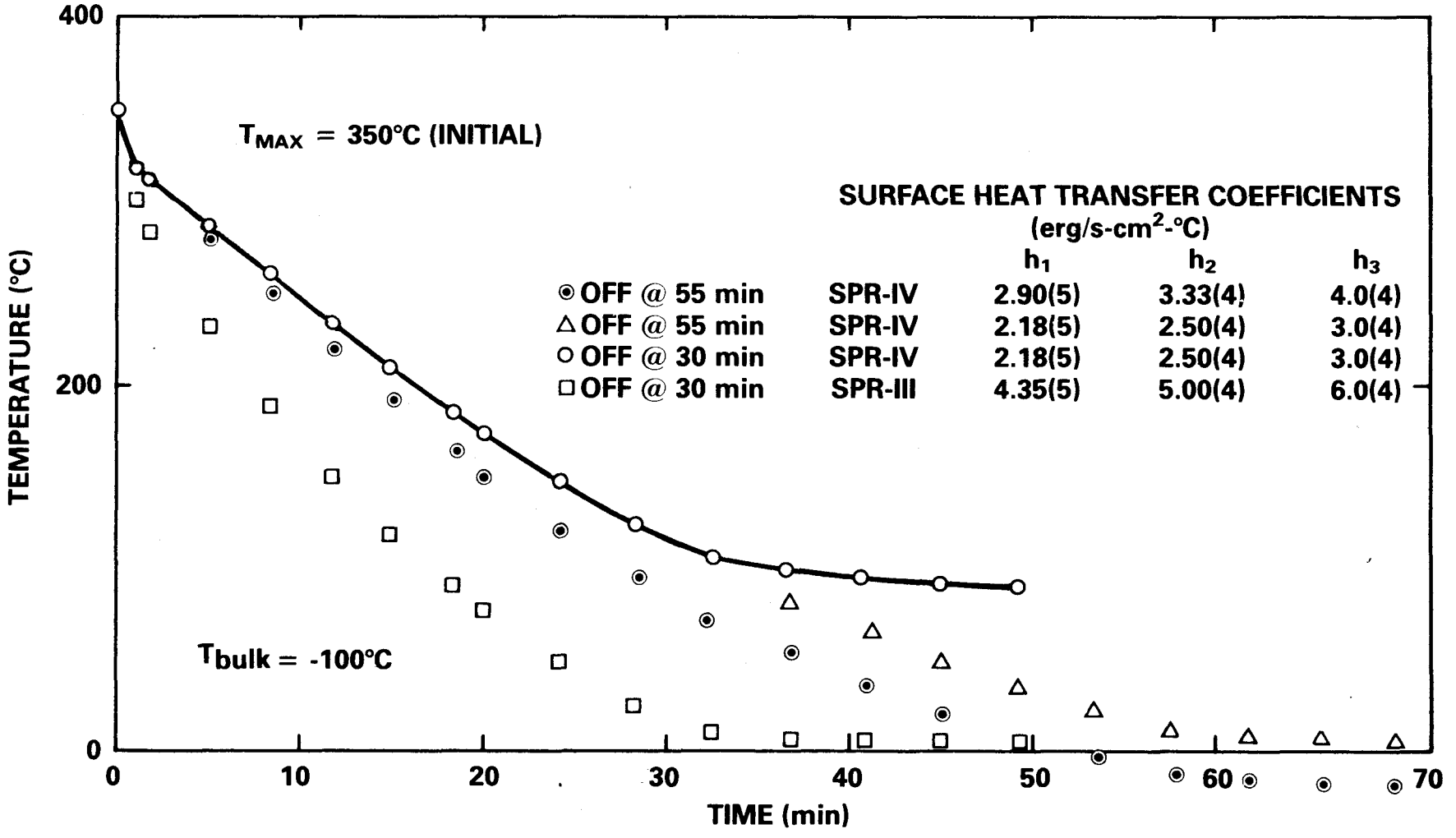

Figure 5.2-6

Maximum Plate Temperature During Cooldown for SPR-IV

Table 5.2-1

Estimated Regional Heat Transfer Coefficients

for SPR-III

Coil Setup	Heat Transfer Coeff (10^{-4} erg/s-cm^2-°C) $T_{max} \sim 270$°C for plate Region 1	Region 2	Region 3
16	40.0	4.0	4.0
4	43.5	5.0	6.0

Table 5.2-2

Geometric Scaling of SPR Heat Transfer Coefficients

SPR-III Heat Transfer Coeff (10^{-4} erg/s-cm^2-°C)	SPR-IV ARC Ratio Factor	SPR-IV Length Ratio Factor	SPR-IV Heat Transfer Coeff (Approx)
43.5	1.453 to 1.539	1.333	21.8
5.0	1.453 to 1.539	1.333	2.5
6.0	1.453 to 1.539	1.333	3.0

h(SPR-IV) = h(SPR-III)/(ARC Ratio * Length Ratio)

change of liquid nitrogen level was noted during the extended steady state operations and converted to a gas flow rate. The flow rates derived from the two methods were in good agreement. These measurements indicated that the coolant mass flow rate was in the range of 45 to 50 g/s. This flow rate was used to estimate the heat transfer characteristics of plate cooling based on parallel duct heat transfer correlations for laminar flow (duct width of .0508 cm, 20 mils). The improvement of the parallel duct heat transfer over the previous gas jet cooling method is indicated in Figure 5.3-1. In this calculation the flow rate over the end surfaces of the plate (1.59 cm thick) was taken to be 1.79 g/s. This flow equates to a flow over a plate in a stack of 15,* in which the total flow of 25 g/s is equally distributed between gaps (1.79 g/s per interior plate). As indicated in Figure 5.3-1 cooldown time with this method is about half the time for jet cooling. Increasing the thickness of the plates will increase cooldown time in a manner inversely proportional to plate thickness providing the mass flow rate is the same. However, for a fixed core length increasing plate thickness will also increase average mass flow rate through the channels between plates, assuming constant gas supply to the reactor. This compensating effect of the increased mass flow with plate thickness on cooldown time is shown in Figure 5.3-2.

Cooling a single plate as indicated above can be put in the perspective of cooldown of a complete stack of plates as shown in Figure 5.3-3. In this model, the upper plate has more gas flow alloted for it by including an additional gas channel above the plate. The additional gas flow that the upper plate receives offsets reduced "channel" inlet temperature as a result of being at the end of the plenum; and in the actual SPR-IV core it offsets the effect of axial temperature peaking near this location in the lower core-half.

For the stack the flow rate was taken as 10.74 g/s at this inlet so that flow through each gap was 1.79 g/s. Shown in Figure 5.3-4 are time snap shots of the temperature profile in the stack at 30 minutes for different sets of parameters or conditions. In Figure 5.3-4(b), the nominal cooldown profile is represented. Plates 3 and 4 which are one plate separated from the boundary plates exhibit behavior similar to the single plate model described above. The enhanced cooling of the top plate is evident in this figure.

*In the final design each core half contains 9 plates. The thickness of each of the 8 B plates is 1.083 inches.

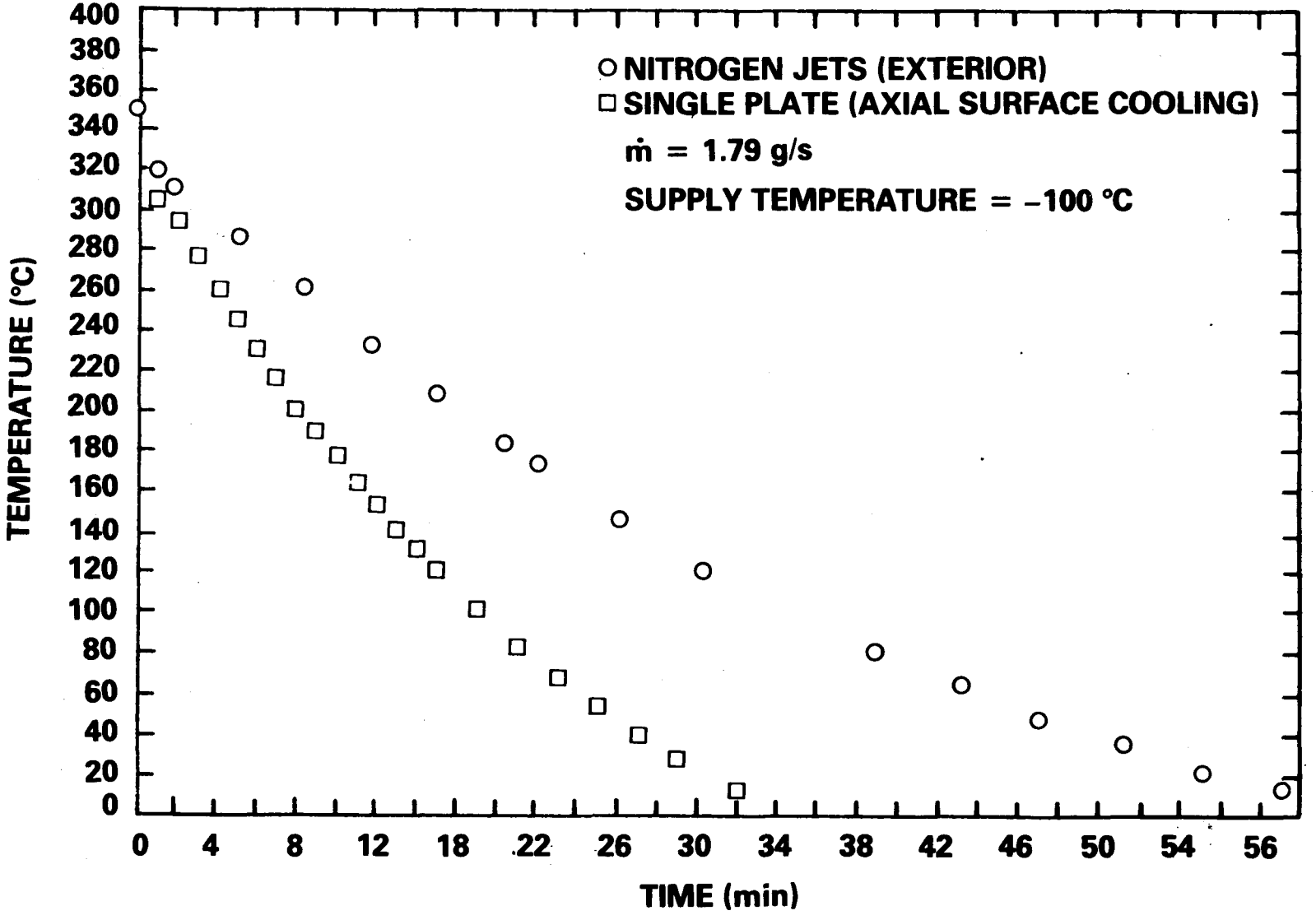

Figure 5.3-1
Maximum Fuel Plate Temperature History

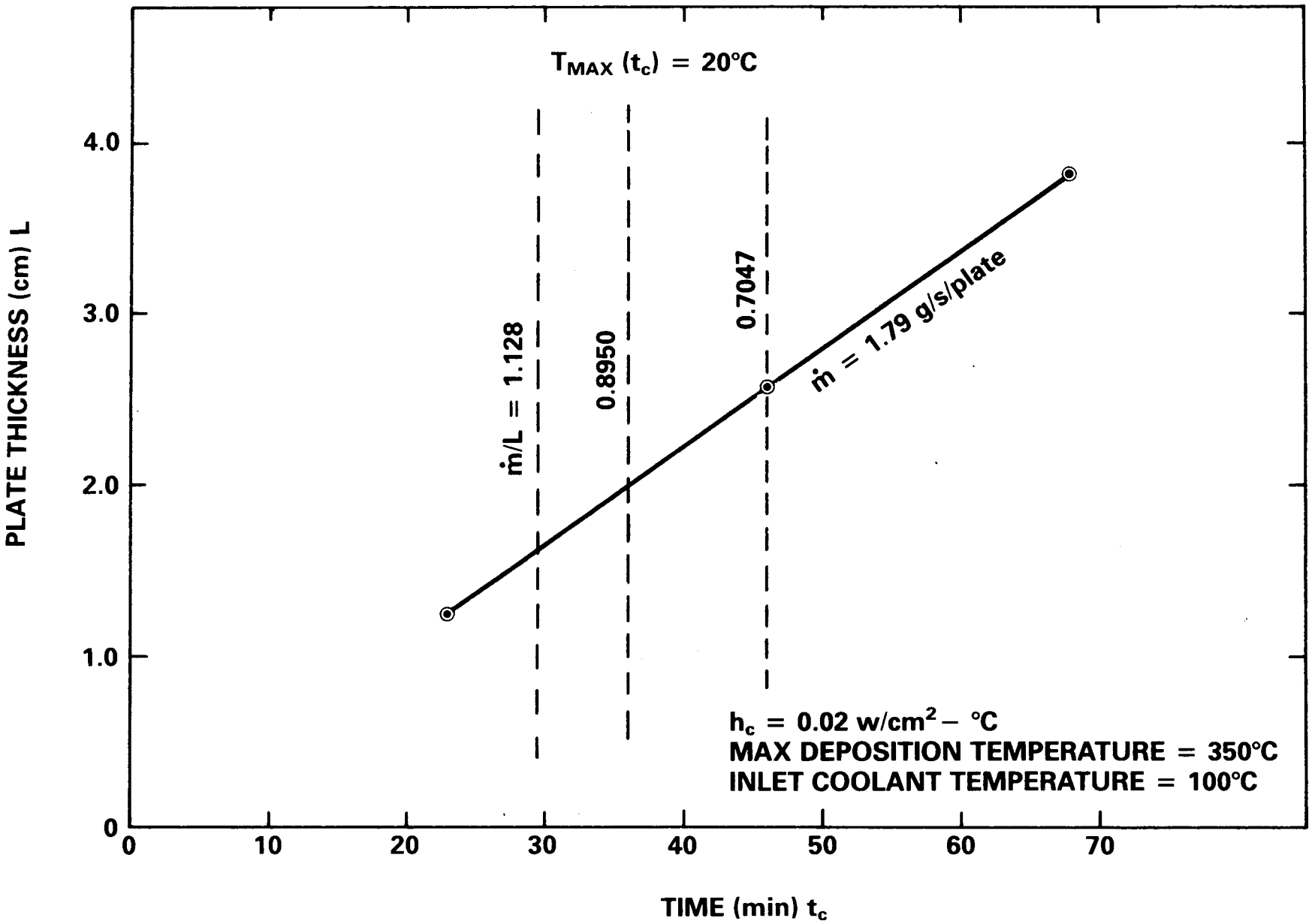

Figure 5.3-2

Cooldown Time Based on Maximum Plate Temperature T_{max} (t_c = 20°C)

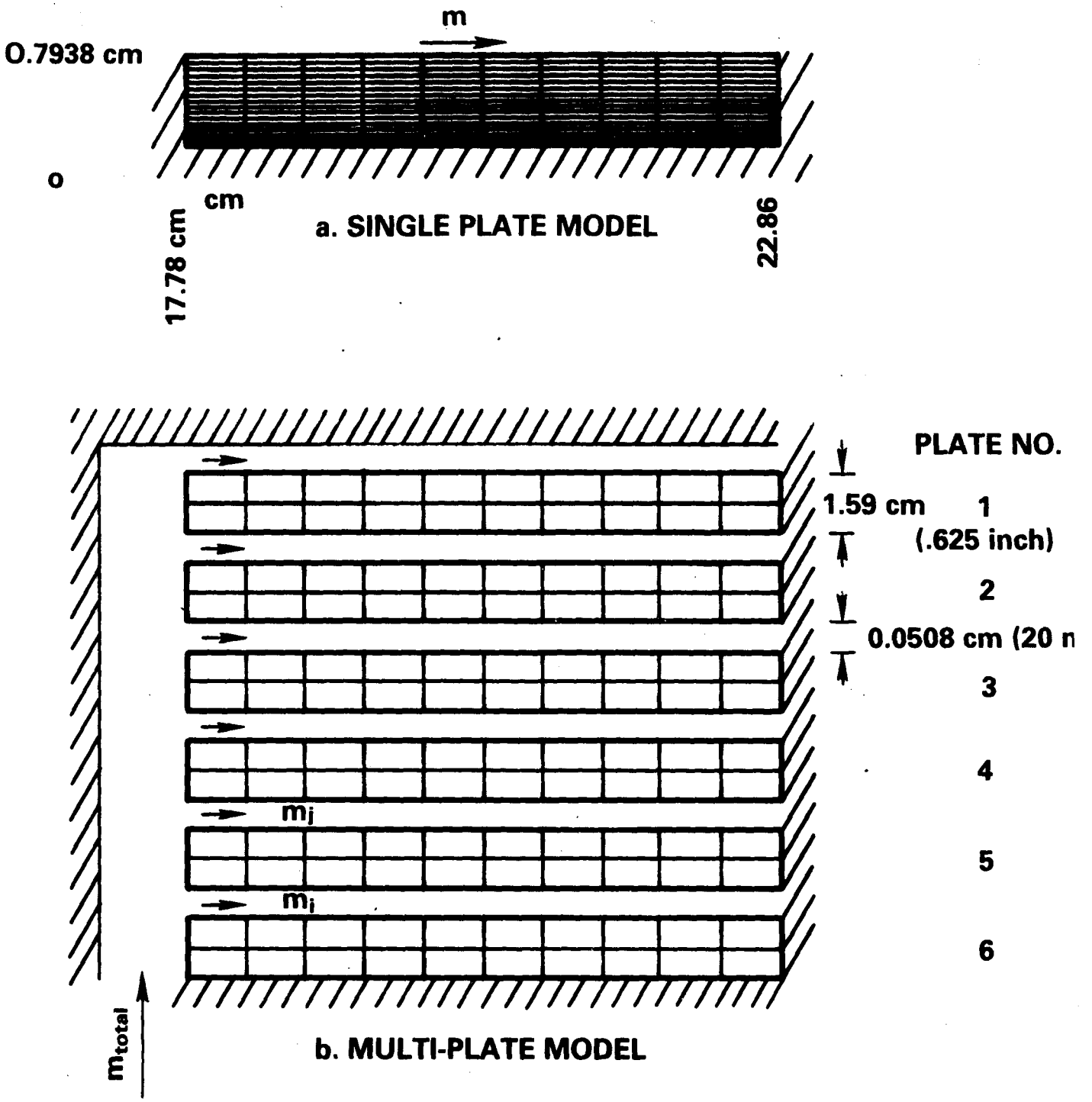

Figure 5.3-3

SPR-IV Heat Transfer Models for Gap Flow Cooling

Temperatures (K)

	1	2	3	4	5	6	7	8	9	10	11	12	Plate #
1	0	0	0	0	0	0	0	0	0	0	0	0	
2	→0	306	329	343	350	349	341	325	304	277	245	0	
3	0	306	329	343	350	349	341	325	304	277	245	0	1
4	0	306	329	343	350	349	341	325	304	277	245	0	
5	→0	306	329	343	350	349	341	325	304	277	245	0	
6	0	306	329	343	350	349	341	325	304	277	245	0	2
7	0	306	329	343	350	349	341	325	304	277	245	0	
8	→0	306	329	343	350	349	341	325	304	277	245	0	
9	0	306	329	343	350	349	341	325	304	277	245	0	3
10	0	306	329	343	350	349	341	325	304	277	245	0	
11	→0	306	329	343	350	349	341	325	304	277	245	0	
12 $\dot{m}_j$	0	306	329	343	350	349	341	325	304	277	245	0	4
13	0	306	329	343	350	349	341	325	304	277	245	0	
14 $\dot{m}_i$	→0	306	329	343	350	349	341	325	304	277	245	0	
15	0	306	329	343	350	349	341	325	304	277	245	0	5
16	0	306	329	343	350	349	341	325	304	277	245	0	
17	→0	306	329	343	350	349	341	325	304	277	245	0	
18	0	306	329	343	350	349	341	325	304	277	245	0	6
19	↑ 0	306	329	343	350	349	341	325	304	277	245	0	
20	0	0	0	0	0	0	0	0	0	0	0	0	

$\dot{m}_{tot}$

(a) Input

	1	2	3	4	5	6	7	8	9	10	11	12
1	0	0	0	0	0	0	0	0	0	0	0	0
2	-65	-53	-34	-23	-15	-10	- 6	- 3	0	0	2	0
3	-68	-12	-10	- 8	- 5	- 3	0	0	2	3	3	0
4	-73	-12	-10	- 7	- 4	- 2	0	1	2	3	3	0
5	-76	-49	-21	-10	- 5	- 2	0	2	3	4	5	0
6	-78	- 7	- 5	- 2	0	2	4	5	6	7	8	0
7	-81	- 8	- 5	- 2	0	2	4	5	7	7	8	0
8	-83	-52	-20	- 3	- 2	0	3	5	7	8	9	0
9	-84	- 6	- 4	- 1	1	4	6	8	9	10	10	0
10	-87	- 6	- 4	- 1	1	4	6	8	9	10	10	0
11	-88	-55	-20	- 6	0	3	5	8	9	11	12	0
12	-89	- 5	- 2	1	4	6	9	11	12	13	13	0
13	-91	- 5	- 2	1	4	7	9	11	12	13	14	0
14	-92	-56	-17	- 3	3	7	10	12	14	16	17	0
15	-93	0	3	7	10	13	15	17	19	20	20	0
16	-95	0	3	7	10	13	16	18	19	20	21	0
17	-96	-53	- 9	6	13	17	20	22	24	25	26	0
18	-97	16	19	21	24	26	28	29	30	31	31	0
19	-99	19	21	23	25	27	28	30	31	31	32	0
20	0	0	0	0	0	0	0	0	0	0	0	0

(b) h_{gap} = 2.0(5)[erg/cm^2-S-K], h_{plenum} = 2.0(4), $\dot{m}_{tot}$ = 10.74 g/s

	1	2	3	4	5	6	7	8	9	10	11	12
1	0	0	0	0	0	0	0	0	0	0	0	0
2	-99	-83	-60	-45	-36	-29	-25	-21	-18	-16	-15	0
3	-99	-31	-29	-26	-23	-21	-18	-16	-15	-14	-13	0
4	-99	-30	-28	-25	-22	-20	-18	-16	-14	-13	-13	0
5	-99	-69	-37	-25	-19	-16	-13	-11	-10	- 8	- 8	0
6	-99	-17	-15	-12	-10	- 8	- 6	- 4	- 3	- 2	- 2	0
7	-99	-17	-15	-12	- 9	- 7	- 5	- 3	- 2	- 1	- 1	0
8	-99	-64	-27	-14	- 8	- 4	- 1	0	1	2	3	0
9	-99	- 7	- 5	- 2	0	2	5	6	8	6	9	0
10	-99	- 7	- 4	- 1	1	3	5	7	8	9	10	0
11	-99	-60	-19	- 4	2	6	9	11	13	14	15	0
12	-99	2	5	8	11	14	16	18	19	20	21	0
13	-99	3	5	9	12	14	17	19	20	21	21	0
14	-99	-55	- 9	7	14	18	21	24	26	27	28	0
15	-99	15	14	22	25	28	30	32	34	34	35	0
16	-99	16	19	23	26	29	31	33	34	35	36	0
17	-99	-47	5	24	31	35	38	40	42	43	43	0
18	-99	39	41	43	45	47	49	50	51	51	52	0
19	-99	42	43	45	46	48	49	51	51	52	52	0
20	0	0	0	0	0	0	0	0	0	0	0	0

(c) h_{gap} = 2.0(5), h_{plenum} = 0.0, $\dot{m}_{tot}$ = 10.74

Figure 5.3-4
SPR-IV Cooldown at 30 minutes (18 O.D. Multi-Phase)

	1	2	3	4	5	6	7	8	9	10	11	12
1	0	0	0	0	0	0	0	0	0	0	0	0
2	-43	-43	-43	-43	-43	-43	-43	-43	-43	-43	-43	0
3	-45	234	235	236	237	238	239	239	240	240	240	0
4	-50	234	235	236	237	238	239	239	240	240	240	0
5	-52	-52	-52	-52	-52	-52	-52	-52	-52	-52	-52	0
6	-54	231	233	234	235	236	327	237	238	238	238	0
7	-59	231	233	234	235	236	237	237	238	238	238	0
8	-61	-61	-61	-61	-61	-61	-61	-61	-61	-61	-61	0
9	-63	229	230	232	233	234	235	235	236	236	236	0
10	-68	229	230	232	233	234	235	235	236	236	236	0
11	-70	-70	-70	-70	-70	-70	-70	-70	-70	-70	-70	0
12	-73	227	228	229	231	232	232	233	233	234	234	0
13	-77	227	228	229	231	232	232	233	233	234	234	0
14	-80	-80	-80	-80	-80	-80	-80	-80	-80	-80	-80	0
15	-82	224	226	227	228	229	230	231	231	231	232	0
16	-87	224	226	227	228	229	230	231	231	231	232	0
17	-90	-90	-90	-90	-90	-90	-90	-90	-90	-90	-90	0
18	-92	222	223	225	226	227	228	228	229	229	229	0
19	-97	222	223	225	226	227	228	228	229	229	229	0
20	0	0	0	0	0	0	0	0	0	0	0	0

(d) $\dot{m}_j$ = o, h_{plenum} = 2.0(4), $\dot{m}_{tot}$ = 10.74

	1	2	3	4	5	6	7	8	9	10	11	1
1	0	0	0	0	0	0	0	0	0	0	0	
2	-42	-26	- 9	- 1	3	6	8	11	12	13	14	
3	-46	- 1	9	3	6	8	10	12	13	14	15	
4	-55	- 1	1	3	6	8	10	12	13	14	15	
5	-68	-26	- 3	2	5	7	9	11	13	14	14	
6	-63	- 2	0	3	6	8	10	12	13	14	14	
7	-69	- 3	0	3	5	8	10	11	13	14	14	
8	-72	-32	- 6	0	3	5	8	10	11	12	13	
9	-74	- 6	- 3	0	3	5	8	9	11	12	12	
10	-78	- 7	- 3	0	2	5	7	9	11	11	12	
11	-81	-38	- 9	- 3	0	3	5	8	9	10	11	
12	-82	- 9	- 6	- 2	0	3	6	7	9	10	10	
13	-86	-10	- 6	- 2	0	3	5	7	9	10	10	
14	-88	-42	-11	- 4	0	2	5	7	9	10	10	
15	-89	-10	- 5	- 2	0	3	6	8	9	10	11	
16	-92	-10	- 6	- 2	1	4	6	8	10	11	11	
17	-94	-42	- 5	- 1	2	5	7	9	11	12	12	
18	-95	- 3	0	3	5	8	10	11	13	13	14	
19	-98	0	1	4	6	8	10	12	13	14	14	
20	0	0	0	0	0	0	0	0	0	0	0	

(e) h_{gap} = 4(5), h_{plenum} = 4(4), $\dot{m}_{tot}$ = 10.74

	1	2	3	4	5	6	7	8	9	10	11	12
1	0	0	0	0	0	0	0	0	0	0	0	0
2	-95	-94	-91	-89	-87	-86	-84	-83	-82	-81	-80	0
3	-96	-84	-83	-83	-82	-81	-80	-80	-79	-79	-79	0
4	-96	-84	-83	-82	-82	-81	-80	-79	-79	-78	-78	0
5	-96	-93	-88	-85	-83	-81	-80	-79	-78	-78	-77	0
6	-97	-81	-80	-79	-78	-78	-77	-76	-75	-75	-75	0
7	-97	-81	-80	-79	-78	-77	-76	-76	-75	-75	-75	0
8	-97	-93	-87	-83	-81	-79	-77	-76	-75	-74	-74	0
9	-97	-79	-78	-77	-76	-75	-74	-73	-72	-72	-72	0
10	-98	-79	-78	-77	-76	-75	-74	-73	-72	-72	-71	0
11	-98	-93	-86	-82	-79	-76	-75	-73	-72	-71	-70	0
12	-98	-76	-75	-74	-73	-72	-70	-69	-69	-68	-68	0
13	-98	-76	-75	-74	-73	-71	-70	-69	-68	-68	-67	0
14	-98	-92	-84	-79	-75	-72	-70	-68	-67	-66	-65	0
15	-98	-71	-70	-69	-67	-65	-64	-63	-62	-61	-61	0
16	-99	-71	-70	-68	-67	-65	-63	-62	-61	-61	-60	0
17	-99	-91	-79	-72	-67	-64	-62	-60	-58	-57	-56	0
18	-99	-59	-58	-57	-55	-54	-53	-52	-51	-51	-51	0
19	-99	-57	-57	-56	-54	-53	-52	-52	-51	-50	-50	0
20	0	0	0	0	0	0	0	0	0	0	0	0

(f) h_{gap} = 2.0(5), h_{plenum} = 2.0(4), $\dot{m}_{tot}$ = 2 * 10.74

	1	2	3	4	5	6	7	8	9	10	11	12
1	0	0	0	0	0	0	0	0	0	0	0	0
2	-99	-98	-95	-93	-91	-90	-88	-87	-86	-85	-84	0
3	-99	-88	-87	-87	-86	-85	-84	-84	-83	-83	-83	0
4	-99	-87	-87	-86	-85	-85	-84	-83	-83	-83	-82	0
5	-99	-96	-91	-88	-86	-84	-83	-82	-81	-81	-80	0
6	-99	-83	-82	-82	-81	-80	-79	-78	-78	-78	-77	0
7	-99	-83	-82	-81	-81	-80	-79	-78	-78	-77	-77	0
8	-99	-95	-89	-85	-82	-81	-79	-77	-76	-76	-75	0
9	-99	-79	-78	-77	-76	-75	-74	-73	-73	-72	-72	0
10	-99	-79	-78	-77	-76	-75	-74	-73	-72	-72	-72	0
11	-99	-94	-86	-81	-78	-75	-73	-72	-71	-70	-69	0
12	-99	-74	-73	-72	-71	-69	-68	-67	-66	-66	-65	0
13	-99	-74	-73	-72	-70	-69	-68	-67	-66	-65	-65	0
14	-99	-93	-82	-76	-72	-69	-66	-65	-63	-62	-61	0
15	-99	-66	-65	-64	-62	-60	-59	-58	-57	-56	-56	0
16	-99	-66	-65	-63	-61	-60	-58	-57	-56	-55	-55	0
17	-99	-90	-76	-67	-61	-58	-55	-53	-51	-50	-49	0
18	-99	-59	-50	-48	-47	-46	-45	-44	-43	-43	-42	0
19	-99	-48	-48	-47	-46	-45	-44	-43	-42	-42	-42	0
20	0	0	0	0	0	0	0	0	0	0	0	0

(g) h_{gap} = 2.0(5), h_{plenum} = 0.0, $\dot{m}_{tot}$ = 2 * 10.74

Figure 5.3-4 (cont'd)

In Figures 5.3-4(c) - (g), the effect of heat transfer variations on the stack cooling performance is indicated. Figure 5.3-4(c) shows that the plenum heat transfer does affect end plate cooldown, but as indicated in Figure 5.3-4(d) can not be used without plate flow-through since the plenum heat transfer coefficient is too low for a plenum duct width of .64 cm (.25 inch). A comparison of Figures 5.3-4(e) - (g) shows the stack cooldown is sensitive to mass flow rate but rather insensitive to small variations in the plenum and/or plate-to-plate gap or duct heat transfer coefficient.

Analysis shows that the interior plenum cooling method offers a significant improvement over the exterior tube cooling configuration both in simplicity of design and heat transfer performance. A final design will include a separate plenum for each core-half to allow physical separation of the core halves following pulsing. The plenum sizing at a duct width of .64 cm (.25 inch) assures neglible plenum pressure drops, and provides nearly equal distribution of inlet gas at all radial ducts.

5.4 External Nitrogen Cooling System

The SPR external cooling system upgrade was initiated following an analysis of the current SPR system. The analysis determined that the SPR cooling system could be significantly improved if the operator had positive control of cooling gas temperature and flow rate entering the reactor. In this respect there are two requirements that a cooling system must satisfy: (1) provide cooling gas to the reactor at low temperature immediately upon demand, and (2) maintain cooling gas temperature and flow rate at the reactor for extended periods of operation. The importance of these requirements to the efficient operation of the reactor facility has been discussed in Section 5.3. To accomplish the first requirement the upgrade system must be capable of complete system chill-down prior to supplying the reactor with cooling gas. To maintain gas temperature nearly constant heat transfer must be maintained independent of climatic variations and evaporator coils must be kept free of heavy condensation. These requirements have provided a baseline set of specifications for a SPR external cooling system upgrade, Figure 5.4-1. The design of the upgrade has been made by the BDM Corporation [5-3]. Pertinent excerpts from Reference 5-3, restating specifications and a description of the system are included in Section 5.4.2.

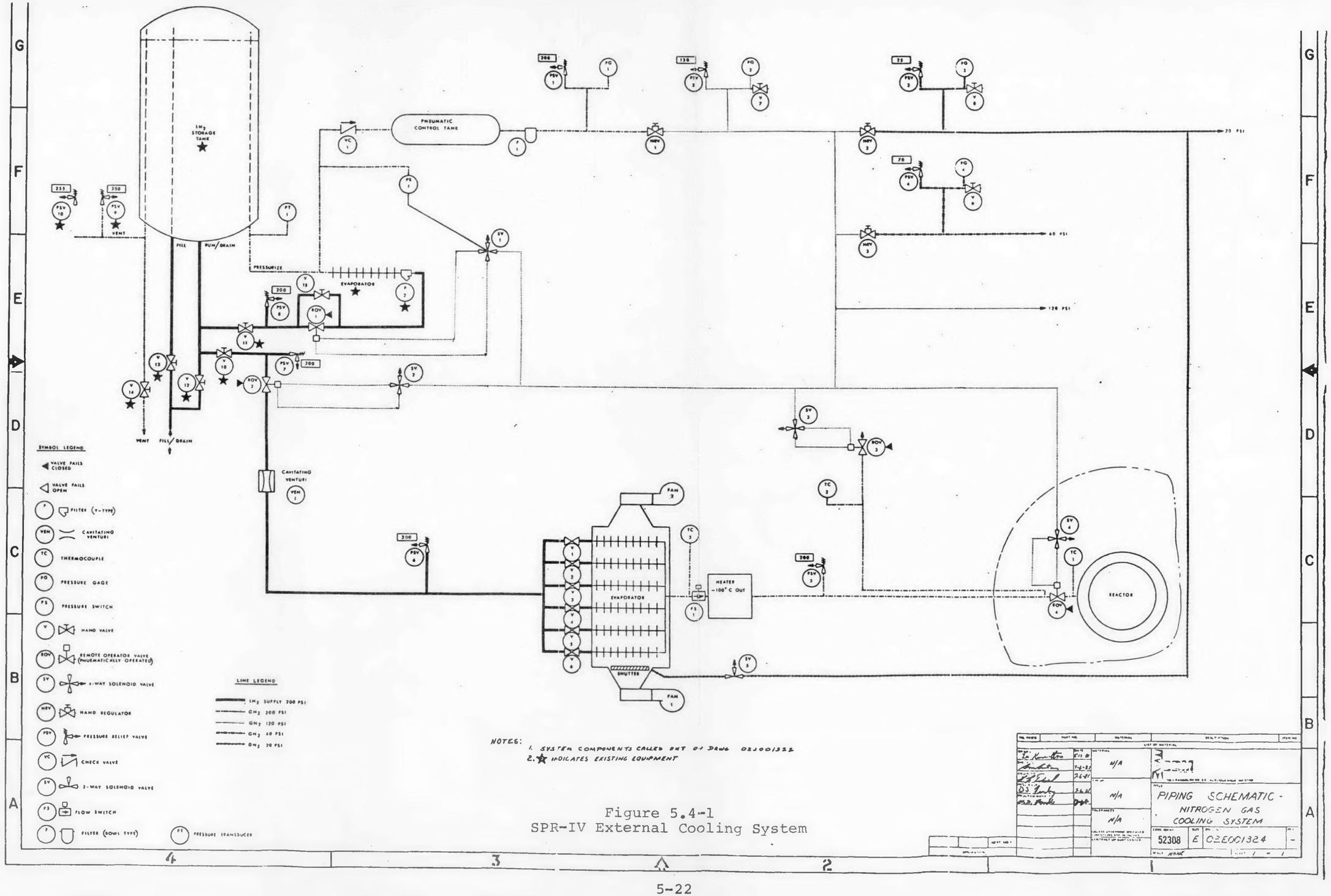

Figure 5.4-1
SPR-IV External Cooling System

5.4.1 Design Requirements

1. Flow rate and temperatures must be 50 to 90 grams/sec of N_2 at minus 100° + 10°C at the reactor stand.

2. Additional regulated N_2 ambient temperature supplies are required at 20 psig, 60 psig, and 120 psig.

3. Reuse as much of existing system as possible.

4. All automatic controls, with manual over-rides, are to be located in the existing control room. Locations of controls must be coordinated with the SPR operational staff.

5. The design should, where practical, minimize the time required that SPR be out of service during installation.

5.4.2 System Description and Operation

5.4.2.1 Description of the Nitrogen Gas Cooling System

The nitrogen gas cooling system is composed of two subsystems -- the reactor cooling subsystem and the pressure control subsystem. Both systems use the LN_2 stored in the storage tank for the control pressure and cooling gas. The piping schematic drawing 02E001324, Figure 5.4-1, can be referenced to supplement this description.

1. Pressure Control Subsystem -- The pressure control system supplies pneumatic control to all remote operated valves, evaporator shutter, and tank pressure pressurization for the nitrogen gas cooling system. In addition it will be used for other functions in the reactor area independent of the cooling system. To analyze the operation of this subsystem, a description of each component will be useful. Main control of the gaseous nitrogen, GN_2, supply is done in the control room.

   a. LN_2 Storage Tank -- This tank stores liquid nitrogen to be used for both cooling the reactor and supplying the nitrogen for the pneumatic controls. The pressure in this tank will be maintained at 190 psi.

b. V 11 -- This hand valve is used to shut off the LN_2 supply to ROV 1. The only time that it needs to be closed is when repair is being made either to the PSV 8 or ROV 1 or for GN_2 conservation when the system is to be shut down for long periods of time.

c. PSV 8 -- This is a pressure relief valve set at 200 psi. Its purpose is to relieve pressure in the line between V 11 and ROV 1 in case of LN_2 lockup if both valves are closed and subsequent pressure buildup takes place.

d. ROV 1 -- This is a remotely operated valve controlled by a preset pressure switch. When open, it allows the LN_2 to flow to the Y filter F 2 and to the evaporator coils. These coils then evaporate the LN_2 producing gaseous nitrogen, GN_2, at 190 psig. The GN_2 then pressurizes both the LN_2 storage tank and the pneumatic control tank.

e. V 15 -- This valve is normally closed during operation. It is used to allow LN_2 into the evaporator when actual pressure is too low to operate the ROV. This will allow system pressure to build up to operating conditions.

f. VC 1 -- This is a check valve which allows the GN_2 into the pneumatic control tank but stops the flow in the other direction. During down time to the LN_2 storage tank such as when it is vented for filling, the pneumatic control tank can maintain pressure for pneumatic operation.

g. PS 1 -- This is a pressure switch that can be set in the field. It switches 28 VDC power to the solenoid valve SV 1 which opens ROV 1 when pressure in the LN_2 storage tank drops below the set pressure. Power is supplied to it from the control panel in the control building.

h. SV 1 -- This is a four way solenoid valve that operates on 28 VDC. 120 psi GN_2 is fed into the valve and diverted to the top of the remotely operated valve ROV 1. This pressurizes the valve in the closed position.

When activated, the solenoid valve vents the pressure from the top of the cylinder and pressurizes the bottom of the cylinder thus opening the ROV.

i. F 1 -- This is a T filter which filters the GN_2 coming from the pneumatic control tank.

j. PSV 1 -- This pressure relief valve is set at 200 psig and is used to guard against a LN_2 lock up between ROV 1 and HRV 1.

k. PG 1 -- This is a pressure gage used to measure the pressure in the pneumatic control tank.

l. HRV 1 -- This is a hand regulator valve which regulates the GN_2 pressure from the control tank to a pressure of 120 psig for the ROV supply.

m. PSV 2 -- This pressure relief valve is used to relieve pressure in case of a runaway hand regulator valve. It is set at 130 psig and sized to handle the maximum flow through the HRV.

n. PG 2 -- This pressure gage measures the output pressure from HRV 1.

o. V 7 -- This hand valve is used to bleed line pressure when reducing the pressure in the line to a lower value.

The balance of the system provides the same protection and supplies pressures at different desired settings.

2. Reactor Cooling Subsystem

The function of the cooling subsystem is to regulate mass flow and temperature of gaseous nitrogen to cool the reactor. The system is composed of pneumatically operated valves controlled by a remote control panel located in the control room. For operation the pressure control subsystem must be functioning. To analyze the operation of this subsystem a description of each component will be useful.

a. LN_2 Storage Tank -- This tank supplies the liquid nitrogen used to cool the reactor. It supplies the liquid to the system at pressure of 190 psig.

b. V 10 -- This is a manual valve which is used to isolate the remote operated valve from the tank.

c. PSV 7 -- This pressure relief valve protects the line between V 11 and ROV 2 from liquid lockup.

d. ROV 2 -- This remote operated valve is controlled from the control panel with a switchmarked LN_2 supply through SV 2. When open, the ROV allows LN_2 to flow to the cavitating venturi.

e. Cavitating Venturi -- This device has a variable throat area which, due to the pressure drop through the venturi, converts the LN_2 to a vapor and creates supersonic flow. By keeping the differential pressure above a minimum level required to cause cavitation, flow rates can be set and maintained independent of upstream pressure. Different flow rates can be obtained by varying the nozzle area. The nitrogen recondenses to a liquid in the expansion nozzle of the cavitating venturi and travels to the evaporator. A pressure relief valve, PSV 6, is in the line to protect the line from liquid lockup.

f. Evaporator -- The evaporator changes the LN_2 into GN_2 at a temperature below the desired operating conditions. Six hand valves control the amount of surface area at ambient temperature exposed to the LN_2. The fans and shutter are controlled remotely in the control room. The valve settings and number of fans on will depend on ambient conditions and flow rate desired.

g. TC 3 -- This is a thermocouple installed to measure the outlet temperature of the GN_2 after the evaporator. The readout is in the control room.

h. FS 1 -- This is a flow switch used to detect gas flow in the line. If no flow is detected the flow switch will interrupt power to the heater for protection of the heater.

i. Heater -- This is a process air heater used for final control of the temperature of the GN_2 before its entry into the reactor. It has an internal thermostat which turns the heater on and off when conditions dictate.

j. ROV 4 -- This remotely operated valve allows the conditioned gas to enter the reactor. It is operated in the control room by a switch labeled reactor supply.

k. TC 1 -- This thermocouple measures the temperature before entry into the reactor.

l. TC 2 -- This thermocouple measures the temperature of the GN_2 that is dumped when chilldown conditions are being used.

m. ROV 3 -- This remote operated valve is operated in the control room to dump the system for quick cooldown to operating temperature. It is operated by a switch labeled chill.

The balance of the system components such as the SV for control pressure operates the same as previous examples.

References

5-1 TAC2D: A General Purpose Two-Dimensional Heat Transfer Computer Code, GA-8868.

5-2 L. L. Bonzon, B. F. Estes, J. S. Philbin, J. A. Reuscher, Sandia Pulse Reactor-III (SPR-III): Safety Analysis Report, SLA-74-0349, Sandia National Laboratories, Albuquerque, NM (October 1974).

5-3 External Nitrogen Cooling System for the Sandia Pulse Reactor Facility, Report No. BDM/A-81-367-TR, BDM Corporation, Albuquerque, NM (September 1981).

6.0 Summary

This report summarizes the design and analysis for the SPR-IV reactor and cooling system. The reactor provides a large central cavity with a usable diameter of 34.3 cm and a height of 51.9 cm. The fuel alloy is fully enriched uranium alloyed with ten weight percent molybdenum, the same as SPR-II/III. The core is composed of 18 fuel plates with a total fuel mass of 532 kg. The reactor is similar to SPR-III, but larger; and improvements have been made in several important areas. The core cooling system has been redesigned to provide improved cooling for steady state operation as well as for post-pulse cool down. This necessitated a change in fuel plate design to accommodate coolant flow through.

The nitrogen coolant supply system has also been redesigned to provide for a greater mass flow rate and a remote control system for maintaining the temperature of the coolant. The cooling system will permit core cool down faster than SPR-III even though the mass of SPR-IV is twice that of SPR-III. It also provides for efficient cooling during steady state operations.

Upper and lower axial reflectors and auxiliary reflectors at the top of the core are used to provide uniform neutron fluence distributions in the cavity and to reduce the reactivity worths of experiments. Depending upon the experiment configuration, the worth can be reduced by a factor of two to five which places smaller requirements on the control margin for the reactor. The shroud for the reactor incorporates a layer of lead for tailoring the neutron-to-gamma ratio for external experiments as well as providing some shielding for personnel during maintenance and set-up operations. All of the mechanical systems were examined for improvements in operation and maintenance. Both the burst element and the safety block drive systems have been modified. The burst element will be driven by a linear induction motor eliminating the current pneumatic-hydraulic system.

The thermomechanical analysis has indicated that for nominal operations of the core, the stresses in the fuel and support structure will be no greater than those currently experienced satisfactorily in SPR-III.

The nominal operating characteristics in the pulse mode are a fluence of 5.6 x 10(+14) neutrons/cm**2 in the central cavity, a pulse width at half maximum power of 125 microsec, and a maximum fuel temperature increase of 400 C. Steady state power will be limited to less than 60 kw.

Appendix A

Material No. Densities

Material	Element	Number Density ($x10^{-24}$)
U-10-Mo (93% Enriched) ρ = 17.06 g/cc	U-235 U-238 MO	0.03666 0.00264 0.01070
4340 Steel ρ = 7.9 g/cc	Fe Ni Cr	0.08148 0.00154 0.00073
SS ρ = 7.92 g/cc	Fe Ni Cr Mo	0.05848 0.00975 0.01558 0.00124
Copper ρ = 8.94 g/cc	Cu	0.0848
Boron powder ρ = 1.3 g/cc 90% enriched	B-10 Density factors	0.07047 0.654* to 1.0
Boron loaded Silastic ρ_{mix} = 0.696 61.5 w/o B (93% en) 38.5 w/o Silgard ρ_B = 2.45 g/cc $\rho_{Silgard}$ = 0.325 g/cc	B-10 Carbon Si O H	0.0240 0.003939 0.002233 0.002470 0.01178
Aluminum ρ = 27 g/cc	AL	0.0602
Lead, ρ = 11.35 g/cc	Pb	0.033
Graphite ρ = 1.7 g/cc	Carbon	0.0855
Air ρ = 0.976x10 -3 g/cc	N O	$3.222x10^{-5}$ $8.563x10^{-6}$

(*) The B-10 density for the thimble region was assumed to be 0.07047*0.654* volume fraction (if applicable) in the final calculations.

Appendix B

Volume Fractions For Volume-Averaged Regions

Region	Material	Volume Percent
Shroud	Silastic	0.399
	AL	0.601
Cavity Thimble	SS-304	0.5
	B-Powder (90% enriched)	0.5
Radial Reflector Zone	Reflector Material (Cu or C)	0.6667
	Steel	0.0556
	Void	0.2777